



8-2015

Biodegradable Nano-Hybrid Polymer Composite Networks for Regulating Cellular Behavior

Charles Henley Sprague

University of Tennessee - Knoxville, cspragu2@vols.utk.edu

Follow this and additional works at: https://trace.tennessee.edu/utk_gradthes

 Part of the [Biology and Biomimetic Materials Commons](#), [Biomaterials Commons](#), [Dental Materials Commons](#), [Materials Chemistry Commons](#), [Medical Biotechnology Commons](#), [Molecular, Cellular, and Tissue Engineering Commons](#), [Other Pharmacy and Pharmaceutical Sciences Commons](#), [Polymer Chemistry Commons](#), and the [Polymer Science Commons](#)

Recommended Citation

Sprague, Charles Henley, "Biodegradable Nano-Hybrid Polymer Composite Networks for Regulating Cellular Behavior. " Master's Thesis, University of Tennessee, 2015.
https://trace.tennessee.edu/utk_gradthes/3455

This Thesis is brought to you for free and open access by the Graduate School at TRACE: Tennessee Research and Creative Exchange. It has been accepted for inclusion in Masters Theses by an authorized administrator of TRACE: Tennessee Research and Creative Exchange. For more information, please contact trace@utk.edu.

To the Graduate Council:

I am submitting herewith a thesis written by Charles Henley Sprague entitled "Biodegradable Nano-Hybrid Polymer Composite Networks for Regulating Cellular Behavior." I have examined the final electronic copy of this thesis for form and content and recommend that it be accepted in partial fulfillment of the requirements for the degree of Master of Science, with a major in Biomedical Engineering.

Shanfeng Wang, Major Professor

We have read this thesis and recommend its acceptance:

Roberto S. Benson, Gajanan S. Bhat

Accepted for the Council:

Carolyn R. Hodges

Vice Provost and Dean of the Graduate School

(Original signatures are on file with official student records.)

**Biodegradable Nano-Hybrid Polymer Composite Networks for Regulating Cellular
Behavior**

A Thesis Presented for the
Master of Science
Degree
The University of Tennessee, Knoxville

Charles Henley Sprague

August 2015

Copyright © 2015 by Charles H. Sprague

All rights reserved.

Acknowledgements

I would like to express my sincere appreciation and thanks to my advisor, Professor Shanfeng Wang. He is a tremendous mentor, researcher, and scholar. I am very blessed to have an academic advisor as caring and professional as him. I am very thankful for the time and support that Dr. Wang has given me during my studies at the University of Tennessee. Throughout this experience with Dr. Wang, I have gained valuable insight in the engineering and science community, from writing scholarly literature to performing and designing projects.

I would also like to thank my committee members, Dr. Benson and Dr. Bhat for reviewing my thesis and serving on my committee. I value their knowledge and professionalism that they have showed throughout my graduate studies. I respect their willingness to talk on both personal and academic matters.

I would like to express my sincere gratitude for all of the professors at UT who taught me in the engineering field. I am glad to have been a part of these courses taught by such intelligent professors.

I would like to thank my colleagues and coworkers: Dr. Xifeng Liu, Jinbo Dou, Anchao Feng and Qingya Zeng. They have always been there to help in all regards. I have been blessed to have the opportunity to work with such hardworking and supportive students.

Finally, I would like to thank my parents and two older brothers. They have always been there to support me and guide me in the right direction.

Abstract

Photo-crosslinkable polymeric biomaterials have emerged in the field of biomedical research to promote tissue regeneration. For example, scaffolds that can be crosslinked and hardened *in situ* have been known to make suitable implant alternatives. Since injectable and photo-crosslinkable biomaterials offer the advantage of being minimally invasive, they have emerged to compete with autografts, a current highly invasive method to repair diseased tissue. A series of novel photo-crosslinkable, injectable, and biodegradable nano-hybrid polymers consisting of poly(ϵ -caprolactone fumarate) (PCLF) and polyhedral oligomeric silsesquioxane (POSS) has been synthesized in our laboratory via polycondensation. To engineer the material properties of the nano-hybrid networks, varied weight compositions of POSS (ϕ_{POSS}) were combined with PCLF. The material properties of uncrosslinked and crosslinked PCLF-*co*-POSS samples were characterized by gel permeation chromatography, thermogravimetric analysis, dynamic mechanical analysis, and differential scanning calorimetry. Surface properties were also analyzed via the water contact angle. From the analysis, we have found that higher weight percentages of POSS resulted in higher stiffnesses and thermal degradation temperatures, but lower crystallinities. Further, PCLF-*co*-POSS ($\phi_{\text{POSS}} = 5\%$, 10% and 20%) samples had higher wettability, as indicated by smaller water contact angles. The increase in wettability was likely due to POSS's ability to enhance porosity. To enhance the study for bone repair applications, the PCLF-*co*-POSS ($\phi_{\text{POSS}} = 20\%$) nanocomposite was supplemented with 20% hydroxyapatite (HA) nanoparticles and formed into disks with smooth and microgrooved surfaces. By tailoring PCLF-*co*-POSS material properties, substrates can be engineered to entice attachment, proliferation, and differentiation of mouse pre-osteoblastic MC3T3-E1 cells and rat primary aortic smooth muscle cells, targeting for bone and cardiovascular tissue engineering applications.

Table of Contents

Chapter I. Medical Polymers for Tissue Engineering Applications	1
1.1 Background.....	2
1.2 Tissue Engineering.....	3
1.2.1 Autografts	4
1.2.2 Allografts.....	5
1.2.2 Xenografts	5
1.3 Cell-Cell/Cell-ECM Interactions	5
1.3.1 Growth Factors.....	7
1.3.2 Growth Factors and Cancer.....	8
1.4 Biomaterials.....	9
1.4.1 Polymeric Biomaterials.....	11
1.4.2 Protein-Material Interactions	14
1.4.3 Cell-Material Interactions	15
1.5 Conclusion.....	16
References.....	17
Chapter II. POSS-containing Polymer Nanocomposites for Tissue Engineering Applications: A Literature Review.....	22
2.1 Introduction	23
2.2 Properties.....	24
2.2.1 POSS Properties	24
2.2.2 POSS with Variable Functional Groups	26
2.2.3 Effects of POSS on Crystallinity	29
2.2.4 POSS Thermal Properties.....	30
2.3 Biomedical Applications.....	31
2.3.1 Orthopedic Applications.....	31
2.3.2 Cardiovascular Applications	36
2.3.3 Dental Applications	38
2.3.4 Drug Delivery	39
2.3.5 Common POSS Nano-Hybrids for Tissue Engineering Applications	40
2.4 Conclusions	40
References.....	42
Chapter III. Experimental Procedures of Polymer Synthesis, Fabrication, Characterization, and Cell Studies.....	56
3.1 Introduction	57
3.2 Synthesis and Characterization of PCLF and PCLF-co-POSS	57
3.2.1 PCLF Synthesis	57
3.2.2 PCLF-co-POSS Synthesis.....	58
3.2.3 Fabrication of HA-containing PCLF-co-POSS	59

3.2.4 Polymer Purification	60
3.2.5 Photo-crosslinking PCLF, PCLF-co-POSS, and PCLF-co-POSS/HA	60
3.3 Characterization of uncrosslinked and crosslinked PCLF and PCLF-co-POSS	61
3.3.1 Gel permeation chromatography (GPC)	61
3.3.2 ¹ H NMR and FTIR	61
3.3.3 Gel fraction and swelling ratio	62
3.3.4 Differential scanning calorimetry (DSC)	62
3.3.5 Thermogravimetric analysis (TGA)	62
3.3.6 Dynamic mechanical analysis (DMA)	63
3.3.7 Water contact angles	63
3.3.8 Surface topography characterization	63
3.4 Cell attachment and proliferation	64
3.4.1 MC3T3-E1 cells	64
3.4.2 Smooth muscle cells	64
3.4.3 In vitro cell attachment and proliferation	64
3.4.4 Focal adhesion characterization	66
3.5 Cell differentiation	66
3.5.1 ALP activity and calcium content	66
3.5.2 MC3T3-E1 Gene Expression	67
3.5.3 SMC Gene Expression	68
References	70
Chapter IV. Regulation of Pre-osteoblastic MC3T3-E1 and Smooth Muscle Cells on Smooth Disks of Photo-crosslinked PCLF and PCLF-co-POSS	72
Abstract	73
4.1 Introduction	73
4.2 Results and Discussion	74
4.3 Structural characterizations	74
4.4 Photo-crosslinking	77
4.5 Water contact angle	78
4.6 Mechanical properties	79
4.7 Thermal properties	80
4.8 Cell attachment and proliferation	82
4.8.1 MC3T3-E1 cells cultured on PCLF and PCLF-co-POSS disks	83
4.8.2 SMCs cultured on PCLF and PCLF-co-POSS disks	85
4.9 Focal adhesions	87
4.9.1 MC3T3-E1 focal adhesions	87
4.9.2 SMC focal adhesions	88
4.10 Cell differentiation	90
4.10.1 ALP and calcium content	90
4.10.2 MC3T3-E1 Gene Expression	91

4.10.2 SMC Gene Expression	92
4.10 Conclusions	92
References	94
Chapter V. Regulation of MC3T3-E1 Cells on Smooth and Microgrooved PCLF-co-POSS/HA Nanocomposite Substrates.....	98
Abstract	99
5.1 Introduction	100
5.2 Results and Discussion	100
5.2.1 Photo-crosslinking	100
5.2.2 Thermal and Mechanical Properties.....	101
5.2.3 Surface topography characterization	103
5.3 Cell attachment and proliferation	103
5.3.1 Focal adhesions	106
5.4 ALP activity and calcium content	108
5.5 Gene expression.....	109
5.6 Further discussion.....	110
5.7 Conclusions	111
References	112
Chapter VI. Summary	116
Vita.....	119

List of Tables

Table 1.1 Common growth factors and their functions used in TE applications.	8
Table 1.2 Common biomaterials used and the biomedical application for each material [32].	10
Table 1.3 Commonly used and FDA-approved polymers and their applications.....	12
Table 1.4 Properties of each functional group and the effect that it has on protein and cell interactions [40].	15
Table 2.1 POSS varieties and uses.....	26
Table 2.2 Mechanical properties of commercially available PU-based polymers [86].	38
Table 2.3 Commonly used POSS-containing polymer nanocomposites for tissue engineering applications [104,105].	40
Table 3.1 MC3T3-E1 oligonucleotide primer sequences for real-time PCR.	68
Table 3.2 SMC oligonucleotide primers for real-time PCR.....	69
Table 4.1 Molecular Weight Information of PCLF and PCLF-co-POSS.	74
Table 4.2 Gel Fraction and Swelling Ratio values.	78
Table 4.3 Thermal Properties of PCLF, PCLF-co-POSS and POSS.....	80
Table 5.1 Thermal properties of crosslinked $\phi_{\text{POSS}} = 20\%$ and PCLF-co-POSS/HA.	102

List of Figures

Figure 1.1 Common tissue engineering approaches.	3
Figure 2.1 General structure of POSS.	25
Figure 2.2 A spinal fracture with several separated bone fragments within the vertebra.	32
Figure 2.3 Proliferation of MC3T3-E1 cells cultured on the surface of PCL/PEG3.4k-POSS, PCL/PEG8.0k-POSS, and PCL/PEG8.0k electrospun scaffolds as a function of the time in culture [78].	34
Figure 2.4 Cell attachment and proliferation on photo-crosslinked PCLTA-POSS substrates with varied mechanical properties. (a) Tensile moduli, (b) normalized cell attachment, (c) Fluorescence images of the cells stained with rhodamine-phalloidin (red) and DAPI (blue).	35
Figure 2.5 EPC capture on PCU-POSS substrates and tricalcium phosphate (TCP) positive control [82].	37
Figure 3.1 Synthesis of PCLF.	58
Figure 3.2 Synthesis of PCLF- <i>co</i> -POSS.	59
Figure 3.3 Fabrication of Microgrooved PCLF- <i>co</i> -POSS/HA.	59
Figure 3.4 Photo-crosslinking of PCLF- <i>co</i> -POSS.	61
Figure 4.1 ¹ H NMR spectra of PCLF, PCLF- <i>co</i> -POSS, and POSS. S = solvent.	76
Figure 4.2 FTIR spectra of PCLF, PCLF- <i>co</i> -POSS, and POSS.	77
Figure 4.3(a) Gel fractions and (b) swelling ratios of PCLF and PCLF- <i>co</i> -POSS in CH ₂ Cl ₂	78
Figure 4.4 Stress vs strain curves of photo-crosslinked PCLF and PCLF- <i>co</i> -POSS. Inset: magnification of the slope.	79
Figure 4.5 TGA curves of (a) PCLF, PCLF- <i>co</i> -POSS, and POSS and (b) photo- crosslinked PCLF and PCLF- <i>co</i> -POSS.	81
Figure 4.6 DSC (a) heating curve of PCLF and PCLF- <i>co</i> -POSS (b) photo-crosslinked PCLF and PCLF- <i>co</i> -POSS. (c) cooling curves of PCLF and PCLF- <i>co</i> -POSS (d) photo-crosslinked PCLF and PCLF- <i>co</i> -POSS.	82
Figure 4.7 MC3T3-E1 cell attachment and proliferation. (a) Fluorescent images stained with rhodamine-phalloidin (red) and DAPI (blue) on crosslinked PCLF and PCLF- <i>co</i> -POSS disks at days 1, 2, and 4 post-seeding. (b) Normalized cell attachment at 4 h. (c) Cell numbers at days 1, 2, and 4. (d) Proliferation index of MC3T3-E1 cells. (e) MC3T3-E1 cell area at 1 day. *, <i>p</i> < 0.05 relative to PCLF for cell attachment and cell area, and PCLF and $\phi_{\text{POSS}} = 5\%$ for cell number and PI. +, <i>p</i> < 0.05 relative to PCLF for cell number and PI. #, <i>p</i> < 0.05 relative to $\phi_{\text{POSS}} = 5\%$ at day 4. Scale bar of 200 μm is applicable to all.	84
Figure 4.8 SMC cell attachment and proliferation. (a) Fluorescent images stained with rhodamine-phalloidin (red) and DAPI (blue) on crosslinked PCLF and PCLF- <i>co</i> -POSS disks at days 1, 2, and 4 post-seeding. (b) Normalized cell attachment at 4 h. (c) Cell numbers at days 1, 2, and 4. (d) Proliferation index of SMCs. (e) SMC cell area at 1 day. *, <i>p</i> < 0.05 relative to PCLF and $\phi_{\text{POSS}} = 5\%$ for all graphs. +, <i>p</i> < 0.05 relative to PCLF at day 4. Scale bar of 200 μm is applicable to all.	86

Figure 4.9 (a) Fluorescent images of MC3T3-E1 cells stained with RP (red) top row, vinculin (green) middle row, and RP + vinculin bottom row. (b) FA density. (c) FA area. (d) FA elongation. *, $p < 0.05$ relative to PCLF and $\phi_{\text{POSS}} = 5\%$ for density and relative to all other samples for area and elongation. +, $p < 0.05$ relative to PCLF for all data. Arrows indicate FA protrusions. Scale bar of 40 μm is applicable to all.	88
Figure 4.10 (a) Fluorescent images of SMCs stained with RP (red) top row, vinculin (green) middle row, and RP + vinculin bottom row. (b) FA density. (c) FA area. (d) FA elongation. *, $p < 0.05$ relative to PCLF and $\phi_{\text{POSS}} = 5\%$ for density and relative to all other samples for area and elongation. Arrows indicate FA protrusions. Scale bar of 40 μm is applicable to all.	89
Figure 4.11 ALP activity and calcium content of MC3T3-E1 cells cultured on crosslinked PCLF and PCLF-co-POSS for (a) 7 days. (b) 14 days. *, $p < 0.05$ relative to PCLF at 7 days and PCLF and $\phi_{\text{POSS}} = 5\%$ at 14 days. +, $p < 0.05$ relative to PCLF.	90
Figure 4.12 MC3T3-E1 gene expression levels relative to GAPDH at 14 days. ALP expression (white). OCN expression (gray). *, $p < 0.05$ relative to PCLF. +, $p < 0.05$ relative to PCLF and $\phi_{\text{POSS}} = 5\%$	91
Figure 4.13 SMC gene expression relative to GAPDH at 4 days. Smoothlin expression (white). Calponin expression (gray). *, $p < 0.05$ relative to PCLF and $\phi_{\text{POSS}} = 5\%$	92
Figure 5.1 (a) gel fractions and (b) swelling ratios of PCLF-co-POSS/HA.	101
Figure 5.2 Thermal and mechanical properties of crosslinked $\phi_{\text{POSS}} = 20\%$ and PCLF-co-POSS/HA. (a) Stress vs strain (b) TGA (c) DSC cooling curve (d) DSC heating curve.	102
Figure 5.3 SEM images of (a) $\phi_{\text{POSS}} = 20\%$. (b) smooth PCLF-co-POSS. (c) microgrooved PCLF-co-POSS/HA.	103
Figure 5.4 MC3T3-E1 cell attachment and proliferation. (a) Fluorescent images stained with rhodamine-phalloidin (red) and DAPI (blue) on $\phi_{\text{POSS}} = 20\%$ and PCLF-co-POSS/HA disks at days 1, 2, and 4 post-seeding. (b) Normalized cell attachment at 4 h. (c) Cell numbers at days 1, 2, and 4. (d) Proliferation index of MC3T3-E1 cells. (e) MC3T3-E1 cell area at 1 day. *, $p < 0.05$ relative to $\phi_{\text{POSS}} = 20\%$ for cell number at 4 days, PI, and relative to microgrooved PCLF-co-POSS/HA for cell area. Scale bar of 200 μm is applicable to all.	105
Figure 5.5 (a) Fluorescent images of MC3T3-E1 cells stained with RP (red) top row, vinculin (green) middle row, and RP + vinculin bottom row. (b) FA density. (c) FA area. (d) FA elongation. *, $p < 0.05$ relative to $\phi_{\text{POSS}} = 20\%$ for density, microgrooved PCLF-co-POSS for FA area, and relative to all other samples for elongation. Arrows indicate FA protrusions. Scale bar of 40 μm is applicable to all.	107
Figure 5.6 ALP activity and calcium content of MC3T3-E1 cells cultured on crosslinked $\phi_{\text{POSS}} = 20\%$, PCLF-co-POSS/HA and microgrooved PCLF-co-POSS/HA for (a) 7 days. (b) 14 days. *, $p < 0.05$ relative to all samples at 7 days and $\phi_{\text{POSS}} = 20\%$ at 14 days. +, $p < 0.05$ relative to $\phi_{\text{POSS}} = 20\%$	108
Figure 5.7 MC3T3-E1 gene expression levels relative to GAPDH at 14 days. OPN expression (white). OCN expression (gray). *, $p < 0.05$ relative to $\phi_{\text{POSS}} = 20\%$ for OPN and all samples for OCN.	110

Chapter I. Medical Polymers for Tissue Engineering Applications

1.1 Background

This project combines the interdisciplinary fields of biomedical engineering and materials science engineering to develop suitable polymeric biomaterials for bone and cardiovascular tissue engineering applications. Importance of rehabilitation in both fields is a significant yet challenging problem to solve. Bone trauma, injury, and disease is debilitating and can lead to a consequential decreased quality of life by causing pain, inflammation, and restricting movement. According to the Center for Disease Control (CDC) over 43 million Americans have osteoarthritis (OA) and it is estimated that by 2030 over 67 million Americans will have the disease [1]. Further, according to the International Osteoporosis Foundation, (IOF) osteoporosis affects over 75 million people worldwide, and is partly responsible to the 8.9 million bone fractures per year worldwide, and can induce up to a 10% total bone loss in patients [2]. Another topic discussed in this project is the use of polymeric biomaterials to promote aortic smooth muscle repair caused from cardiovascular disease. According to the CDC, heart disease is the No. 1 cause of death in America, causing over 600,000 deaths per year and equating to medical expenses of over \$108.8 billion per year [3]. To combat bone and cardiovascular ailments, research in the engineering of bio-artificial scaffolds has become an essential approach to enhancing and ultimately rehabilitating these ailments.

Currently the gold standard to heal and regenerate bone and cardiovascular injuries is the autograft procedure, which is performed by harvesting cells or tissue from an area of the body and transplanting them into another region in the body of the same individual. Although autografts have proven to perform well in regenerating tissue and aiding in recovery, serious limitations are still prevalent. Problems associated with autografts include donor site morbidity, immunogenic rejection, and highly invasive surgery [4]. To combat the limitations associated

with autografts, synthetic polymeric biomaterials have been developed with tailorable mechanical and rheological properties to match site specific implantation. Additionally, injectable and crosslinkable viscous polymer solutions have been engineered to be cured and polymerized *in situ* via redox, thermal, or photo initiation, thereby reducing patient down time and mitigating the ill effects of highly invasive surgery. In this project, the use of bio-inspired polymers including poly(ϵ -caprolactone) (PCL) and polyhedral oligomeric silsesquioxane (POSS) has been studied to design biodegradable, osteoconductive, and cyto/hemocompatible substrates for bone and cardiovascular tissue engineering applications.

1.2 Tissue Engineering

Tissue Engineering (TE) is an interdisciplinary branch of engineering and regenerative medicine which uses natural and synthetic materials to regenerate and rehabilitate damaged cells and tissues [5]. TE has proven to be successful in the early stages of repair for bone, blood vessels, cartilage, enamel, and skin. Elementary TE involves cell and tissue culturing techniques to promote growth and generation of targeted tissues [6]. Important factors to consider in successful TE practices include cell attachment, proliferation, differentiation, and gene expression. An advantage of TE is the ability to reduce the need for highly invasive and dangerous procedures such as autografts [7].

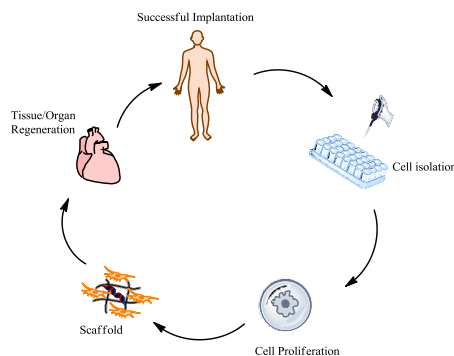


Figure 1.1 Common tissue engineering approaches.

Because cells and tissues can be grown *in vitro*, much research has been devoted to the use of TE for regenerating various connective tissues, collagen, and organs to create successful alternatives for autografts. TE applications can be studied via two mechanisms which involve the regeneration of tissue via natural cells derived from human or animal donors. Alternatively, tissue regeneration can be promoted from the integration of synthetic materials such as polymers, metals, ceramics, and composites with various cell and tissue types appropriate for the targeted rehabilitation site. Further, the latter approach for TE can be further broken down into the sub-field known as biomaterials.

The ultimate goal of TE is to maintain, restore, and improve tissue function [8]. To do this effectively, limitations including cytotoxicity, rejection, and demand need to be addressed. Although artificial tissues and organs such as tracheas, bladders, and hearts have been developed, significant problems of immunorejection and incompatibility still remain. In the design of three-dimensional TE applications which mainly involve the regeneration of organs, the extracellular matrix (ECM) is the main component that needs to be examined. Comprised of polysaccharides and proteins such as collagen, laminin, and fibronectin, the ECM serves as the structural component for tissues [9]. Type I collagen comprises most of the ECM and is the most abundant protein in both the ECM and the body [10].

1.2.1 Autografts

Autografts currently provide the best form of treatment for human tissue regeneration. Autografts are performed by harvesting cells from the same donor that is in need of tissue reconstruction. Autografts are useful especially for bone grafting procedures since they can promote both osteoconduction and osteogenesis [11]. However, autografts can bring discomfort

to patients since secondary surgery is required to harvest tissue.

1.2.2 Allografts

Allografts are similar to autografts in the fact that tissue is harvested from a donor and transplanted into the subject of need; however, with allografts the donor is not the subject of need but rather from another subject of the same species. Allografts offer an advantage over autografts by eliminating donor site morbidity and additional surgery for the patient.

Nevertheless, allografts are still secondary to autografts because of problems such as immune-incompatibility and disease transmission [12].

1.2.2 Xenografts

Xenografts are similar to allografts by transplanting tissue from a separate donor to the subject of need; however, the donor in a xenograft will be from a different species, most commonly derived from bovine. Xenografts are not optimal forms of treatment as they have the potential to pose serious risks to the subject in need. Risks include cross-species disease transmission, immunorejection, and bacterial and viral infections [13].

1.3 Cell-Cell/Cell-ECM Interactions

The ECM is an essential scaffold for tissue and organ development as well as, regulation of cell behavior including cell-cell and cell-ECM interactions. These interactions are imperative in the control of cell behavior including, the regulation of cell shape, development, migration, proliferation, and function [9]. Further the cell-cell and cell-ECM interactions can be an essential indication of whether or not a tissue engineered construct will be biocompatible for separate individuals. Cell-cell and cell-ECM interactions play a crucial role in ECM control and

regulation. For example, cell-ECM interactions regarding chondrocytes and the ECM have shown that chondrocytes, because of their multitude of receptors can influence ECM homeostatic balance therefore, affecting the ECM signaling system [14]. Essential approaches that TE depends on are successful cell and tissue migration, proliferation, and differentiation of which are all influenced by cell-ECM interactions [15,16]. Cell-ECM interactions are capable of regulating cell functions via receptor mediated signaling by triggering integrin and ligand binding interactions. For example, osteoprogenitor cells and osteoblasts have been shown to significantly express the $\alpha_5\beta_1$ integrin thereby, the design of a biomaterial aimed to enhance the expression of the $\alpha_5\beta_1$ integrin is an important factor to consider for bone TE applications [12]. Further, smooth muscle cells tend to express α_v containing integrins, especially $\alpha_v\beta_3$ during angiogenesis (e.g., formation of new blood vessels) [17]. Because of cell-ECM interactions, receptor mediated signaling is able to control vital physiological pathways and regulate growth factors to stimulate cell proliferation and adhesion to ECM scaffolds for successful TE applications.

Although the ECM is responsible for cell signaling and regulation within microenvironments, the ECM is also needed to fulfill further roles of ensuring structural integrity for newly formed tissue [18]. ECM for successful TE applications should have the desired mechanical properties to support itself and the surrounding forces acting on it. The ECM has the ability to control specific transduction pathways for attachment, proliferation, and differentiation; however, selectively activating targeted pathways still remains unsolved thus, posing challenges for immunogenic compatibility. An important pathway influenced by cell-ECM interactions is the mitogen-activated protein kinase (MAPK) pathway. MAPK is responsible for the regulation of growth factors and cell phenotype, both essential to TE. MAPKs are protein kinases which

regulate three amino acids including serine, threonine, and tyrosine [19]. MAPK can control growth factors and induce cell signaling for cell division by their ability to act as an “on/off” switch. This is accomplished by MAPK ability to add phosphate groups to neighboring proteins, therefore activating or deactivating specific growth pathways [20]. Studies have demonstrated that MAPK activation plays a role in regulating osteogenesis and promoting bone growth. Mouse pre-osteoblastic MC3T3-E1 cells cultured on stiff poly ethylene glycol (PEG) substrates have shown to increase alkaline phosphatase (ALP), osteocalcin (OCN), and bone sialoprotein (BSP) gene expression levels as well as, significantly increase MAPK activity thereby, enhancing the ability to regenerate bone tissue [21]. Although MAPK is critical to cell growth and proliferation, factors to promote significant upregulation of MAPK activation has proven to be a problem as this can lead to tumor and malignancy formation.

1.3.1 Growth Factors

Growth factors also play a critical role in regulating cell growth, proliferation, and survival necessary for TE. Growth factors are polypeptides that signal cells to respond to different biological environments [22]. Growth factors interact with the signaling components of the ECM such as, ligands and growth factor receptors to ensure correct cell function and signal transduction for regenerating tissue in different locations. Various growth factors play a vital role in the development, inhibition, and stimulation of specific tissues. For example, certain growth factors have the ability to entice growth of blood vessels, bone, cartilage, and skin. However, downregulating and upregulating signal transduction induced by growth factors, which is necessary for proper cell function, still remains a challenge. Further, specific growth factors can be delivered to the site of interest to improve wound healing, functional tissue development, and hormone delivery [23]. In order to deliver growth factors to site specific locations to promote cell

attachment and proliferation, polymer carriers with incorporated growth factors have been used to sustain the release of the bioactive molecules as the polymer degrades over time [24]. Table 1.1 lists common growth factors for tissue regeneration.

Table 1.1 Common growth factors and their functions used in TE applications.

Growth Factor	Function
Angiopoietin	Growth of veins and arteries
Bone Morphogenetic Protein (BMP)	Promote bone and cartilage growth
Epidermal Growth Factor (EGF)	Regulate cell growth, proliferation, and differentiation
Fibroblast Growth Factor (FGF)	Regulate wound healing
Growth Differentiation-8 (GDF-8)	Regulate skeletal muscle growth and differentiation
Insulin-like Growth Factor-1 (IGF-1)	Regulate glycogen synthesis in osteoblasts
Platelet-derived Growth Factor (PDGF)	Development of blood vessel formation
Transforming Growth Factor Alpha (TGF- α)	Activates pathways for cell proliferation and differentiation
Transforming Growth Factor Beta (TGF- β)	Activates pathways for cell proliferation and differentiation
Tumor Necrosis Factor (TNF)	Regulate apoptosis
Vascular Endothelial Growth Factor (VEGF)	Regulate blood vessel formation

1.3.2 Growth Factors and Cancer

Although growth factors are imperative for the regulation of cell growth, proliferation, differentiation, and migration, which are all necessary for the regeneration and formation of new

tissue, growth factors have been shown to contribute to malignancy formation and cancer progression. Specifically, growth factors promote cancer progression by influencing cell invasion across tissue barriers, clonal expansion, and colonization of cells in distant niches [25].

Oncogenic mutations result in uncontrollable growth factor stimulation thereby, promoting tumorigenesis [26,27]. For example, overexpression of genes that release IGF-1 has been linked to increased risk of colorectal cancer as well as, increased tumor size [28]. Further, increased levels of IGF-1 have been shown to stimulate breast cancer cell proliferation, because IGF-1 and IGF-1 receptor (IGF-1R) signaling pathways are upregulated by breast cancer tumors, induced from mutations in breast cancer susceptibility genes 1 and 2 (BRCA1/2) [29].

1.4 Biomaterials

Biomaterials encompass the use of synthetic materials such as metals, ceramics, polymers, and composites for biological integration. Biomaterials science is closely related to TE and requires multidisciplinary study from medicine, biology, engineering, chemistry, and physics. Advantages of synthetic biomaterials are less invasive surgeries, faster recovery; and tailorable mechanical, chemical, and topographical properties to match site specific applications. The ultimate goal of biomaterials is to improve physiological function, aid in healing, and replace living tissue as an implant. Biomaterials have emerged in the field of regenerative medicine and have proven to be successful scaffolds to repair cells, tissues, and organs [30]. Biomaterials can be defined as a nonviable materials used in a medical device aimed to be integrated into biological systems [31]. Human applications for biomaterials include a wide variety of targeting such as joint replacements, drug delivery, nerve regeneration, and vascular stents. Table 1.2 represents the current commonly used biomaterials and their applications.

Table 1.2 Common biomaterials used and the biomedical application for each material [32].

Tissue Engineering Application	Biomaterial
Joint Replacement	Cobalt-chromium, Titanium, Ti-Al-V, Stainless Steel
Bone and Dental Cement	Poly(methyl methacrylate) (PMMA), Hydroxyapatite (HA)
Dental Implant	Titanium, Ti-Al-V, polyhedral oligomeric silsesquioxane (POSS), HA, Calcium Phosphate
Ligament	Dacron
Blood Vessels	(PCL), Polycarbonate Urea (PCU), Teflon, POSS, polyurethane (PU)
Kidney	Cellulose, Polyacrylonitrile (PAN)
Lungs	Silicone, Polytetrafluoroethylene (PTFE)
Contact Lenses	Si-acrylate, PMMA, Polyhydroxyethylmethacrylate (PolyHEMA)
Corneal Regeneration	Hydrogels, Collagen

In order to engineer appropriate biomaterials for suitable use in human subjects, the designed material must proceed through a wide variety of tests and regulatory standards before being approved. In order to understand whether or not a biomaterial will be suitable for implantation, the material must first be in a purified and sterilized form and be an acceptable substrate for culturing cells, and enticing cellular adsorption, proliferation, and differentiation [32]. Currently the study of biomaterials focuses heavily on synthesizing and characterizing materials, as the chemical composition, mechanical, and, rheological properties of the material will allow for prior understanding of its use as a viable biomaterial before physiological and biological experiments are carried out. When a biomaterial is designed, precise reactions with

specific proteins and cells can be tailored for specific applications thereby, making the design process imperative for ensuring proper cell-material interactions [32]. Further, biomaterials must possess an important trait of being biocompatible within the desired biological system. This is a critical step in biomaterial fabrication and implantation since incompatible implants are liable to cause severe harm and injury to patients including immunorejection, inflammation, infection, surgical defects, and impaired healing [33]. Since biocompatibility is highly regulated, all materials intended for medical implantation must meet advanced standards and undergo testing regulated by the International Organization for Standardization (ISO). Specifically, to test for biocompatibility, ISO 10993 must be performed on the desired material aimed for biomedical use [34]. The ISO 10993 standard tests for a wide variety of material interactions including, cytotoxicity interactions with blood (hemocompatibility), carcinogenicity, and risk management assessments [35].

1.4.1 Polymeric Biomaterials

Polymers are among the most commonly encountered materials throughout daily life and have many important applications for everyday use. More importantly, polymers have the ability to be suitable biomaterials as they can be easily modified to fit specific needs of the body.

Polymers are viable components for engineering both two-dimensional and three-dimensional scaffolds. The development of polymer scaffolds has recently had a significant impact on the field of TE by providing cells and tissues favorable environments for growth and sustainability.

In the design of polymer scaffolds for TE applications, cellular cues used to promote adsorption and differentiation are important parameters to consider. For example, polymer scaffolds with variable surface properties can provide stem cells with physical cues such as stiffness, size, and shape to determine what type of primary cell they will differentiate into.

Specifically, mimicking the microenvironments of site specific areas for targeted regeneration can allow for stem cell differentiation needed for *in vitro* cell and tissue growth, which is essential for repair [36]. The table below lists current commonly used Food and Drug Administration (FDA) approved biomaterials.

Table 1.3 Commonly used and FDA-approved polymers and their applications.

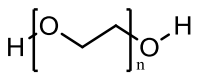
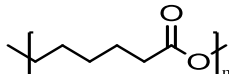
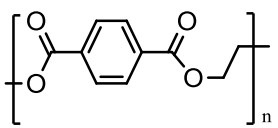
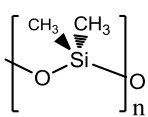
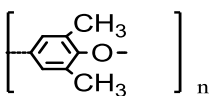
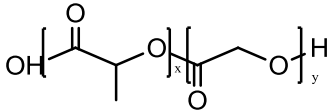
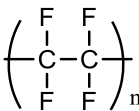
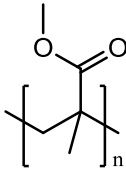
Polymeric Biomaterial	Application
PEG 	Cartilage, bone tissue, drug delivery, and gene therapy
PCL 	Smooth muscle and bone tissue
Dacron® Polyethylene Terephthalate (PET) 	Vascular grafts, Infection resistance
Polydimethylsiloxane (PDMS) 	Sensing and cell separation
Poly(<i>p</i> -phenylene oxide) (PEO) 	Biomimetic, cartilage, and bone tissue engineering

Table 1.3 Commonly used and FDA-approved polymers and their applications. Continued.

Polymeric Biomaterial	Application
poly(lactic- <i>co</i> -glycolic acid) PLGA	Skin grafts, wound healing, and bone repair
	
PTFE	Catheters, sutures, and cosmetic surgery
	
PMMA	Contact lenses, bone cement, and dental prosthetics
	

To further regulate cell behavior, polymers with tunable topographical, mechanical, and chemical properties designed to promote specific cell behavior can be categorized as smart biomaterials [37]. Polymeric biomaterials can serve many different functions from repairing and replacing tissue to being used for drug and gene therapy [38]. Recently, controlling the biodegradation rate of biopolymers has become useful for allowing cells and tissue to grow on substrates and form mechanically stable networks thereby, allowing the polymer to degrade over time while leaving only the newly formed tissue. Common biodegradable polymers that have proven to be successful when interfaced with human tissue include PCL, PPF, PEG, PLGA, and poly(L-lactic acid) (PLLA). Further, novel biomaterials have been developed to possess both

biodegradable and injectable properties which can allow for less invasive surgical procedures. Injectable and biodegradable polymers are typically cohesive and gel-like solutions designed to be injected and crosslinked *in situ* [38]. Many of these polymers are thermogelling diblock and triblock copolymers which take advantage of their ability to be hardened via temperature differences inside and outside the body [39]. Injectable polymers can also be photo-crosslinked and hardened *in situ* with ultraviolet (UV) light. Photo-crosslinkable polymers have shown promise for applications in bone, dental regeneration, and vascular grafts.

1.4.2 Protein-Material Interactions

Proteins are considered natural polymers and are categorized into four different stages of structure including primary, secondary, tertiary, and quaternary. Proteins are large biomolecules comprised of a sequence of twenty amino acids, determined by the DNA of the cell. Proteins are responsible for many actions in the body such as, transporting molecules, replicating DNA, and regulating hormones. Protein-material interactions are an imperative aspect to consider when designing biomaterials for implantation. Protein-material interactions are responsible for determining whether or not a biomaterial will be biocompatible [40]. When materials are implanted into a physiological system, a protein monolayer is formed around the material (e.g., stent, catheter, joint replacement, or TE scaffold) within a matter of minutes. It is understood that when cells are cultured onto foreign synthetic surfaces that the actual cells are not in direct contact with the molecular structure of the material, but rather the cells attach onto the monolayer of proteins. When materials are selected for human applications, the specific material for use is not bioactive. The bioactivity of the material is determined by the ability of proteins to adsorb to the surface of the material [40]. The proteins adsorbed to the surface of the biomaterial are responsible for controlling the action of cells and tissues. Techniques to influence protein

adsorption to material surfaces can be achieved by surface modification and grafting techniques. By exposing proteins to various functional groups, protein adsorption can be altered. For example, the use of methyl (-CH₃), hydroxyl (-OH), amine (-NH₂), and carboxylic (-COOH) groups can be used to affect protein and cell behavior [41]. However, there is still an issue in controlling the protein adsorption behavior to influence cell activity. Table 1.4 lists the effects on cells of each functional group described above.

Table 1.4 Properties of each functional group and the effect that it has on protein and cell interactions [40].

Functional Group	Properties	Effects
- CH ₃	Neutral; Hydrophobic	Promote leukocyte adhesion and phagocyte migration
- OH	Neutral; Hydrophilic	Increases osteoblast proliferation
- NH ₂	Positive; Hydrophilic	Increases myoblast proliferation, and differentiation of osteoblasts
-COOH	Negative; Hydrophilic	Increases affinity for albumin and fibronectin

1.4.3 Cell-Material Interactions

Cell-material interactions are a fundamental but critical topic in biomaterials research. Similar to, and dependent upon protein-material interactions, cell-material interactions play a large role in determining specific cues for cell influence and behavior [41]. Materials engineered with altered surface properties by micropatterning techniques to induce features such as microgrooves, pores, and channels have been used to improve cell attachment and density. As discussed earlier in protein-material interactions, when cells attach to the material surface they are not in direct contact with the material surface, but rather attached to the proteins adsorbed to the surface, therefore the ability to influence protein adsorption onto the substrate is critical [40].

Another important aspect to consider for proper cell attachment and enhanced cell-material interactions are focal adhesions (FAs). FAs are complex organelles comprised of over 150 proteins [42]. Since FAs are located at the interface between the cytoskeleton and the ECM, these proteins are responsible for the cell attachment [42]. In turn, FAs serve to anchor the cells to biomaterial surfaces.

1.5 Conclusion

As reviewed above, the integration between TE and biomaterials has allowed for the improvement of interfacing synthetic materials with physiological systems. The use of biomaterials for TE applications has proven to be successful in the advancement of biomedicine by improving the understanding of cellular responses to implanted materials. Numerous techniques for polymeric biomaterials have been developed to guide cell behavior and enhance cell migration, proliferation, and differentiation, which are essential to regenerative medicine. Specific techniques used to improve the viability of biomaterials include the uses of biodegradable, injectable, and photo-crosslinkable polymer systems. By understanding the interactions between proteins, cells, and biomaterials, the engineering of novel polymeric systems can be tailored for specific needs and continue to improve regenerative medicine.

References

1. Wegner, N., Lundberg, K., Kinloch, A., Fisher, B., Malmström, V., Feldmann, M., Venables, P. (2010). Autoimmunity to Specific Citrullinated Proteins Gives The First Clues to the Etiology of Rheumatoid Arthritis. *Immunological Reviews*, 233(1), 34-54.
2. Hannan, M., Felson, D., Dawson-Hughes, B., Tucker, K., Cupples, L., Wilson, P., Kiel, D. (2000). Risk Factors for Longitudinal Bone Loss in Elderly Men and Women: the Framingham Osteoporosis Study. *Journal of Bone and Mineral Research*, 15(4), 710-720.
3. American Heart Association. (1988). *Heart Facts*. The Association.
4. Betz, R. (2002). Limitations of Autograft and Allograft: New Synthetic Solutions. *Orthopedics*, 25(5 Suppl), 561-570.
5. Polak, J. (2006). Stem Cells and Tissue Engineering: Past, Present, and Future. *Annals of the New York Academy of Sciences*, 352-366.
6. Chapekar, M. (2000). Tissue Engineering: Challenges and Opportunities. *Journal of Biomedical Materials Research*, 617-620.
7. Duncan, D., Breuer, C. (2011). Challenges in Translating Vascular Tissue Engineering to the Pediatric Clinic. *Vascular Cell*, 3, 23-23.
8. Sala CC, Ribes MA, Muiños TF, Sancho LR, Chicón PL(2013) Current Applications of Tissue Engineering in Biomedicine. *Journal of Biochip & Tissue Chips*2:
9. Alberts B, Johnson A, Lewis J, Et Al. *Molecular Biology of the Cell*. 4th Edition. New York: Garland Science; 2002.
10. Gieringer, M. (2011). Radiotherapy and Wound Healing: Principles, Management and Prospects (Review). *Oncology Reports*, 26(2), 299-307.

11. Oryan, A., Alidadi, S., Moshiri, A., Maffulli, N. (2014). Bone Regenerative Medicine: Classic Options, Novel Strategies, and Future Directions. *Journal of Orthopaedic Surgery and Research*, 9, 18-18.
12. Robertson, A. (2006). Current Trends in the Use of Tendon Allografts in Orthopaedic Surgery. *Journal of Bone and Joint Surgery - British Volume* 12(2), 988-992.
13. Xebach, M. (1998). Xenotransplantation: Problems and Prospects. *Annual Review of Medicine*, 49, 301-310.
14. Chondrocytes-ECM Interactions in Human Osteoarthritis. (1999). *Advances in Experimental Medicine and Biology*, 455, 413-417.
15. Chen, S., Fitzgerald, W., Zimmerberg, J., Kleinman, H., Margolis, L. (2007). Cell-Cell and Cell-Extracellular Matrix Interactions Regulate Embryonic Stem Cell Differentiation. *Stem Cells*, 25(3), 553-561.
16. Petrie, T., Reyes, C., Burns, K., García, A. (2008). Simple Application of Fibronectin-Mimetic Coating Enhances Osseointegration Of Titanium Implants. *Journal of Cellular and Molecular Medicine*, 13(8b), 2602-2612.
17. Brooks, P., Clark, R., Cheres, D. (1994). Requirement of Vascular Integrin Alpha V Beta 3 for Angiogenesis. *Science*, 569-571.
18. Rosso, F., Giordano, A., Barbarisi, M., Barbarisi, A. (2004). From Cell-ECM Interactions to Tissue Engineering. *Journal of Cellular Physiology*, 174-180.
19. Waskiewicz, A. (1997). Mitogen-Activated Protein Kinases Activate the Serine/Threonine Kinases Mnk1 And Mnk2. *The EMBO Journal*, 16(8), 1909-1920.

20. Cargnello, M., Roux, P. (2011). Activation and Function of the Mapks and Their Substrates, the MAPK-Activated Protein Kinases. *Microbiology and Molecular Biology Reviews*, 75, 50-83.
21. Khatiwala, C., Peyton, S., Metzke, M., Putnam, A. (2007). The Regulation of Osteogenesis by ECM Rigidity In MC3T3-E1 Cells Requires MAPK Activation. *Journal of Cellular Physiology*, 211(3), 661-672.
22. Lee, K., Silva, E., Mooney, D. (2010). Growth Factor Delivery-Based Tissue Engineering: General Approaches and a Review of Recent Developments. *Journal of the Royal Society Interface*, 8, 153-170.
23. Whitaker, M., Quirk, R., Howdle, S., Shakesheff, K. (2001). Growth Factor Release From Tissue Engineering Scaffolds. *Journal of Pharmacy and Pharmacology*, 53, 1427-1437.
24. Babensee, J., Mcintire, L., Mikos, A. (N.D.). Growth Factor Delivery for Tissue Engineering. *Pharmaceutical Research*, 17(5), 497-504.
25. Witsch, E., Sela, M., Yarden, Y. (2010). Roles for Growth Factors in Cancer Progression. *Physiology*, 2, 85-101.
26. Wang, S., Yu, Y., Criswell, T., Debusk, L., Lin, P., Zent, R., Arteaga, C. (2010). Oncogenic Mutations Regulate Tumor Microenvironment through Induction of Growth Factors and Angiogenic Mediators. *Oncogene*, 23, 3335-3348.
27. Cross, M., Dexter, T. (1991). Growth Factors in Development, Transformation, and Tumorigenesis. *Cell*, 64(2), 271-280.
28. Shiratsuchi, I., Akagi, Y., Kawahara, A., Kinugasa, T., Romeo, K., Yoshida, T., Shirouzu, K. (2011). Expression Of IGF-1 And IGF-1R And Their Relation To Clinicopathological Factors In Colorectal Cancer. *Anticancer Res.*, 31(7), 2541-2545.

29. Kang, H., Yi, Y., Kim, H., Hong, Y., Seong, Y., Bae, I. (2012). BRCA1 Negatively Regulates IGF-1 Expression Through an Estrogen-Responsive Element-Like Site. *Cell Death and Disease*, 3, E336-E336.
30. Murphy, S., Atala, A. (2012). Organ Engineering - Combining Stem Cells, Biomaterials, and Bioreactors to Produce Bioengineered Organs for Transplantation. *Bioessays*, 35(3), 163-172.
31. Parida, P., Behera, A., Mishra, S. (2012). Classification of Biomaterials Used in Medicine. *International Journal of Advances in Applied Sciences*, 1(3), 31-35.
32. Ratner, B., Hoffman, A. (2004). Biomaterials and Biomaterials Science. in *Biomaterials Science an Introduction to Materials in Medicine*. (2nd Ed.). Burlington: Elsevier.
33. Stynes, G., Kiroff, G., Morrison, W., Kirkland, M. (2008). Tissue Compatibility of Biomaterials: Benefits and Problems of Skin Biointegration. *ANZ Journal of Surgery*, 78(8), 654-659.
34. Muller, U. (2008). *in vitro* Biocompatibility Testing Of Biomaterials and Medical Devices. *Med Device Technol.*, 19(2), 32-34.
35. Use of International Standard ISO-10993, 'Biological Evaluation of Medical Devices Part 1: Evaluation and Testing' (Replaces #G87-1 #8294).
36. Higuchi, A., Ling, Q., Chang, Y., Hsu, S., Umezawa, A. (2013). Physical Cues of Biomaterials Guide Stem Cell Differentiation Fate. *Chemical Reviews*, 3297-3328.
37. Control of Microenvironmental Cues with a Smart Biomaterial Composite Promotes Endothelial Progenitor Cell Angiogenesis. (2012). *ECM Journal*, 90-106.
38. Kohane, D., Langer, R. (2007). Polymeric Biomaterials in Tissue Engineering. *Pediatric Research*, 63(5), 487-491.

39. Dhandayuthapani, B., Yoshida, Y., Maekawa, T., Kumar, D. (2011). Polymeric Scaffolds in Tissue Engineering Application: A Review. *International Journal of Polymer Science*, 2011, 1-19.
40. Latour, R. (N.D.). *Biomaterials: Protein–Surface Interactions*. 1-13.
41. Yao, X., Peng, R., Ding, J. (2013). Cell-Material Interactions Revealed via Material Techniques of Surface Patterning. *Advanced Materials*, 25(37), 5257-5286.
42. Oakes, P., Gardel, M. (2014). Stressing the Limits of Focal Adhesion Mechanosensitivity. *Current Opinion in Cell Biology*, 30, 68-73.

**Chapter II. POSS-containing Polymer Nanocomposites for Tissue Engineering
Applications: A Literature Review**

2.1 Introduction

The emerging application for nanomaterials in biomedical research has become a particular area of interest for engineers and scientists. A nano cage-like molecule known as polyhedral oligomeric silsesquioxane (POSS) has recently become a nanomaterial of interest for its promising benefits in developing tunable biomaterials for tissue engineering applications. In the field of biomedical research, interdisciplinary collaboration has become commonplace and essential to the advancement of healthcare. POSS nanomaterial research has the ability to coalesce the work of several engineering and science disciplines such as biomedical engineering, materials science, nanotechnology, and biotechnology. Since POSS is typically used to form nano-hybrid polymeric networks and copolymers, the involvement of material science and organic chemistry is imperative. Additionally, since POSS copolymers can be formed into biomaterials such as hydrogels, thin disks, and injectable molded scaffolds; biomedical engineers also play a large role to integrate novel polymer constructs into biological systems, thereby facilitating potential human use. Originally, POSS was developed by the United States Air Force for aerospace engineering purposes. Thanks to its impressive material properties, this nanomaterial has been introduced into biomedical research [1-5]. The small diameter (1.5 nm) and innate ability of POSS to promote material integrity of polymers has demanded the interest of many researchers, and is emerging as an integral aspect to improve polymeric biomaterials for biomedical research [6]. Further, using POSS in polymer systems allows for specific tailoring of biomaterials for bone, cardiovascular, dental, and neural tissue engineering applications. Also the fact that POSS does not evoke a significant immune response or induce cytotoxicity when implanted makes it an ideal additive to proven biomaterials [7]. Attributes of POSS include the ability to slow biodegradation time therefore, allotting more time for cells to proliferate and

attach onto the surfaces [8, 10]. Also since POSS can be copolymerized with fumarate containing polymers such as poly(ϵ -caprolactone fumarate) (PCLF) and poly propylene fumarate (PPF), these polymer systems tend to promote a favorable environment for cells, as fumarate is a natural compound found in mammalian cell metabolism [11]. Additionally, when POSS-containing nanocomposites incorporate fumarate, the rate of biodegradation becomes less of a problem as the body can easily excrete these compounds as waste. Because of the ease of excretion and enhanced biocompatibility, surgical patients would be provided with more comfort and less downtime, as the need for additional surgeries would be diminished [12-15]. Throughout this chapter we will discuss several biomedical applications of POSS but, more specifically we will be reviewing the mechanical and rheological properties of POSS in addition to using POSS for bone, cardiovascular, and dental tissue engineering applications. From the review we will be able to showcase the synergistic effects that POSS displays as being both biocompatible and osteoconductive from cell study evidence.

2.2 Properties

2.2.1 POSS Properties

It is widely known that increasing POSS loading in a polymer system allows for enhancement and control of material properties, thus making POSS a viable component for anisotropic tissue properties. By varying the weight percentage of POSS, specific polymers can be tailored in order to satisfy variable *in-situ* microenvironments, and therefore ultimately leading to the creation of an implant with increased biocompatibility. As stated earlier, POSS is a nano-scale oligomer with a cage diameter of 1.5 nm [12]. POSS is comprised of several Si-O bonds which are responsible for the cage-like structure. Two factors can explain the ability of

POSS to strengthen polymers. Firstly, the nature of short silicon and oxygen bonds require high energies to be broken (Figure 2.1). The property of short Si-O bonds in POSS also contributes to a slower degradation time [15,16].

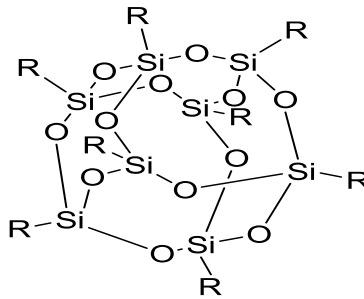


Figure 2.1 General structure of POSS.

Figure 2.1 is the general structure of POSS which contains several Si-O bonds with *R* groups attached to each silicon atom. It is evident in the figure that the assembly of Si-O bonds is the backbone of the cage-like structure. Since POSS has short Si-O bonds, significant energy is required to break the bonds therefore, enhancing POSSs ability to promote material integrity and strengthening properties as well as, improving chemical and thermal stability [17-20]. Moreover, these short bonds are a key attribute of POSS, which allows it impose slower biodegradation when integrated into degradable polymer networks [17,21-23]. Additionally, POSS is able to strengthen polymers because of the fact that it has the ability to increase crosslinking density in polymer systems. Specific POSS molecules that are known to increase crosslinking density significantly include methacryl, isobutyl, and tris norbornenylethyl POSS. However, not all types of POSS are able to increase crosslinking density, and in some instances POSS molecules such as, norbornenylethyl POSS decreases crosslinking density [24]. Cross-linked polymers are stiffer, and thus are desirable for tissue scaffolds subjected to excessive compressive and tensile forces, such as bone grafts [25-28]. When designing scaffolds for various applications, it is

imperative to understand that POSS loading affects material stiffness and thermal and chemical stability [29].

2.2.2 POSS with Variable Functional Groups

Table 2.1 POSS varieties and uses.

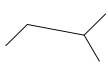
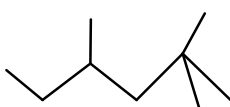
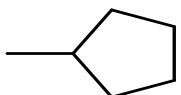
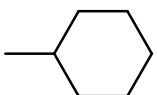
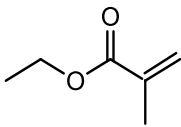
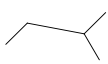
Full Name	Structure	Uses
Isobutyl POSS	R= 	Porogen
Isooctyl POSS	R= 	Porogen
Cyclopentyl POSS	R= 	Surface Modifications
Cyclohexyl POSS	R= 	Surface Modifications
Methacrylate isobutyl POSS	R ₁ =  R ₂₋₈ = 	Increases T _g

Table 2.1 POSS varieties and uses. Continued.

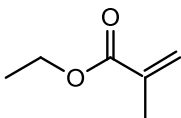

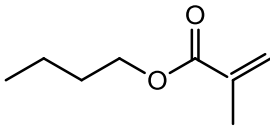
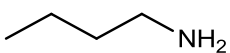
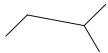
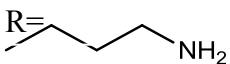
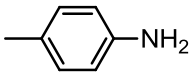
Full Name	Structure	Uses
Methacrylate ethyl POSS	$R_1=$ 	Increase hydrophobicity and toughness
Methacryl Isobutyl POSS	$R_{2-8}=$  $R_1=$ 	Increase hydrophobicity and toughness
Aminopropylisobutyl POSS	$R_1=$  $R_{2-8}=$ 	Grafting agent
Octa-Aminopropyl POSS	$R=$ 	Grafting agent
Octa-Aminophenyl POSS	$R=$ 	Grafting agent

Table 2.1 POSS varieties and uses. Continued.

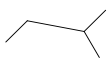
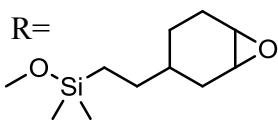
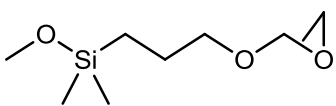
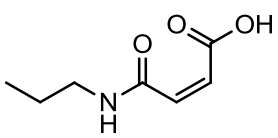
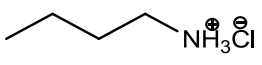
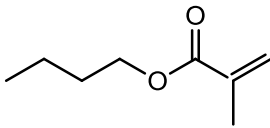
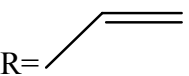
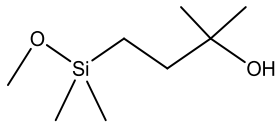
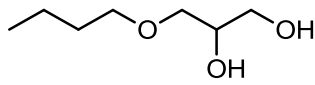
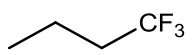
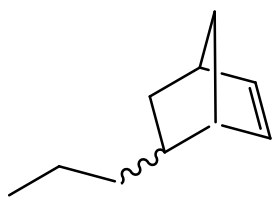
Full Name	Structure	Uses
Octa-isobutyl POSS	R= 	Porogen
Octa-epoxycyclohexyldimethylsilyl POSS	R= 	Cure accelerator
Octa-glycidyl dimethylsilyl POSS	R= 	Cure accelerator
Octa-Maleic Acid POSS	R= 	Peptide/Amino acid dispersion
Octa-Ammonium POSS	R= 	Drug delivery and dendrimers
Octamethacryl POSS	R= 	Increase T _g
Octa-methyl POSS	R= —	Improve hydrophobicity Crosslinking agent
Octa-vinyl POSS	R= 	

Table 2.1 POSS varieties and uses. Continued.

Full Name	Structure	Uses
Octa-3-hydroxy-3-methylbutyldimethylsiloxy POSS	R= 	PU crosslinker and adhesion promotion
1,2-propanediolisobutyl POSS	R= 	Increase strength and toughness
Trifluoropropyl POSS	R= 	Reduce surface energy
Norbornenylethylethyl POSS	R= 	Toughening agent

2.2.3 Effects of POSS on Crystallinity

POSS has been shown to act as a nucleating agent to promote or decrease crystal and spherulite formation for several nano-hybrid networks, therefore increasing crystallization rates and temperatures [32]. Advantages of nucleating agents include enhanced physical and optical properties such as stiffness, toughness, heat distortion, hardness, and clarity [32-37]. Studies have revealed that overall crystallinity decreases while POSS occupies a higher weight

percentage of the crosslinked nanocomposite. Specifically polypropylene (PP) and octa-vinyl POSS composites have proven that POSS increases crystallization rate and temperature while decreasing total crystallinity when compared to PP alone. Further supported from this study was that POSS greatly reduced the amount of spherulite formation of PP because of the heterogeneous nucleating effect of POSS [38,39].

2.2.4 POSS Thermal Properties

POSS has the ability to promote thermal stability of a nanocomposite. When analyzing thermal degradation of a polymer via thermogravimetric analysis (TGA), the addition of POSS has proven to increase total weight percent residue, which is due to the silicon's ability to increase the inorganic phase [40-43]. Thermal degradation has been studied on several functionalized POSS molecules including octahydride-POSS, polyvinyl-POSS, methyl-POSS, isooctyl-POSS, and isobutyl-POSS. From the studies, isooctyl-POSS and isobutyl-POSS degrade at the highest temperatures ranging from 307 ° to 372 °C respectively, while octahydride-POSS had the lowest degradation temperature at 157 °C [44]. POSS also improves thermal stability by protecting the surface layer of a polymer matrix and restricting the diffusion of oxygen into the matrix. When POSS-containing nanocomposites are heated, POSS degrades first and evolves into a superficial ceramic-like protective layer over the polymer [45-48]. Because POSS can decrease heat transfer by acting as a protective layer, POSS has also been used as flame retardants [49-53]. Furthermore, differential scanning calorimetry (DSC) has been used to show that the glass transition temperature (T_g) increases in correlation to the increase of POSS aggregates in polymer networks [54-60].

2.3 Biomedical Applications

2.3.1 Orthopedic Applications

The fact that POSS can be used to tailor and enhance material properties has sparked interest in its use for bone-tissue-engineering applications [61-64]. POSS can be used to generate autologous bone grafts for individuals with recent bone trauma, injuries, or osteoporosis. In order to examine the material properties effected by POSS, copolymers and polymer blends such as, PPF-*co*-POSS, PCLF-*co*-POSS, poly(ϵ -caprolactone) triacrylate (PCLTA)/POSS, polyethylene glycol (PEG)/POSS, and polyurethane (PU)/POSS were first synthesized via polycondensation with varied weight percentages of POSS, then photo-crosslinked. Once crosslinked, the samples were then swelled in organic solvents such as methylene chloride or acetone then dried for several days in a vacuum. Because POSS can induce porosity onto the surfaces of polymer systems, porosity variations can be analyzed via imaging and the use of the sessile drop technique. Surface imaging techniques are typically analyzed via scanning emission microscopy (SEM) and atomic force microscopy (AFM). It is known that an increase in POSS loading will induce a higher surface porosity thereby, increasing surface wettability [65,66]. Advantages of polymer substrates engineered with POSS include, the ability for the polymer networks to entice cell differentiation, elicit a promising surface for protein and cellular adsorption and, promote osteoconductivity, and gene expression [19,67-70]. Furthermore, POSS nano-composites tend to induce porosity with a pore diameter ranging from 1.41 to 3.10 nm, which makes simulating the natural porous structure of bone tissue less of a challenge and thereby, making POSS a suitable additive in the development of a bone mimetic material [64]. Since POSS-containing polymer systems can simulate the natural environment of bone as well as, stimulate bone regeneration, it is ideal to use as a scaffold for heterologous bone grafting [64-68]. Further, POSS performs well

in the ability to easily control and enhance the material properties of polymer networks for anisotropic bone tissue [26,67]. Because POSS has an impact on material properties as well as, inducing surface porosity, several research ideas have been assimilated based upon using POSS monomers in the development of copolymers aimed to entice bone growth and promote regeneration. For example, osteoconductive POSS has been studied to create injectable and crosslinkable polymer resins that can be cured via UV light *in situ* [71,72]. In the treatment of spinal injuries, the use of POSS is important in the synthesis of a copolymer because it not only allows for a tunable polymer network with desired material properties but, also allows for a polymer that can be hardened *in situ* thus, being less invasive to surgical patients (Figure 2.2). A spinal fracture contains many bone fragments which contribute to inflammation, pain, restricted movement, and slow recovery time.

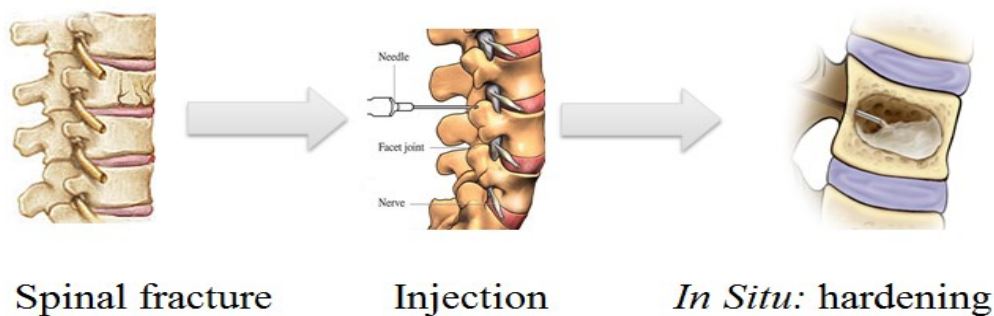


Figure 2.2 A spinal fracture with several separated bone fragments within the vertebra.

As shown above, it is evident that an osteoconductive and, photo-crosslinkable polymer could offer desired healing benefits for patients by providing a possible outpatient spinal surgery. Because of the minimally invasive nature of this procedure, faster recovery would be expected. With regards to treating the injury, POSS would be a viable component in the engineering of a copolymer with tailorable mechanical characteristics that can exhibit similar mechanical properties of bone such as stiffness, toughness, and elasticity. In particular, stiffness and

toughness are imperative parameters to consider when treating bone related spinal injuries, since the spine is responsible for being able to withstand immense yet constant forces such as compressive, tensile, torsional, and external forces. Typical spinal injuries are known to occur at compressive forces exceeding 1720 N [72]. Further, evidence has shown that spinal injuries related to torsion tend to occur at a torque of 13.6 N·m and a rotation of 114 ° [72]. With these pre-factors in mind, the tailorable effects of POSS would be highly desired in the design of a copolymer that showcases strong material properties by being able to withstand high loading forces yet, possess high enough elastic properties to account for spinal torsion. Another advantage of POSS is to simulate the characteristics of hydroxyapatite [HA, $\text{Ca}_{10}(\text{PO}_4)_6(\text{OH})_2$], which is the main mineral found in bone and teeth [73,74]. HA is a common biomaterial used since its surface properties display porosity and its structural properties exhibit hardness, which is essential to bone. However, HA tends to be very brittle and cannot be applied to a load-bearing site therefore; alternatives have been desired. Research has shown that the use of POSS could be a feasible replacement to HA. The use of POSS with bio-inspired polymers such as PEGF, PCLF, or PPF is excellent for generating bone grafts, as these nano-composite networks would be both osteoconductive and offer low toxicity to cells [74]. Studies have shown that PEG or PCL/POSS scaffolds are a great choice to use for the promotion of bone growth and bone grafts, as this particular scaffold has an uncanny ability to promote osteoblast cell differentiation and proliferation [73-75]. Specific cell lines that have responded well to POSS composite scaffold have been the mouse pre-osteoblastic MC3T3-E1 cells. Studies regarding the use of fumarate in POSS-containing nanohybrid polymer networks have proven to maximize MC3T3-E1 cell functions including proliferation, differentiation, and gene expression [76-78].

Additionally, studies have examined the use of PEG and PCL with POSS to form copolymers synthesized via polycondensation at room temperature under nitrogen for 12 h. Specifically, a polymer blend consisting of PEG or PCL/POSS was evaluated on the ability to promote pre-osteoblastic MC3T3-E1 mouse cell proliferation in comparison to a PCL/PEG copolymer and PCL alone (Figure 2.3).

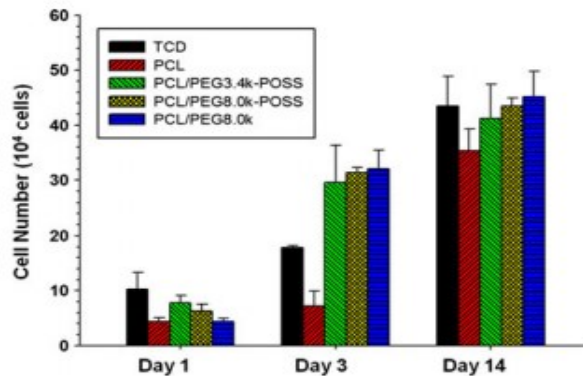


Figure 2.3 Proliferation of MC3T3-E1 cells cultured on the surface of PCL/PEG3.4k-POSS, PCL/PEG8.0k-POSS, and PCL/PEG8.0k electrospun scaffolds as a function of the time in culture [78].

Further, the polymer blend showed promising cell proliferation as the number of cells on the POSS substrates was far greater than PCL alone. This is because of POSS siloxanes have the ability to induce higher free surface energy and stimulate higher cell attachment [78]. Studies have further suggested that the use of POSS as a material strength enhancer to induce surface stiffness tends to promote mouse pre-osteoblastic MC3T3-E1 cell proliferation and differentiation, as the cells have been shown to favor stiffer surfaces with a modulus of elasticity (E) of 1GPa rather than a softer surface where (E) is 1KPa. Similar results have been gathered where the same MC3T3-E1 cell line was cultured on PCLTA-POSS substrates where (E was 420 or 14 KPa) [69].

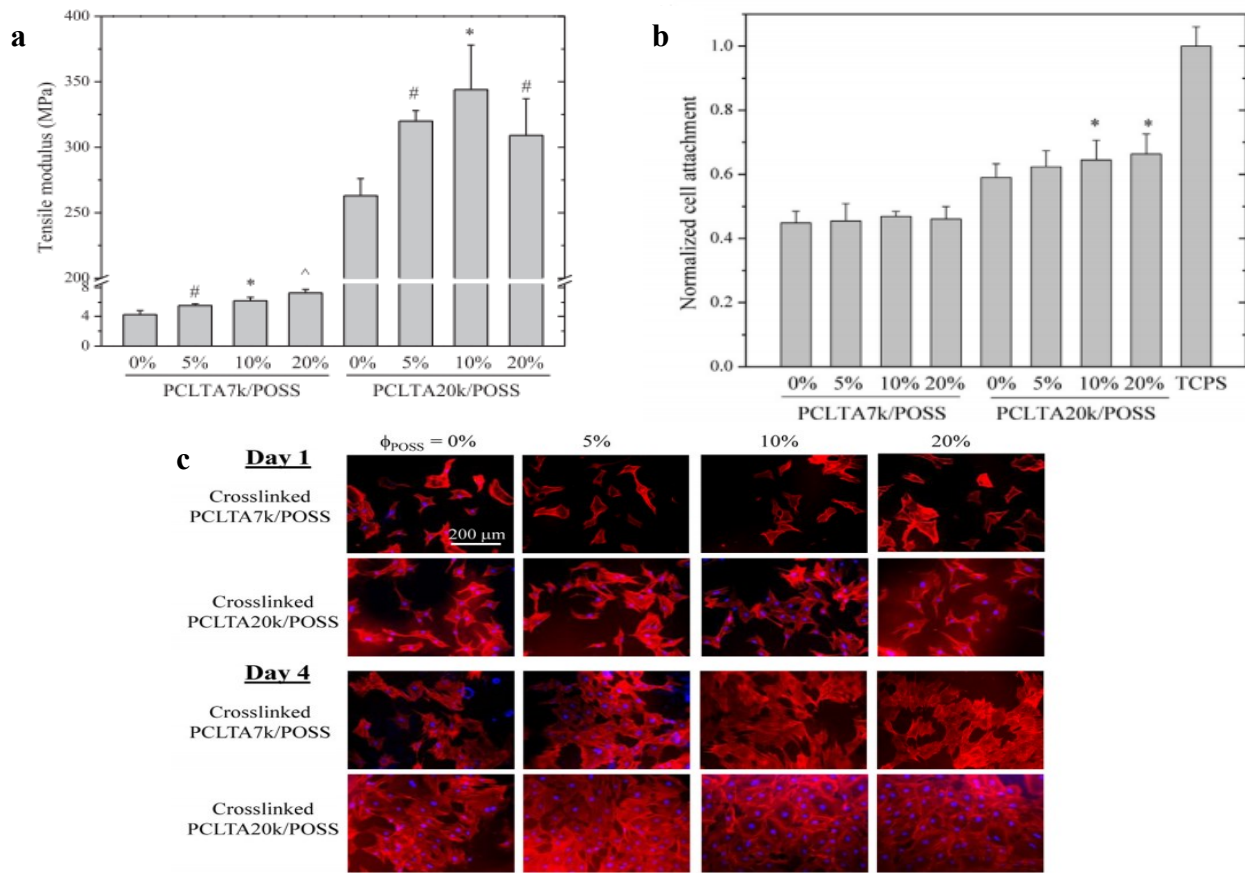


Figure 2.4 Cell attachment and proliferation on photo-crosslinked PCLTA-POSS substrates with varied mechanical properties. (a) Tensile moduli, (b) normalized cell attachment, (c) Fluorescence images of the cells stained with rhodamine-phalloidin (red) and DAPI (blue).

Shown in Figure 2.4 above, it is evident that an increase in POSS loading increases the overall average tensile moduli in PCLTA matrices. Moreover, normalized cell attachment and proliferation is enhanced with an increase in POSS composition. It is evident from the two studies that POSS looks to be a promising nanomaterial for biomaterial scaffolds to promote bone tissue regeneration.

Finally POSS has also been studied for implant coatings. More specifically POSS has been considered as an additive into polymer hip implants. Since hip implants are inserted into the femur and are always in contact with the surrounding bone, the osteoconductive and biocompatibility properties of POSS have been favored in this area [79].

2.3.2 Cardiovascular Applications

Vascular engineering is an area of research aimed at integrating living cells, biomaterial scaffolds, and even animal cells to formulate biocompatible smooth muscle cell (SMC) tissue for organ repair and replacement [5]. The goal of cardiovascular tissue engineering is to ultimately entice SMC tissue to grow in human subjects without eliciting significant immune response or rejection. To create an effective polymer that simulates the environment of the cardiovascular system, several materials have been studied including POSS. In addition to being biocompatible and providing satisfactory cell-material interactions, the use of POSS in the cardiovascular system provides many advantages to polymer systems, such as the enhancement of mechanical, chemical, and thermal properties, which includes viscoelasticity, calcification resistance, and wettability [8,17,80-83]. Furthermore, since POSS has been shown to increase stiffness and rigidity, it has been used for coatings in arterial stents and drug eluting stents. The use of POSS in a polycarbonate urea (PCU) copolymer has demonstrated that POSS is not only hemocompatible with vascular SMCs but also exhibits anti-inflammatory properties and evokes negligible immunoreactivity [83-85]. Also evidence from thromboelastography (TEG) has shown that POSS exhibits anti-thrombogenic properties when implanted into vascular architecture therefore, amplifying the effectiveness of drug eluting stents [83]. Surface topography analysis such as (AFM) and transmission emission microscopy (TEM) have confirmed that POSS nanocomposite rich surfaces have the ability to repel both platelets and proteins responsible for stenosis formation [85]. Due to the antithrombogenic and bio-inert nature of POSS, it can be used further in stent therapy in order to aid in the delivery of blood thinning medications to an obstructed area.

Studies have indicated that PCU-POSS enhanced cell capture of endothelial progenitor cells (EPCs) on POSS containing substrates used for cardiovascular stent applications while maintaining non-cytotoxic to surrounding cells. Recent studies have shown that PCU-POSS has been biofunctionalized onto the polymer surface with anti-CD34 by the use of fumed silica (Figure 2.5).

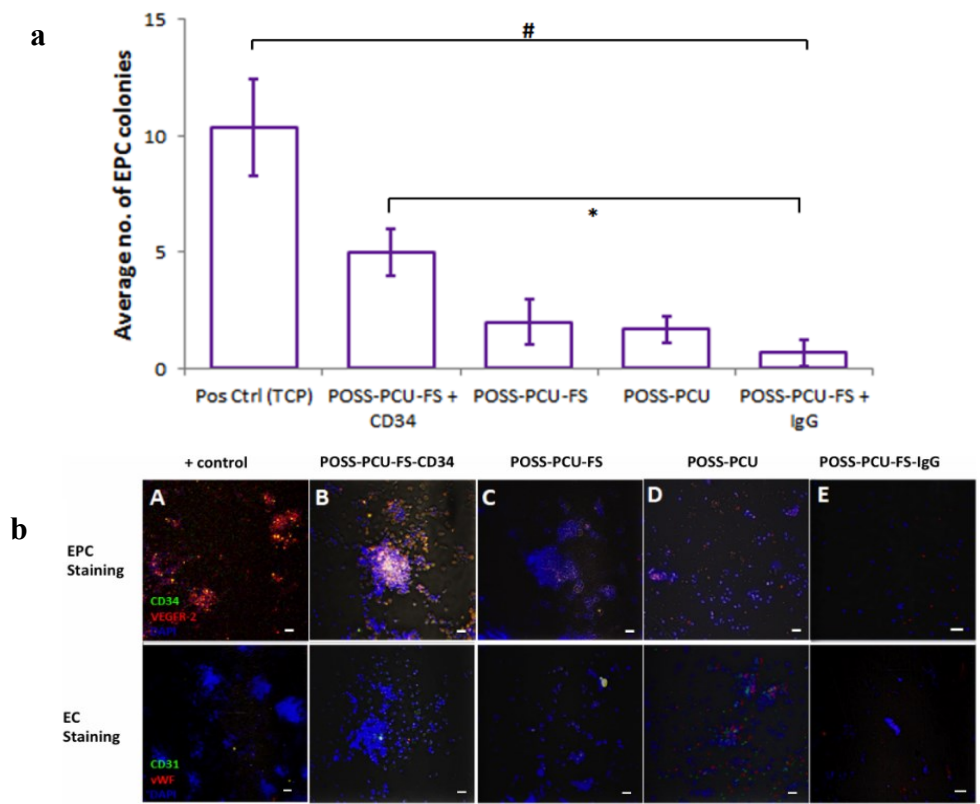


Figure 2.5 EPC capture on PCU-POSS substrates and tricalcium phosphate (TCP) positive control [82].

As shown above, it is evident that the biofunctionalized PCU-POSS substrate enhances EPC adhesion. The use of PCU-POSS is intriguing in its ability to promote *in situ* endothelialization thus, making this substrate an exceptional design for hemocompatibility, long term viability, and vessel restoration [82].

POSS-PCU polymer substrates have also proven to be successful scaffolds for its use in the development in heart valve leaflets because of the superior ability of POSS to enhance mechanical properties such as tensile strength and strain when compared to conventional PU substrates.

Table 2.2 Mechanical properties of commercially available PU-based polymers [86].

Polymer	Hardness (Shore A)	Tear Strength (N mm⁻¹)	Tensile Strength (N mm⁻²)	Elongation at Break (%)
Elastane ® (PEU)	85	55	48.3	570
Chronoflex ® C	80	45	37.9-45.5	400-490
Elasteon TM	75-90	50-80	20-30	500-750
POSS-PCU	84	50 ± 1.2	53.6 ± 3.4	704.8 ± 38

2.3.3 Dental Applications

Not only is POSS a great promoter of SMCs and bone tissue growth but, it is also used in the dental field to restore enamel. POSS has become very popular in dental research for the prevention of tooth decay as well as, dental regeneration [87]. This field is quite similar to research with regards to bone, since HA is also the main mineral found in teeth [88]. An interesting attribute of POSS which inspires researchers to use this material for dental research is the very small size of the POSS particles. POSS particles are typically 1.5 nm in diameter thus, making these particles significant vehicles to fill micro-cracks and pores within teeth when combined with polymethylmethacrylate (PMMA) and methylmethacrylate (MMA) matrices [88-92]. HA naturally contains 2.4 nm diameter tubules throughout its structure, which can allow for foreign debris and bacteria to infiltrate these small spaces and cause decay to the tooth and surrounding bone. POSS molecules smaller than 2.4 nm have been used to infiltrate the HA tubules and act as a shield to food particles and harmful bacterial which promote decay [93].

Another advantage to using POSS for dental applications is because of the fact that PMMA-POSS and MMA-POSS resins can be photo-crosslinked easily and cured with UV light thereby, allowing for fast in office procedures for patients. Studies have shown that POSS containing MMA and PMMA nanocomposites have proven to be suitable materials for dental implants and resins because of the increased compressive strength and shear stress of the dental filler [94, 95].

2.3.4 Drug Delivery

Additional biomedical uses for POSS have been studied including revolutionary novel drug delivery applications. POSS has proven to be a successful drug delivery carrier because of its ability to be easily functionalized and biologically inert [96, 97] POSS particles have shown promise for first generation poly(amidoamine) (PAMAM) dendrimer formation because of their nanocage-like structure. Dendrimers are a topic of interest for anti-cancer, diabetic, neural and, ocular regeneration, and tissue engineering applications [98-101]. Advantages of dendrimers include their ability to encapsulate therapeutic drug agents thus, protecting them from degradative enzymes and chemical breakdown. Moreover, dendrimers have the ability to deliver site specific drugs because of external chemical functionalization for direct cell targeting. Evidence has shown that self-assembled PAMAM-POSS based dendrimers loaded with insulin improved the dispersion and diffusion of insulin through cell membranes. Further evidence showed that the PAMAM-POSS dendrimer cores protected insulin for up to two hours [102]. PAMAM-POSS dendrimers have also been self-assembled into bilayers in which, anti-cancer drugs and folic acid have been loaded into for ligand binding and receptor mediated endocytosis [103].

2.3.5 Common POSS Nano-Hybrids for Tissue Engineering Applications

Table 2.3 Commonly used POSS-containing polymer nanocomposites for tissue engineering applications [104,105].

POSS Blends and Copolymers	Tissue Engineering Application
PPF-co-POSS	Bone
PEG-POSS	Bone/Vascular
PCL-POSS	Bone/Vascular
PU-POSS	Bone/Vascular
PCU-POSS	Vascular
PLLA-POSS	Vascular
PEG-co-POSS	Bone/Vascular/Drug Delivery
PVA-POSS	Drug/Gene Delivery
POSS-PEG-PLA	Drug/Gene Delivery
POSS-Methacrylate	Dental
POSS-MMA	Dental
POSS-PMMA	Dental

2.4 Conclusions

Throughout this review we have suggested the various biomedical uses and benefits associated with POSS. After examining the ability of POSS to be used in conjunction with many polymers to enhance material properties while still providing a biocompatible substrate, we can conclude that POSS is an effective nanomaterial for cancer therapy, drug delivery, and tissue engineering applications. Furthermore, since POSS has been shown to be osteoconductive and a

suitable replacement to HA, POSS is ideal to use for bone and dental regeneration. Ultimately, the use of POSS for biomedical research has become an interesting topic due to the wide variety of its applications and recent promising studies. Based upon the topics discussed throughout this chapter, we can conclude that POSS is a valuable nano-material and has many advantages to contribute to the advancement of polymer science and biomedicine.

References

1. Thomas, S., Stephen, R. (2009). Nanocomposites: State of the Art, New Challenges and Opportunities. In Rubber Nanocomposites: Preparation, Properties and Applications (1st ed., Vol. 1, p. 896). Wiley.
2. Discher, D. (2005). Tissue Cells Feel and Respond to the Stiffness of Their Substrate. *Science*, 310, 1139-1143.
3. Li, G., Cho, H., Wang, L., Toghiani, H., Pittman, C. (2005). Synthesis and Properties of Poly(isobutyl methacrylate-co-butanediol dimethacrylate-co-methacryl oolyhedral oligomeric silsesquioxane) Nanocomposites. *Journal of Polymer Science Part A: Polymer Chemistry*, 355-372.
4. Utracki, L. (2004). Clay-Containing Polymeric Nanocomposites (Vol. 1, p. 785). Shrewsbury: Rapra Technology.
5. Wu, J., Mather, P. (2009). POSS Polymers: Physical Properties and Biomaterials Applications. *Polymer Reviews*, 25-63.
6. Rizvi, S., Yildirimer, L., Ghaderi, S., Seifalian1, A. (2012). A Novel POSS-Coated Quantum Dot for Biological Application. *International Journal of Nanomedicine*, 7, 3915–3927.
7. Fillion, T., Xu, J., Prasad, M., Song, J. (2011). In Vivo Tissue Responses to Thermal-Responsive Shape Memory Polymer Nanocomposites. *Biomaterials*, 32(4), 985-991.
8. Raghunath, Joanne, George Georgiou, and David Armitage. Degradation Studies on Biodegradable Nanocomposite Based on Polycaprolactone/polycarbonate (80:20%) Polyhedral Oligomeric Silsesquioxane. *Biomaterials & Tissue Engineering*. Wiley InterScience, 4 Sept. 2008.

9. Kannan, R., Salacinski, H., Butler, P., Seifalian, A. (2005). Polyhedral Oligomeric Silsesquioxane Nanocomposites: The Next Generation Material for Biomedical Applications. *Accounts of Chemical Research*, 879-884.
10. Kannan, R., Salacinski, H., Edirisinghe, M., Hamilton, G., Seifalian, A. (2006). Polyhedral Oligomeric Silsesquioxane–Polyurethane Nanocomposite Microvessels for an Artificial Capillary Bed. *Biomaterials*, 27, 4618-4626.
11. Temenoff, J., Kasper, F., Mikos, A. (2007). Fumarate-based Macromers as Scaffolds for Tissue Engineering Applications. *Topics in Tissue Engineering*, 3.
12. Sheikh, F A., Nasser A. Barakat, B.S Kim, Santosh Aryal, Myung-Seob Khil, and Hak-Yong Kim. Self-assembled Amphiphilic Polyhedral Oligosilsesquioxane (POSS) Grafted Poly(vinyl alcohol) (PVA) Nanoparticles. *Materials Science and Engineering: C* 29.3 (2009): 869-76.
13. Gu, X., Wu, J., Mather, P. (2011). Polyhedral Oligomeric Silsesquioxane (POSS) Suppresses Enzymatic Degradation of PCL-Based Polyurethanes. *Biomacromolecules*, 3066-3077.
14. Wang, W., Guo, Y., Otaigbe, J. (2009). The Synthesis, Characterization and Biocompatibility of Poly(ester urethane)/Polyhedral Oligomeric Silsesquioxane Nanocomposites. *Polymer*, 5749-5757.
15. Feher, F., Budzichowski, T. (1991). Heterosilsesquioxanes: Synthesis and characterization of Group 15 containing polyhedral oligosilsesquioxanes. *Organometallics*, 812-815.
16. Pielichowski, K., Njuguna, J. (2005). Thermal degradation of polymeric materials. Shawbury: Rapra Technology.

17. Janowski, B., Pielichowski, K. (2008). Thermo (Oxidative) Stability of Novel Polyurethane/POSS nanohybrid Elastomers. *Thermochemica Acta*, 51-53.
18. Kopesky, E., Haddad, T., Cohen, R., Mckinley, G. (2008). Thermomechanical Properties of Poly(methyl methacrylate)s Containing Tethered and Untethered Polyhedral Oligomeric Silsesquioxanes. *Macromolecules*, 8951-8951.
19. Kopesky, E., Mckinley, G., Cohen, R. (2006). Toughened Poly(methyl methacrylate) Nanocomposites by Incorporating Polyhedral Oligomeric Silsesquioxanes. *Polymer*, 47(1), 299-309.
20. Li, G., Wang, L., Toghiani, H., Daulton, T., Koyama, K., Pittman, C. (2001). Viscoelastic and Mechanical Properties of Epoxy/Multifunctional Polyhedral Oligomeric Silsesquioxane Nanocomposites and Epoxy/Ladderlike Polyphenylsilsesquioxane Blends. *Macromolecules*, 34(25), 8686-8693.
21. Kannan, R, Y., Henryk J. Salacinski, Marianne Odlyha, Peter E. Butler, Alexander M. Seifalian. (2006). The Degradative Resistance of Polyhedral Oligomeric Silsesquioxane Nanocore Integrated Polyurethanes: An In Vitro Study. *Biomaterials* 27.9 1971-979.
22. Schwab, J. J. Lichtenhan, J. D. (1998), Polyhedral oligomeric silsesquioxane(POSS)-based polymers. *Applied Organometallic Chemistry*, 12: 707–713.
23. Wu, J., Haddad, T., Kim, G., Mather, P. (2007). Rheological Behavior of Entangled Polystyrene–Polyhedral Oligosilsesquioxane (POSS) Copolymers. *Macromolecules*, 544-554.
24. Constable, G., Lesser, A., Coughlin, E. (2001). Morphological and Mechanical Evaluation of Hybrid Organic–Inorganic Thermoset Copolymers of Dicyclopentadiene and Mono- or Tris (norbornenyl)-Substituted Polyhedral Oligomeric Silsesquioxanes. *Macromolecules*, 1276-1282.

25. Ayandele, E., Sarkar, B., Alexandridis, P. (2012). Polyhedral Oligomeric Silsesquioxane (POSS)-Containing Polymer Nanocomposites. *Nanomaterials*, 2, 445-475.
26. Guizhi, L., Wang, L., Ni, H., Pittman, C. (2001). Polyhedral Oligomeric Silsesquioxane (POSS) Polymers and Copolymers: A Review. *Journal of Inorganic and Organometallic Polymers*, 11(3), 123-154.
27. Kopesky, E., Haddad, T., Cohen, R., McKinley, G. (2005). Thermomechanical Properties Of Polyhedral Oligomeric Silsequioxane- Poly(Methyl Methacrylate) Nanocomposites. *Macromolecules*, 37(24), 8992-9004.
28. Zhao, Y., Schiraldi, D. (2005). Thermal and mechanical properties of polyhedral oligomeric silsesquioxane (POSS)/polycarbonate composites. *Polymer*, 46(25), 11640-11647.
29. Fu, J., Shi, L., Chen, Y., Yuan, S., Wu, J., Liang, X., Zhong, Q. (2008). Epoxy nanocomposites containing mercaptopropyl polyhedral oligomeric silsesquioxane: Morphology, Thermal Properties, and Toughening Mechanism. *Journal of Applied Polymer Science*, 340-349.
30. Kuo, S., Chang, F. (2011). POSS Related Polymer Nanocomposites. *Progress in Polymer Science*, 36(12), 1649-1696.
31. Polymers and Copolymers Containing Covalently Bonded Polyhedral Oligomeric Silsesquioxanes Moieties. (2010). *Advances in Silicon Science*, 3, 167-207.
32. Hato, M., Ray, S., Luyt, A. (2008). Nanocomposites Based on Polyethylene and Polyhedral Oligomeric Silsesquioxanes, 1 - Microstructure, Thermal and Thermomechanical Properties. *Macromolecular Materials and Engineering*, 293, 752-762.
33. Lee, B., Roy, S., Sadhan, J. (2010). Nanoscale Structure in Polymers II: Polymer Nanocomposites. Nanoscale Dispersion of POSS in PP Assisted by Sorbitol Nucleating Agents.

34. Mather, R. (2006). Medical polymers 2006: Cologne, Germany, 6 - 7 June 2006; [5th International Conference Focusing on Polymers Used in the Medical Industry; conference proceedings]. Shawbury, Shrewsbury: Rapra Technology.
35. Pistor, V., Conto, D., Ornaghi, F., Zattera, A. (2012). Microstructure and Crystallization Kinetics of Polyurethane Thermoplastics Containing Trisilanol Isobutyl POSS. *Journal of Nanomaterials*, 1-8.
36. Wu, J., Ge, Q., Burke, K., Mather, P. (2005). Crystallization of POSS in a PEG Based Multiblock Polyurethane: Toward a Hybrid Hydrogel. *MRS Proceedings*, 487.
37. Mukhopadhyay, S. (2012). Nanoparticles and Polymer Nanocomposites. In *Nanoscale multifunctional materials science and applications* (p. 108). Hoboken, N.J.: Wiley.
38. Zhou, Z., Cui, L., Zhang, Y., Zhang, Y., Yin, N. (2008). Isothermal Crystallization Kinetics of Polypropylene/POSS Composites. *Journal of Polymer Science Part B: Polymer Physics*, 46, 1762-1772.
39. Qiu, Z., Pan, H. (2009). Preparation, crystallization And Hydrolytic Degradation of Biodegradable poly(L-lactide)/Polyhedral Oligomeric Silsesquioxanes Nanocomposite. *Composites Science and Technology*, 70, 1089-1094.
40. Carvalho, H., Suzana, A., Santilli, C., Pulcinelli, S. (2014). Structure and thermal behavior of PMMA-polysilsesquioxane organic-inorganic hybrids. *Polymer Degradation and Stability*, 104, 112-119.
41. Choi, J., Yee, A., Laine, R. (2003). Organic/Inorganic Hybrid Composites from Cubic Silsesquioxanes. Epoxy Resins of Octa(dimethylsiloxyethylcyclohexylepoxide) Silsesquioxane. *Macromolecules*, 5666-5682.

42. Jung, C., Hwang, I., Choi, J. (2014). Preparation of Flexible PLA/PEG-POSS Nanocomposites by Melt Blending and Radiation Crosslinking. 23-28.
43. Kumar, A., Depan, D., Tomer, N., Singh, R. (2009). Nanoscale Particles for Polymer Degradation and Stabilization—Trends and Future Perspectives. *Progress in Polymer Science*, 34, 479-515.
44. Fina, A., Tabuani, D., Carniato, F., Frache, A., Boccaleri, E., Camino, G. (2005). Polyhedral oligomeric silsesquioxanes (POSS) Thermal Degradation. *Thermochimica Acta*, 440, 36-42.
45. Kumar, S., Butola, B., Joshi, M. (2012). POSS/Polypropylene Hybrid Nanocomposite Monofilaments by Reactive Extrusion. *Fibers and Polymers*, 14, 428-435.
46. Lewicki, J., Pielichowski, K., Jancia, M., Hebda, E., Albo, R., Maxwell, R. (2014). Degradative and Morphological Characterization of POSS Modified Nanohybrid Polyurethane Elastomers. *Polymer Degradation and Stability*, (104), 50-56.
47. Liu, Y., Huang, Y., Liu, L. (2007). Thermal Stability of POSS/Methylsilicone Nanocomposites. *Composites Science and Technology*, 67(13), 2864-2876.
48. Liu, Y., Huang, Y., Liu, L. (2008). Influence of Methacryl Polyhedral Oligomeric Silsesquioxane on the Thermal and Mechanical Properties of Methylsilicone Resin. *Journal of Applied Polymer Science*, 2989-2995.
49. Fina, A., Tabuani, D., Frache, A., Camino, G. (2005). Polypropylene–polyhedral oligomeric silsesquioxanes (POSS) Nanocomposites. *Polymer*, 46, 7855-7866
50. Kiliaris, P., Papaspyrides, C. (2010). Polymer/Layered Silicate (Clay) Nanocomposites: An Overview of Flame Retardancy. *Progress in Polymer Science*, 35, 902-958.

51. Pavlidou, S., Papaspyrides, C. (2008). A review On Polymer–Layered Silicate Nanocomposites. *Progress in Polymer Science*, 33, 1119-1198.
52. Wilkie, C. (2010). *Fire retardancy of polymeric materials* (2nd ed., p. 1064). Boca Raton: CRC Press.
53. Zhang, W., Li, X., Guo, X., Yang, R. (2010). Mechanical and Thermal Properties And Flame Retardancy of Phosphorus-containing polyhedral oligomeric silsesquioxane (DOPO-POSS)/Polycarbonate Composites. *Polymer Degradation and Stability*, 95, 2541-2546.
54. Fox, D., Novy, M., Brown, K., Harris, R. (2014). Flame Retarded Poly(lactic acid) Using POSS-Modified Cellulose. 2. Effects of Intumescent Flame Retardant Formulations on Polymer Degradation and Composite Physical Properties. 106, 54-62.
55. Kopesky, E., Boyes, S., Treat N., Cohen, R., Mckinley, G. (2008). Thermorheological Properties Near the Glass Transition of Oligomeric Poly(methyl methacrylate) Blended with Acrylic Polyhedral Oligomeric Silsesquioxane Nanocages. *Rheologica Acta*, 45(6), 971-981.
56. Lewicki, J., Pielichowski, K., Jancia, M., Hebda, E., Albo, R., Maxwell, R. (2014). Degradative And Morphological Characterization Of POSS Modified Nanohybrid Polyurethane Elastomers. *Polymer Degradation and Stability*, (104), 50-56.
57. Liu, Y., Fangchiang, M. (2009). Polyhedral oligomeric silsesquioxane Nanocomposites Exhibiting Ultra-Low Dielectric Constants through POSS Orientation into Lamellar Structures. *Journal of Materials Chemistry*, 3643-3643.
58. Lopes, G., Junges, J., Fiorio, R., Zeni, M., Zattera, A. (2011). Thermoplastic Polyurethane Synthesis Using POSS as A Chain Modifier. *Materials Research*, 698-704.

59. Xu, H., Kuo, S., Lee, J., Chang, F. (2002). Preparations, Thermal Properties, and Tg Increase Mechanism of Inorganic/Organic Hybrid Polymers Based on Polyhedral Oligomeric Silsesquioxanes. *Macromolecules*, 8788–8793.
60. Zou, J. (2011). Poly(L-lactide) nanocomposites containing octaglycidylether polyhedral oligomeric silsesquioxane: Preparation, structure and properties. *Express Polymer Letters*,5(8), 662-673.
61. Alves, F., Scholder, P., Nischang, I. (2013). Conceptual Design of Large Surface Area Porous Polymeric Hybrid Media Based on Polyhedral Oligomeric Silsesquioxane Precursors: Preparation, Tailoring of Porous Properties, and Internal Surface Functionalization. *ACS Applied Materials & Interfaces*, 5, 2517-2526.
62. Morrison, J., Love, C., Manson, B., Shannon, I., Morris, R. (2002). Synthesis of Functionalised Porous Network Silsesquioxane Polymers. *Journal of Materials Chemistry*, 3208-3212.
63. Shi, X., Sitharaman, B., Pham, Q., Liang, F., Wu, K., Billups, W., Mikos, A. (2007). Fabrication of Porous Ultra-Short Single-Walled Carbon Nanotube Nanocomposite Scaffolds for Bone Tissue Engineering. *Biomaterials*, 28(28), 4078-4090.
64. Wei, Z., Luo, X., Zhang, L., Luo, M. (2014). POSS-Based Hybrid Porous Materials with Exceptional Hydrogen Uptake at Low Pressure. *Microporous and Mesoporous Materials*,193, 35-39.
65. Alves, F., Scholder, P., Nischang, I. (2013). Conceptual Design of Large Surface Area Porous Polymeric Hybrid Media Based on Polyhedral Oligomeric Silsesquioxane Precursors: Preparation, Tailoring of Porous Properties, and Internal Surface Functionalization. *ACS Applied Materials & Interfaces*, 5(7), 2517-2526.

66. Alves, F., Nischang, I. (2013). Tailor-Made Hybrid Organic-Inorganic Porous Materials Based on Polyhedral Oligomeric Silsesquioxanes (POSS) by the Step-Growth Mechanism of Thiol-Ene “Click” Chemistry. *Chemistry - A European Journal*, 19(51), 17310-17313.
67. Wang, K., Cai, L., Wang, S. (2011). Methacryl-Polyhedral Oligomeric Silsesquioxane as a Crosslinker For Expediting Photo-crosslinking of Poly(propylene fumarate): Material Properties and Bone Cell Behavior. *Polymer*, 52(13), 2827-2839.
68. Cai, L., Foster, C., Liu, X., Wang, S. (2014). Enhanced Bone Cell Functions on Poly(ϵ -caprolactone) Triacrylate Networks Grafted with Polyhedral Oligomeric Silsesquioxane Nanocages. *Polymer*, 55, 3836-3845.
69. Kotela, I., Podporska, J., Soltysiak, E., Konsztowicz, K., Blazewicz, M. (2009). Polymer Nanocomposites for Bone Tissue Substitutes. *Ceramics International*, 35, 2475-2480.
70. Murugan, R., Ramakrishna, S. (2005). Development of nanocomposites for bone grafting. *Composites Science and Technology*, 2385-2406.
71. Mirmohammadi, S., Imani, M., Uyama, H., Atai, M. (2013). In Situ Photocrosslinkable Nanohybrids Based on Poly(ϵ -caprolactone fumarate)/Polyhedral Oligomeric Silsesquioxane: Synthesis and Characterization. *Journal of Polymer Research*, 20, 297-297.
72. Blackmore, M., Goswami, T., Chancey, C. (2012). Cervical Spinal Injuries and Risk Assessment. In *Injury and Skeletal Biomechanics*. Intech
73. Engstrand, J., López, A., Engqvist, H., Persson, C. (2012). Polyhedral oligomeric silsesquioxane (POSS)–Poly(ethylene glycol) (PEG) Hybrids As Injectable Biomaterials. *Biomedical Materials*, 3, 035013-035013.

74. Lee, K W., Wang, S., Yaszemski, M., Lu, L. (2008). Physical Properties and Cellular Responses to Crosslinkable Poly(propylene fumarate)/Hydroxyapatite Nanocomposites. *Biomaterials*, 29(19), 2839-2848.
75. Cai, L, Chen, J, A.J. Rondinone, S, Wang. Injectable and Biodegradable Nanohybrid Polymers with Simultaneously Enhanced Stiffness and Toughness for Bone Repair. *Advanced Functional Materials* 22.15 (2012): 3181-190.
76. Armentano, I., Dottori, M., Fortunati, E., Mattioli, S., Kenny, J. (2010). Biodegradable Polymer Matrix Nanocomposites for Tissue Engineering: A Review. *Polymer Degradation and Stability*, 95, 2126-2146.
77. Hatiwala, C., Peyton, S., Metzke, M., Putnam, A. (2007). The Regulation of Osteogenesis by ECM Rigidity in MC3T3-E1 Cells Requires MAPK Activation. *Journal of Cellular Physiology*, 661-672.
78. Kyu, K., Lee, K., Kim, I. (2013). Osteoblastic Cells Culture on Electrospun Poly(ϵ -caprolactone) Scaffolds Incorporating Amphiphilic PEG-POSS Telechelic. *J. Mater Sci: Mater Med*, 24, 2029-2036.
79. Mittal, V. (2013). POSS-Containing Nanocomposite Polymer Coatings. In *Polymer Nanocomposite Coatings*. CRC Press.
80. Molecular Dynamics Simulation of Organiceinorganic Copolymers Based On Methacryl-POSS and Methyl Methacrylate. (2006). *Polymer*, 47, 8219-8227.
81. Shao, Y., Aizhao, P., Ling, H. (2014). POSS End-capped Diblock Copolymers: Synthesis, Micelle Self-assembly and Properties. *Journal of Colloid and Interface Science*, 425, 5-11.

82. Tan, A., Goh, D., Farhatnia, Y., G, N., Lim, J., Teoh, S., Egles, C. (2013). An Anti-CD34 Antibody-Functionalized Clinical-Grade POSS-PCU Nanocomposite Polymer for Cardiovascular Stent Coating Applications: A Preliminary Assessment of Endothelial Progenitor Cell Capture and Hemocompatibility. PLoS ONE, E77112-E77112.
83. Seifalian, Alexander M., Tan, Aaron. Surface Modification Of A Polyhedral Oligomeric Silsesquioxane Poly(carbonate-urea) Urethane (POSS-PCU) Nanocomposite Polymer as a Stent Coating for Enhanced Capture of Endothelial Progenitor Cells. Biointerphases: 23. Biointerphases. Web. 27 Apr. 2014.
84. Solouk, A., Cousins, B., Mirzadeh, H., Seifalian, A. (2014). Biomimetic Modified Clinical-Grade POSS-PCU Nanocomposite Polymer for Bypass Graft Applications: a Preliminary Assessment of Endothelial Cell Adhesion and Haemocompatibility. Materials Science and Engineering C, 46, 400-408.
85. Kannan, R., Salacinski, H., Groot, J., Clatworthy, I., Bozec, L., Horton, M., Seifalian, A. (2005). The Antithrombogenic Potential of a Polyhedral Oligomeric Silsesquioxane (POSS) Nanocomposite. Biomacromolecules, 7(1), 215-223.
86. Kidane, A., Burriesci, G., Edirisinghe, M., Ghanbari, H., Bonhoeffer, P., Seifalian, A. (2009). A Novel Nanocomposite Polymer for Development of Synthetic Heart Valve Leaflets. Acta Biomaterialia, 5(7), 2409-2417.
87. Hong, S. D., J. Chung, and J.H. Lee. A Biocompatibility Study of A Reinforced Acrylic-Based Hybrid Denture Composite Resin with Polyhedraloligosilsesquioxane. Journal of Oral Rehabilitation 34: 389-395.

88. Li, L., Pan, H., Tao, J., Xu, X., Mao, C., Gu, X., Tang, R. (2008). Repair of Enamel by Using Hydroxyapatite Nanoparticles as the Building Blocks. *Journal of Materials Chemistry*, 4079-4079.
89. Fong, H., Dickens, S., Flaim, G. (2004). Evaluation of Dental Restorative Composites Containing Polyhedral Oligomeric Silsesquioxane Methacrylate. *Dental Materials*, 21, 520-529.
90. Gao, F., Tong, Y., Schricker, S., Culbertson, B. (2001). Evaluation Of Neat Resins Based On Methacrylates Modified With Methacryl-POSS, as Potential Organic-Inorganic Hybrids for Formulating Dental Restoratives. *Polymers for Advanced Technologies*, 12(6), 355-360.
91. Wu, X., Sun, Y., Xie, W., Liu, Y., Song, X. (2010). Development of Novel Dental Nanocomposites Reinforced With Polyhedral Oligomeric Silsesquioxane (POSS). *Dental Materials*, 26(5), 456-462.
92. Kenig, S., Y. Maoz, and B. Zalsman. The Effect of Grafted Caged Silica (Polyhedral Oligomeric Silsesquioxanes) on the Properties of Dental Composites and Adhesives. *Journal of Adhesion Science and Technology* 20:1401-1412.
93. Lungu, A., Florea, N., Voicu, G., Iovu, H. (2011). Comparison between Octa - Or Monofunctional POSS Interactions with Dimethacrylate Monomers. *Bulletin Series B*, 73(3), 1454-2331.
94. Wang, W., Sun, X., Huang, L., Gao, Y., Ban, J., Shen, L., Chen, J. (2014). Structure–Property Relationships in Hybrid Dental Nanocomposite Resins Containing Monofunctional and Multifunctional Polyhedral Oligomeric Silsesquioxanes. *International Journal of Nanomedicine*. 9, 841-852.

95. Wu, X., Xie, W., Sun, Y., Sun, S. (2009). Mechanical Properties of Dental Nanocomposites Reinforced with Polyhedral Oligomeric Silsesquioxane(POSS). *Advanced Materials Research*, 345-348.
96. Mccusker, C., Carroll, J., Rotello, V. (2004). Cationic polyhedral oligomeric silsesquioxane (POSS) Units as Carriers for Drug Delivery Processes. *Chemical Communications*, 996-996.
97. Qiongyu, G. (2010). POSS-Based Biodegradable Polymers for Stent Applications: Electroprocessing, Characterization and Controlled Drug Release. *Macromolecular Science and Engineering*.
98. Dvornic, P. (2009). *Silicon-Containing Dendritic Polymers* (p. 428). Dordrecht: Springer.
99. Naka, K., Shinke, R., Yamada, M., Belkada, F., Aijo, Y., Irie, Y., Sakurai, S. (2013). Synthesis of Imidazolium Salt-Terminated Poly(amidoamine)-Typed POSS-Core Dendrimers and Their Solution and Bulk Properties. *Polymer Journal*, 46, 42-51.
100. Tanaka, K., Chujo, Y. (2012). Unique Properties of Amphiphilic POSS and Their Applications. *Polymer Journal*, 247-254.
101. Yao M, Wang J, Gu X, Feng L. (2012) Synthesis and Application of Dendrimers Based on Polyhedral Oligomeric Silsesquioxanes *Progress in Chemistry*, 24(0203): 405-413
102. Kim, K. (2011). Self-Assembled Core-Shell Poly(ethylene glycol)-POSS Nanocarriers for Drug Delivery. *Journal of Biomaterials and Nanobiotechnology*, 201-206.
103. Nair, B., Vaikkath, D., Nair, P. (2013). Polyhedral Oligomeric Silsesquioxane (POSS)-F68 Hybrid Vesicles for Folate Receptor Targeted Anti-Cancer Drug Delivery. *Langmuir*, 340-347.

104. Aziz, A. (2005). Polyhedral Oligomeric Silsesquioxane (POSS) Polymers, Copolymers, and Resin Nanocomposites. In *Macromolecules Containing Metal and Metal-Like Elements* (Vol.4). Hoboken: Wiley-Interscience
105. Liu, Y., Tseng, M., Fangchiang, M. (2008). Polymerization and Nanocomposites Properties of Multifunctional Methylmethacrylate POSS. *Journal of Polymer Science Part A: Polymer Chemistry*, 5157-5166.

**Chapter III. Experimental Procedures of Polymer Synthesis, Fabrication,
Characterization, and Cell Studies**

3.1 Introduction

In this study, I synthesized neat PCLF along with a novel series of PCLF-*co*-POSS nanohybrid polymeric networks with varied weight fractions of POSS ($\phi_{\text{POSS}} = 5\%$, 10% , and 20%), respectively. Neat PCLF and PCLF-*co*-POSS nanohybrids were crosslinked into networks with properties exhibiting low swell ratios and high gel fractions along with tunable mechanical properties, controlled by manipulating crystallinity and crosslinking density. An advantage of these polymeric networks is that they are biodegradable, injectable, and can be molded into various shapes and cured via UV photo-initiation for TE applications. The novel series of PCLF-*co*-POSS nanohybrid networks and pure PCLF were synthesized, characterized, and examined for their TE viability, by analyzing cell-cell and cell-material interactions. The goal of this process was to emphasize the ability of neat PCLF and PCLF-*co*-POSS to enhance adhesion, proliferation, and growth of mouse pre-osteoblastic MC3T3-E1 cells and primary rat aortic smooth muscle cells (SMCs) for bone and cardiovascular regeneration. To advance this study, 20% hydroxyapatite (HA) was integrated into the $\phi_{\text{POSS}} = 20\%$ polymer network to form PCLF-*co*-POSS/HA; a crosslinked nanocomposite with smooth surfaces and surfaces containing microgrooves.

3.2 Synthesis and Characterization of PCLF and PCLF-*co*-POSS

3.2.1 PCLF Synthesis

PCL diols [α,ω -dihydroxy poly(ϵ -caprolactone)] with a nominal molecular weight of 1250 gmol^{-1} was purchased from Sigma-Aldrich (Milwaukee, WI) and used for the synthesis of poly(ϵ -caprolactone fumarate). PCL diol was dried under vacuum at $50 \text{ }^\circ\text{C}$ for at least 12 h prior to the reaction. All other chemicals in this study were purchased from Sigma-Aldrich unless

otherwise noted. Methylene chloride was dried and distilled over calcium hydride (CaH₂) before the reaction. Fumaryl chloride was purified via distillation at 161 °C. Ground potassium carbonate (K₂CO₃) was dried at 100 °C for at least 12 h and then cooled down at vacuum conditions. PCLF was synthesized via polycondensation of PCL with fumaryl chloride in methylene chloride with K₂CO₃ as a proton scavenger [1,2]. PCL diol, fumaryl chloride, and K₂CO₃ were measured out in a molar ratio of 1:0.95:1.2. The PCL diol was dissolved in methylene chloride (1:2v/v) and placed into a 1L three-neck flask along with ground K₂CO₃. The mixture was stirred with a magnetic stir bar to form a slurry, to which fumaryl chloride was then dissolved in methylene chloride (1:1v/v) and added drop wise to the slurry. This reaction occurred at 50 °C under nitrogen for 12 h.

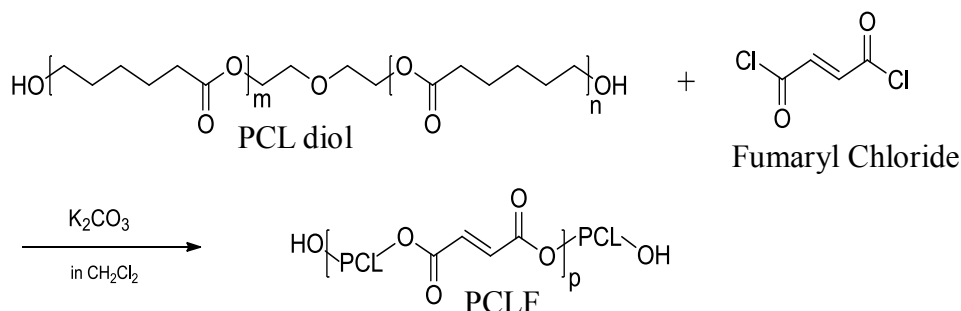


Figure 3.1 Synthesis of PCLF

3.2.2 PCLF-co-POSS Synthesis

PCLF-co-POSS was synthesized via polycondensation of PCL diol and POSS with fumaryl chloride in methylene chloride with K₂CO₃ as a proton scavenger. 1, 2-Propanediol isobutyl POSS purchased from Hybrid Plastics (Hattiesburg, MS) was weighed in varied weight fractions. POSS weight fractions ($\phi_{\text{POSS}} = 5\%$, 10%, and 20%) were dissolved in methylene chloride (1:2 v/v) and placed in a 1L three-neck flask. The mixture was stirred with a magnetic stir bar, to which fumaryl chloride was then dissolved in methylene chloride (1:1v/v) and added

drop wise. This reaction occurred at 50 °C along with dried ground K_2CO_3 under nitrogen for 12 h [3].

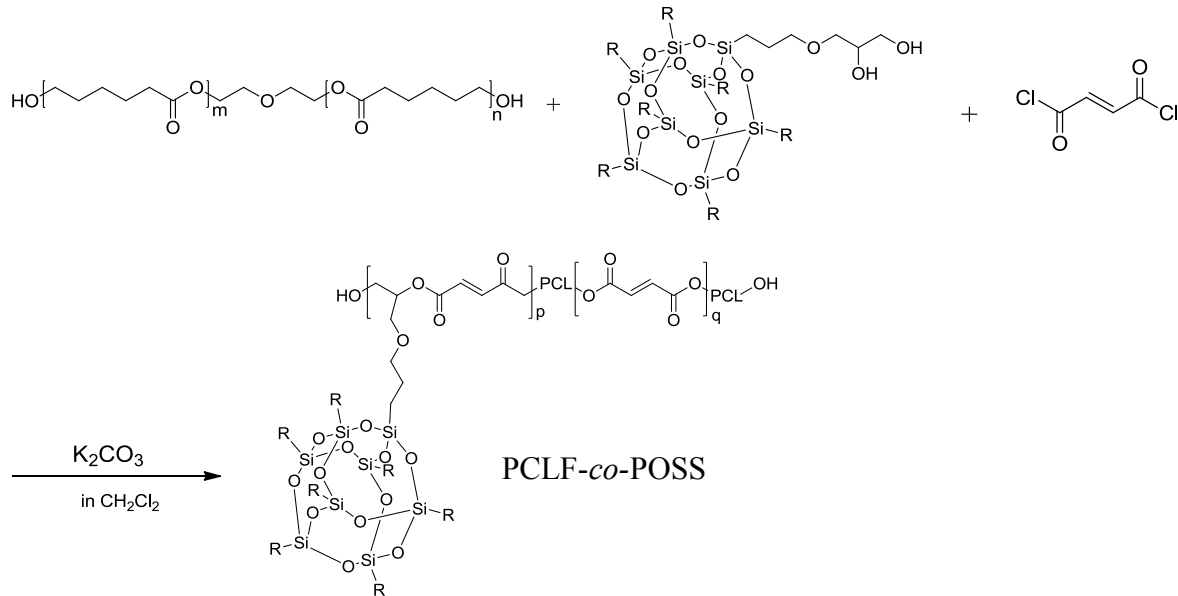


Figure 3.2 Synthesis of PCLF-*co*-POSS

3.2.3 Fabrication of HA-containing PCLF-*co*-POSS

PCLF-*co*-POSS/HA nanocomposites were engineered by incorporating 20% of HA nanoparticles within the PCLF-*co*-POSS ($\phi_{POSS} = 20\%$) network by physical mixing prior to photo-crosslinking.

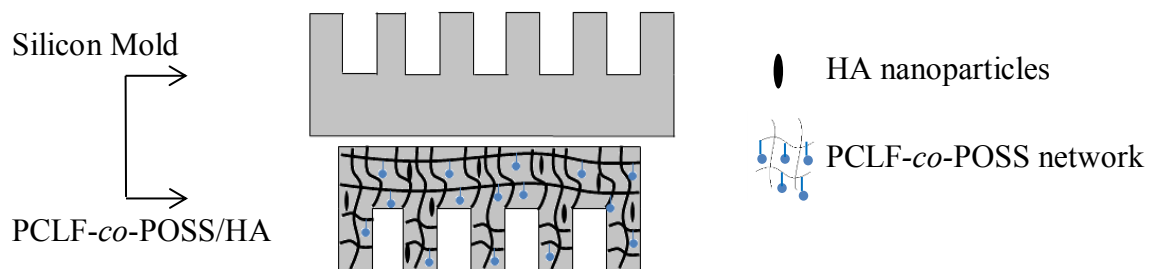


Figure 3.3 Fabrication of Microgrooved PCLF-*co*-POSS/HA

3.2.4 Polymer Purification

After polymerizing for 12 h, the mixture was cooled and placed into centrifuge tubes. The solution was spun down for 12 min at 3000 rpm until the precipitate (K_2CO_3) was removed. The supernatant was then added dropwise to petroleum ether to isolate the polymer. Once isolated, the precipitate was rotary-evaporated then placed under vacuum conditions at 25 °C to remove traces of organic solvent.

3.2.5 Photo-crosslinking PCLF, PCLF-co-POSS, and PCLF-co-POSS/HA

The photo-initiator, phenyl bis(2,4,6-trimethyl benzoyl) phosphine oxide (BAPO, IRGACURE 819, Ciba Specialty Chemicals, Tarrytown, NY) was used as a crosslinking agent. Photo-crosslinking was initiated with a high-intensity long-wave ultraviolet (UV) light (SB-100P, $\lambda=365$ nm, Intensity: $4800 \mu w/cm^2$). In crosslinking, 150 μL of BAPO/ CH_2Cl_2 (300 mg/1.5 mL) solution were mixed with PCLF and PCLF-co-POSS/ CH_2Cl_2 solution (3 g/1 mL) to form a homogenous solution [4-6]. PCLF and PCLF-co-POSS solutions were injected into a mold consisting of two glass plates (2.1mm, thickness) and a Teflon mold to form sheets (10 mm \times 0.5 mm, diameter \times thickness) then subjected to UV light at a distance of ~ 10 cm for 30 min. To form the PCLF-co-POSS/HA with microgrooves, 20% (600 mg) of HA nanoparticles were mixed with $\phi_{POSS} = 20\%$, to which the solution was poured onto a micro-fabricated silicon wafer (5 $\mu m \times 12 \mu m$, groove width \times groove depth) between two glass plates (2.1 mm, thickness) and a silicone spacer (1 mm, thickness). Crosslinked sheets for all samples were removed from the mold then cooled down to room temperature and cut into strips and disks for experiments.

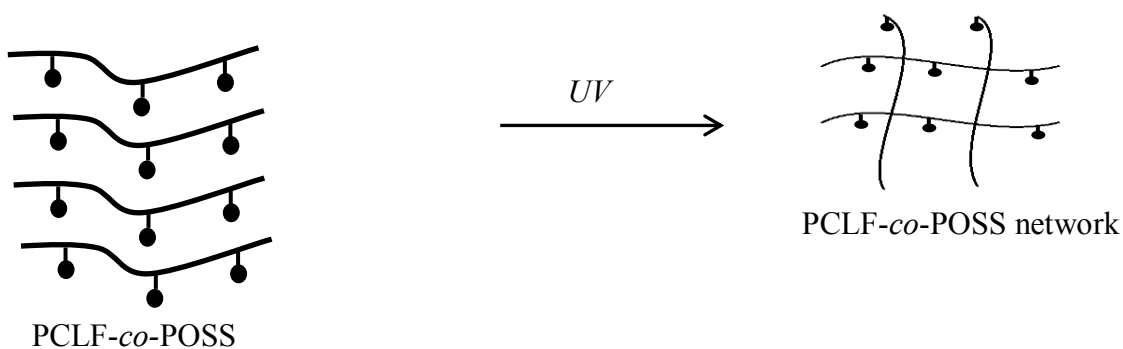


Figure 3.4 Photo-crosslinking of PCLF-*co*-POSS.

3.3 Characterization of uncrosslinked and crosslinked PCLF and PCLF-*co*-POSS

3.3.1 Gel permeation chromatography (GPC)

Gel permeation chromatography (GPC) was performed at room temperature using a GPC system (HLC-83200GPC, TOSOH Biosciences LLC., Tokyo, Japan) with a refractive index indicator to determine the molecular weight and polydispersity index of uncrosslinked PCLF and PCLF-*co*-POSS. Tetrahydrofuran (THF) was the eluent and monodisperse polystyrene samples were used for standard calibration. Cirrus GPC/SEC software (Agilent Technologies, Santa Clara, CA) was used for data processing.

3.3.2 ^1H NMR and FTIR

Chemical structure confirmation was determined by using ^1H Nuclear Magnetic Resonance (^1H NMR) and was carried out with a Varian Mercury 300 spectrometer (Agilent Technologies, Santa Clara, CA) using CDCl_3 solutions containing tetramethylsilane (TMS). Fourier Transform Infrared (FTIR) spectra were gathered on a Perkin Elmer Spectrum Spotlight 300 spectrometer with diamond Attenuated Total Reflectance (ATR).

3.3.3 Gel fraction and swelling ratio

Gel fraction and swelling ratio measurements were performed on PCLF, PCLF-*co*-POSS, and PCLF-*co*-POSS/HA (8 mm × 0.8 mm, diameter × thickness) to determine crosslinking density. The crosslinked disks were then soaked separately in excess CH₂Cl₂ and water for two days then removed and weighed after being blotted quickly. After weighing, the solvent in the disks was evacuated by vacuum and the dry disks were weighed.

3.3.4 Differential scanning calorimetry (DSC)

Differential Scanning Calorimetry (DSC) was used to determine the melting temperature (T_m), crystallization temperature (T_c), and crystallinity (X_c). Samples were implemented using a DSC (TA Q2000, TA Instruments, New Castle, DE) system in a nitrogen atmosphere. To keep a constant thermal history, the uncrosslinked PCLF and PCLF-*co*-POSS, and crosslinked PCLF, PCLF-*co*-POSS, and PCLF-*co*-POSS/HA samples were heated from 25° to 100 °C then cooled to -60 °C at a rate of 10 °C min⁻¹. The subsequent runs were performed at 30 °C and heated to 100 °C at 10 °C min⁻¹ then cooled from 100 ° to -60 °C at the rate of 10 °C min⁻¹. Universal Analysis 2000 supplied by (TA Instruments) was used for data processing.

3.3.5 Thermogravimetric analysis (TGA)

Thermogravimetric analysis (TGA) was used to determine the thermal degradation of uncrosslinked PCLF and PCLF-*co*-POSS, and crosslinked PCLF, PCLF-*co*-POSS, and PCLF-*co*-POSS/HA samples. Samples were implemented using a TGA (TA Q50, TA Instruments, New Castle, DE) thermal analyst system in nitrogen conditions at a heating rate of 20 °C min⁻¹ up to 600 °C. Universal Analysis 2000 was used for data processing.

3.3.6 Dynamic mechanical analysis (DMA)

Dynamic Mechanical Analysis (DMA) was carried out to determine the tensile and modulus properties of crosslinked PCLF, PCLF-*co*-POSS, and PCLF-*co*-POSS/HA specimens. The samples were cut into strips (10 mm × 1.5 mm × 0.5 mm, length x width x thickness) and implemented using a dynamic mechanical analyzer (TA Q800, TA Instruments, New Castle, DE) at 37 °C. Samples were chosen to be elongated up to 200% at a strain rate of 30% min⁻¹. Universal Analysis 2000 was used for data processing.

3.3.7 Water contact angles

Hydrophobicity was determined by measuring water contact angles at 37 °C using a Ramé-Hart NRC C. A. goniometer (Model 100-00-230, Mountain Lakes, NJ). Crosslinked PCLF and PCLF-*co*-POSS disks (8 mm × 0.5 mm, diameter × thickness) were used in the experiment to which 1 μL of distilled water (pH = 7.0) was injected onto the surface of the disks and the measurements were taken after a static time of 30 s. To calculate the contact angle in degrees, a tangent method was used. Three disks were used for four samples to calculate the average and standard deviation.

3.3.8 Surface topography characterization

Surface topography of $\phi_{\text{POSS}} = 20\%$, PCLF-*co*-POSS/HA, and microgrooved PCLF-*co*-POSS/HA were imaged using scanning emission (SEM, Carl Zeiss Auriga, Germany). Samples were sputter-coated with a gold-palladium layer (Emscope SC 500, Elexience) before imaging. SEM images were conducted at an accelerating voltage of 2 kV.

3.4 Cell attachment and proliferation

3.4.1 MC3T3-E1 cells

Mouse MC3T3-E1 pre-osteoblastic cells (CRL-2593, ATCC, Manassas, VA) were used to determine cell attachment, proliferation, mineralization, and gene expression on PCLF, PCLF-*co*-POSS, and PCLF-*co*-POSS/HA substrates. The MC3T3-E1 cells were cultured *in vitro* by using culture medium consisting of Alpha Minimum Essential Medium (α -MEM; Gibco, Grand Island, NY), combined with 10% fetal bovine serum (FBS, Sera-Tech, Germany) and 1% penicillin/streptomycin (Gibco). Culture medium was placed into a polystyrene flask and MC3T3-E1 cells were plated. Prior to seeding, the cell suspension was then incubated in a 5% CO₂, 95% relative humidity incubator at 37 °C. Subcultures of MC3T3-E1 cells were performed at approximately 80% confluency. Trypsin with a concentration of 0.025% was used to detach the cells from the bottom of the polystyrene flask.

3.4.2 Smooth muscle cells

Rat primary SMCs isolated from the aorta were used to examine the ability of PCLF and PCLF-*co*-POSS substrates to influence attachment, proliferation, and gene expression. The SMCs were cultured *in vivo* similarly to the mouse MC3T3-E1 pre-osteoblastic cells as described above; however, α MEM was replaced with Dulbecco's Modified Eagle Medium (DMEM) as a component of the culture medium.

3.4.3 In vitro cell attachment and proliferation

Prior to seeding, PCLF, PCLF-*co*-POSS, and PCLF-*co*-POSS/HA disks (8 mm \times 0.5 mm, diameter \times thickness) were dried in a vacuum, pressed between two glass slides to remove surface inconsistencies, then sterilized in 70% ethanol. The microgrooved PCLF-*co*-POSS/HA

samples were not pressed between two glass slides. After sterilization, PCLF and PCLF-co-POSS disks were separately attached onto 48-well tissue culture polystyrene (TCPS) plates with Silicon-based grease (Dow Corning, Midland, MI) and cleaned with 300 μ L of phosphate buffered saline (PBS, Gibco) prior to seeding. Mouse MC3T3-E1 pre-osteoblastic and rat primary aortic SMCs were trypsinized, centrifuged at 1000 rpm for 2 min, and collected after confluency in the culture flask was achieved. MC3T3-E1 cells and SMCs were then separately seeded onto the polymer substrates at a density of 1.5×10^4 cells/cm². The negative control was the empty TCPS well and the positive control was TCPS seeded with cells. The seeded substrates were then incubated for 4 h to determine cell attachment and 1, 2, 4 days to determine proliferation. A microplate reader at 490 nm (SpectraMax Plus 384, Molecular Devices, Sunnyvale, CA) was used to determine the cell numbers obtained from the adsorption values of the MTS assay, (CellTiter 96 Aqueous One Solution, Promega, Madison, WI) and a standard curve constructed from known cell numbers. Culture medium was removed from the wells containing MC3T3-E1 cell and SMC seeded substrates and the polymer substrates were washed twice with PBS after the cells were cultured in a 5% CO₂ and 95% relative humidity atmosphere at 37 °C for 4 h, 1, 2, 4 days. For fluorescent imaging, the attached cells were fixed in 4% paraformaldehyde (PFA) solution for 10 min. After fixation, the PFA was removed and PBS was used to wash the cells twice. Cells were permeabilised with 0.1% Triton X-100 for 10-20 min. The cytoplasm filaments were stained with rhodamine-phalloidin (RP) and incubated for 1 h at 37°C. After incubating, 4',6-diamidino-2-phenylindole (DAPI) was used to stain the cell nuclei. MC3T3-E1 cell and SMC images were acquired with an Axiovert 25 light microscope (Carl Zeiss, Germany). Proliferation index (PI) was quantified by dividing the cell number at day 4 by

the cell number at day 1. Cell area was determined by using ImageJ software (National Institutes of Health, Bethesda, MD) where averages were taken on 15 non-overlapping cells at day 1.

3.4.4 Focal adhesion characterization

MC3T3-E1 cells and SMCs were cultured on PCLF and PCLF-*co*-POSS disks for 24 h, washed with PBS, fixed in 4% PFA solution, then permeabilised with 0.1% Triton X-100 for 1 h at physiological temperature. Cells were then washed with PBS and incubated in 1% bovine serum albumin (BSA)/PBS for 1 h to reduce background signal. The cells were then treated with monoclonal mouse antibody against vinculin (1:1000 in PBS; Sigma) overnight. Following overnight treatment, cells were washed three times with PBS then cultured in an incubator for 2 h with goat anti-mouse IgG secondary antibody (1:200 in PBS; Sigma). Prior to taking images on a Leica DM6000B fluorescent confocal microscope, the actin filaments of MC3T3-E1 cells were stained with RP for 1 h. The area and density of the focal adhesions were determined by averaging 15 non-overlapping cells by using ImageJ. Further, focal adhesions were characterized on PCLF-*co*-POSS/HA (smooth and microgrooved) disks with MC3T3-E1 cells by using the same protocol described above.

3.5 Cell differentiation

3.5.1 ALP activity and calcium content

After culturing MC3T3-E1 cells on PCLF, PCLF-*co*-POSS, and PCLF-*co*-POSS/HA (smooth and microgrooved) disks for 7 and 14 days, the alkaline phosphatase (ALP) activity and calcium content were determined. Cells were washed with PBS, trypsinized, and centrifuged at 1000 rpm for 4 min. The acquired cell pellet was re-suspended in 1 mL of 0.2% Nonidet P-40

(American Bioanalytical, Natick, MA) and stirred in an ice bath for 2 min. The cell lysate was frozen at 20 °C before determining ALP activity and calcium content. To measure the ALP activity of the cell lysate, a fluorescence-based ALP Detection Kit (St. Louis, MO; Sigma) was used. 20 µL of cell lysate was added into each well of a 96-well plate and incubated at 65 °C for 20 min. After incubating, 20 µL of dilution buffer, 160 µL of fluorescent assay buffer, and 1µL of the 10 mM substrate solution provided in the kit were added into each well followed by 4µL of cell lysate or control enzyme with known concentrations. The absorbance was measured at 340 nm on the microplate reader and the values were quantified using a standard curve constructed with varied amounts of control enzyme. Calcium content was determined by using QuantiChrom calcium assay kit (BioAssay Systems, Hayward, CA). 5 µL of cell lysate was added into each well of a 96-well plate and mixed with 200 µL of working reagent. The samples were incubated at room temperature for 3 min before measuring the optical density at 620 nm on the microplate reader. The absolute calcium content was quantified by using a standard curve with known concentrations [7,8].

3.5.2 MC3T3-E1 Gene Expression

MC3T3-E1 cells were seeded at ~15,000 cells/cm² on crosslinked PCLF, PCLF-co-POSS, and (smooth and microgrooved) PCLF-co-POSS/HA disks, then cultured for two weeks. MC3T3-E1 cells were then trypsinized and total RNA was isolated by using RNeasy Mini Kit (Qiagen, Valencia, CA). mRNA concentrations (ng/µL) were quantified using a Nanodrop 1000 spectrophotometer (Thermo Scientific, Wilmington, DE). After isolating mRNA, cDNA was synthesized by using DyNAmo cDNA synthesis kit (Thermo Scientific). Table 3.1 below shows the oligonucleotide primers (Invitrogen) used for RT and real-time PCR. Osteopontin (OPN) was analyzed for the HA-containing PCLF-co-POSS studies. Real-time PCR reactions were

conducted in 25 μ L of PCR mixture containing each cDNA sample and Power SYBR Green PCR Master Mix (Applied Biosystems, Carlsbad, CA). PCR was carried out on a Peltier Thermo Cycler (PTC-200, MJ Research, Waltham, MA). The PCR amplification protocol was set to thirty cycles of 30 s at 95 °C (denaturation), 30 s at 55 °C (annealing), and 30s at 72 °C (elongation)

Table 3.1 MC3T3-E1 oligonucleotide primer sequences for real-time PCR.

Gene	Primer sequence (5'-3'; F: forward; R: reverse)
Osteocalcin (OCN)	F: CAAGTCCCACACAGCAGCTT R: AAAGCCGAGCTGCCAGAGTT
Osteopontin (OPN)	F: ACACTTTCACCTCCAATCGTCC R: TGCCCTTCCGTTGTTGTCC
ALP	F: GCCCTCTCCAAGACATATA R: CCATGATCACGTCGATATCC
GAPDH	F: ACTTTGTCAAGCTCATTTCC R: TGCAGCGAACTTTATTGATG

3.5.3 SMC Gene Expression

SMCs were seeded at $\sim 15,000$ cells/cm² on crosslinked PCLF and PCLF-co-POSS disks, and cultured for 4 days. Total RNA for SMCs was isolated and quantified by using the protocol described above for MC3T3-E1 cells. Similarly, cDNA was synthesized and real-time PCR was conducted in by using the same experimental procedure for MC3T3-E1 cells. Genes analyzed were calponin, smoothlin, and GAPDH. The oligonucleotide primers (Invitrogen) for RT and real-time PCR are shown in Table 3.2.

Table 3.2 SMC oligonucleotide primers for real-time PCR.

Gene	Primer sequence (5'-3'; F: forward; R: reverse)
Calponin	F: AGTCTACTCTCTTGGCTCTGGCC
	R: CCTGCCTTCTCTCAGCTTCTCAGG
Smoothlin	F: TCGGAGTGCTGGTGAATAC
	R: CCCTGTTTCTCTTCCCTCTGG
GAPDH	F: TCTTCACCACCATGGAGAA
	R: ACTGTGGTCATGAGCCCTT

Refernces

1. Jabbari, E., Wang, S., Lu, L., Gruetzmacher, J. A., Ameenuddin, S., Hefferan, T. E., Yaszemski, M. J. (2005). Synthesis, Material Properties and Biocompatibility of a Novel Self-Crosslinkable Poly(ϵ -caprolactone fumarate) as an Injectable Tissue Engineering Scaffold. *Biomacromolecules*, 6(5), 2503–2511.
2. Cai, L., Chen, J., Rondinone, A. J. Wang, S. (2012), Injectable and Biodegradable Nanohybrid Polymers with Simultaneously Enhanced Stiffness and Toughness for Bone Repair. *Advanced. Functional. Materials*. 22: 3181–3190.
3. Kim, K., Ramasundaram, S., Lee, J. (2008). Synthesis and Characterization of Poly(trimethylene terephthalate) Polyhedral Oligomeric Silsesquioxanes Nanocomposites. *Polymer Composites*, 29(8), 894-901.
4. Wang, S., Yaszemski, M. J., Knight, A. M., Gruetzmacher, J. A., Windebank, A. J., Lu, L. (2009). Photo-crosslinked Poly(ϵ -caprolactone fumarate) Networks for Peripheral Nerve Regeneration: Physical Properties and Preliminary Biological Evaluations. *Acta Biomaterials*, 5(5), 1531–1542.
5. Wang, K., Cai, L., Zhang, L., Dong, J., Wang, S. (2012), Biodegradable Photo-Crosslinked Polymer Substrates with Concentric Microgrooves for Regulating MC3T3-E1 Cell Behavior. *Advanced Healthcare Materials*, 1: 292–301.
6. Wang, K., Cai, L., Wang, S. (2011). Methacryl-Polyhedral Oligomeric Silsesquioxane as a Crosslinker for Expediting Photo-Crosslinking of Poly(propylene fumarate): Material Properties And Bone Cell Behavior. *Polymer*, 52(13), 2827-2839.
7. Isama, K., Tsuchiya, T. (2003). Enhancing Effect of Poly(L-Lactide) on the Differentiation of Mouse Osteoblast-like MC3T3-E1 Cells. *Biomaterials*, 24(19), 3303-3309.

8. Ikarashi, Y., Tsuchiya, T., Nakamura, A. (2000). Effect of Heat Treatment of Poly(L-lactide) on the Response of Osteoblast-like MC3T3-E1 cells. *Biomaterials*, 21(12), 1259-1267.

**Chapter IV. Regulation of Pre-osteoblastic MC3T3-E1 and Smooth Muscle Cells on
Smooth Disks of Photo-crosslinked PCLF and PCLF-co-POSS**

Abstract

Poly(ϵ -caprolactone fumarate) (PCLF) was copolymerized with polyhedral oligomeric silsesquioxane (POSS) with varied weight percentages of POSS ($\phi_{\text{POSS}} = 0\%$, 5%, 10%, and 20%), and photo-crosslinked into polymer substrates. PCLF and PCLF-*co*-POSS ($\phi_{\text{POSS}} = 0\%$, 5%, 10%, and 20%) polymer substrates were characterized for their material properties as well as, their ability to influence mouse pre-osteoblastic MC3T3-E1 cell and rat primary aortic smooth muscle cell (SMC) activity. The increase of (ϕ_{POSS}) within the polymer network showed to increase wettability and significantly improve tensile strength. Further, as (ϕ_{POSS}) was increased, both MC3T3-E1 and SMC attachment, proliferation, and differentiation were improved. Studies suggested that the increase in (ϕ_{POSS}) enhanced material properties and cell favorability for the polymer substrates over neat PCLF.

4.1 Introduction

In this chapter, four different PCLF-*co*-POSS ($\phi_{\text{POSS}} = 0\%$, 5%, 10%, and 20%) injectable, photo-crosslinkable, and degradable nano-hybrid polymer networks were prepared by the methods described above in Chapter III. All of the substrates involved in this study contained smooth surfaces without any further modifications. The structural, physical, mechanical, and thermal properties of all samples were first characterized followed by the analysis of mouse pre-osteoblastic MC3T3-E1 cell and smooth muscle cell (SMC) activity on the substrates. Throughout this study, varied compositions of POSS (ϕ_{POSS}) were used to tailor the properties of the polymer networks to enhance MC3T3-E1 and SMC attachment, proliferation, and differentiation. Both MC3T3-E1 cells and SMCs were analyzed on their ability to attach, proliferate, express genes, and display focal adhesions.

4.2 Results and Discussion

4.3 Structural characterizations

The PCLF and PCLF-*co*-POSS samples were synthesized in the presence of methylene chloride, fumaryl chloride, and K_2CO_3 , and were opaque to white at room temperature when they were semi-crystalline. The weight-average (M_w), number-average (M_n), and polydispersity index (PDI) of PCLF and PCLF-*co*-POSS were determined using GPC (Table 4.1). By increasing ϕ_{POSS} , molecular weight increases, which has an impact on the mechanical, crosslinking, and crystalline properties.

Table 4.1 Molecular Weight Information of PCLF and PCLF-*co*-POSS.

Sample	M_n (gmol ⁻¹)	M_w (gmol ⁻¹)	PDI
PCL diol	1250	2350	1.9
PCLF	3970	5440	1.4
5%	6230	7940	1.3
10%	6890	10600	1.5
20%	7080	10100	1.4

To confirm the chemical structures of PCLF and PCLF-*co*-POSS, ^1H NMR and FTIR spectra in Figures 4.1 and 4.2 were used, respectively. The FTIR spectra transmission peaks at 2940 and 2840 cm^{-1} was due to the methylene (CH_2) groups in PCLF. The carbonyl ($\text{C}=\text{O}$), which is a common characteristic of PCLF, can be seen from the strong peaks at 1730 cm^{-1} . The prominence of the carbonyl peak is due to PCL and the contribution of fumaryl chloride. Peaks at 1260 and 1300 cm^{-1} were due to C-H rocking vibration of the fumarate group. Fumarate and C=C peaks can be seen at 1160 cm^{-1} . Finally, the strong peaks at 1150 cm^{-1} represent the Si-O-Si bonds in POSS. In the ^1H NMR spectra shown in Figure 4.1, all of the chemical shifts were well assigned to the protons in the polymer structures. The peak at 6.8 ppm is the characteristic of fumarate in the samples. Because the chemical shift of fumarate protons was below 7 ppm, the fumarate group in the copolymer is in the *cis*-configuration [1]. Peaks labeled 1, 2, and 3 represent the presence of POSS in the copolymer. It can be observed that a more prominent peak in POSS occurs with an increase in POSS loading.

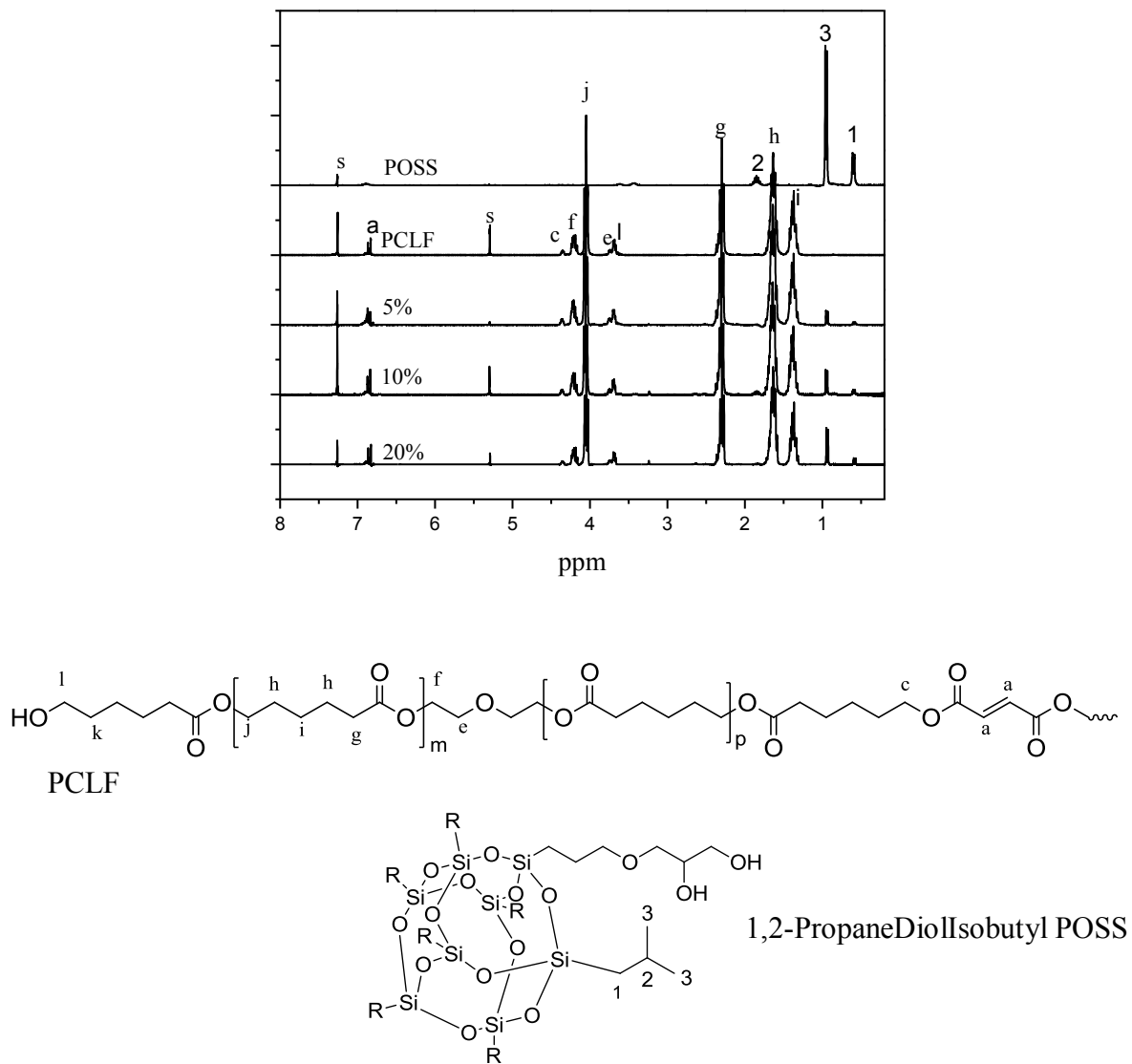


Figure 4.1 ^1H NMR spectra of PCLF, PCLF-co-POSS, and POSS. S = solvent.

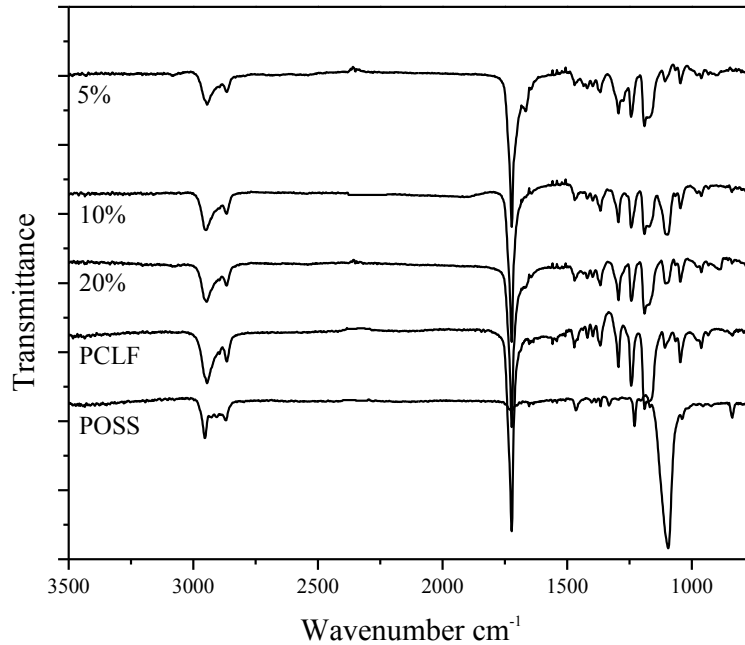


Figure 4.2 FTIR spectra of PCLF, PCLF-*co*-POSS, and POSS.

4.4 Photo-crosslinking

To determine the degree of crosslinking, gel fraction and swelling ratio experiments were performed on all samples (Figure 4.3). The gel fraction of a polymer indicates the integrity of the crosslinked sample whereas; the swelling ratio is a low-cost and effective technique to characterize polymer networks [2,3]. Higher weight percentages of POSS ($\phi_{\text{POSS}} = 10\%$ and 20%) significantly enhanced crosslinking density over PCLF-*co*-POSS ($\phi_{\text{POSS}} = 5\%$) and neat PCLF (Table 4.2). The high crosslinking density was characterized by a high gel fraction and a low swelling ratio. The gel fraction of the PCLF-*co*-POSS ($\phi_{\text{POSS}} = 20\%$) sample had an 8% higher gel fraction and a 26% lower swelling ratio than PCLF alone. Based upon the weight of the original (W_0), dry (W_d), and fully swollen (W_s) PCLF and PCLF-*co*-POSS disks, swelling ratios

and gel fractions were calculated by the equations $\Gamma_o = W_d/W_o \times 100\%$ and $S_o = (W_s - W_d)/W_d \times 100\%$, respectively.

Table 4.2 Gel Fraction and Swelling Ratio values.

Sample	Gel Fraction (%)	Swelling Ratio
PCLF	85 ± 0.2	6.7 ± 1
5%	88 ± 0.4	6.6 ± 1
10%	89 ± 0.2	5.7 ± 1
20%	92 ± 0.1	5.3 ± 1

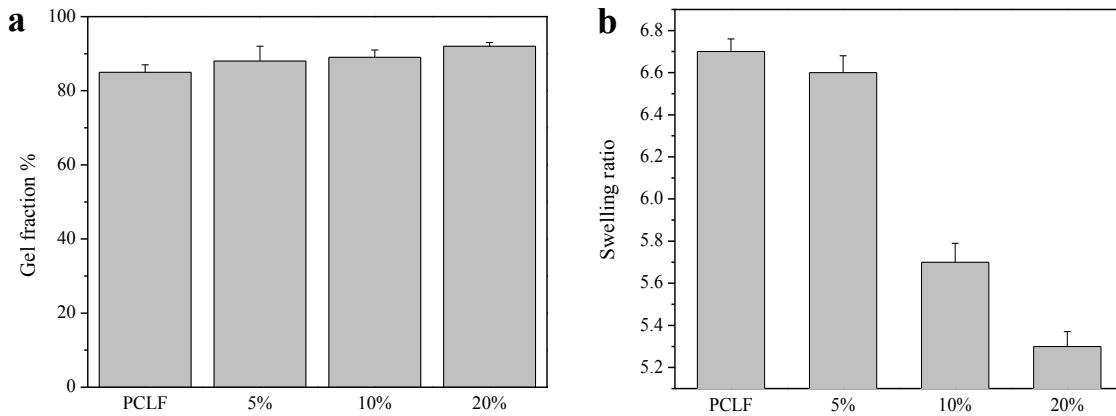


Figure 4.3 (a) Gel fractions and (b) swelling ratios of PCLF and PCLF-*co*-POSS in CH_2Cl_2 .

4.5 Water contact angle

Surface energy and wettability of crosslinked PCLF and PCLF-*co*-POSS was determined by performing water contact angle experiments and measurements. The water contact angle experiment was carried out under physiological conditions (37 °C). Crosslinked PCLF and PCLF-*co*-POSS ($\phi_{\text{POSS}} = 5\%$, 10%, and 20%) samples showed water contact angles of $70 \pm 4^\circ$, $68 \pm 1^\circ$, $67 \pm 2^\circ$, and $65 \pm 4^\circ$, respectively. The higher water contact angle on PCLF can be described by its more hydrophobic nature [4].

4.6 Mechanical properties

The modulus of elasticity (E) measurement for crosslinked PCLF, and PCLF-*co*-POSS was carried out at physiological temperature (37 °C). As evident from Figure 4.4, the covalent incorporation of POSS in the PCLF network enhanced the modulus of elasticity significantly from 3.9 ± 0.9 MPa for neat crosslinked PCLF to 5.1 ± 1.1 , 6.4 ± 0.7 , and 8.0 ± 1.4 MPa for crosslinked PCLF-*co*-POSS with $\phi_{\text{POSS}} = 5\%$, 10%, and 20% respectively. The increase in the modulus of elasticity for higher POSS containing copolymers can possibly be explained by the higher crosslinking density induced from increased POSS loading. Further, elongation was greatest for neat crosslinked PCLF, while the increase in POSS loading hindered elongation but, significantly enhanced stiffness as indicated by the steeper slope.

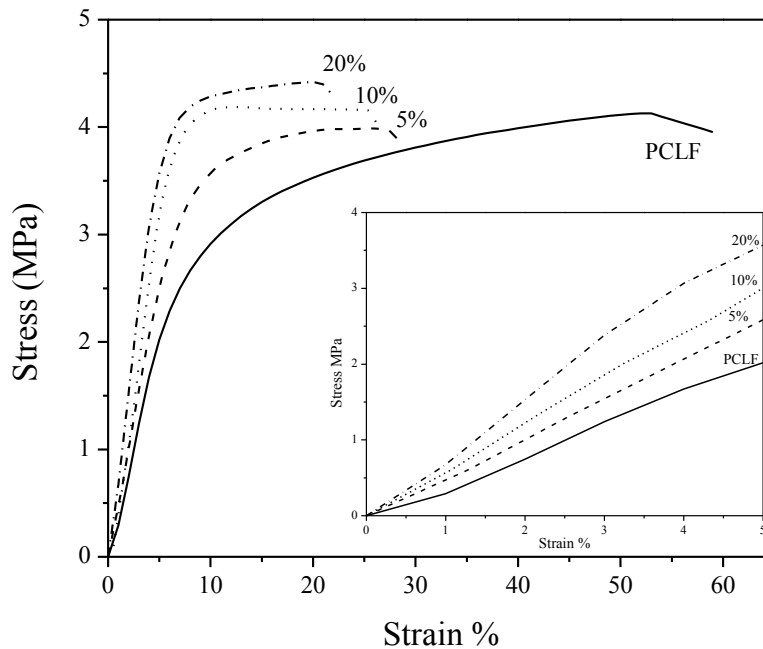


Figure 4.4 Stress vs strain curves of photo-crosslinked PCLF and PCLF-*co*-POSS. Inset: magnification of the slope.

4.7 Thermal properties

TGA curves in Figure 4.5 were used to determine the thermal stability by examining the degradation temperature (T_d) of uncrosslinked PCLF, PCLF-*co*-POSS, POSS, and crosslinked PCLF and PCLF-*co*-POSS. All of the samples had a single degradation step. T_d values of the uncrosslinked and crosslinked samples are shown in Table 4.3. T_d was highest for $\phi_{POSS} = 20\%$; however, PCLF-*co*-POSS samples ($\phi_{POSS} = 10\%$ and 5%) are slightly lower than neat PCLF and POSS, demonstrating the lowest T_d (Table 4.3). Crosslinked samples experienced a higher T_d than the uncrosslinked samples. Similar to the uncrosslinked samples, the crosslinked T_d was highest for $\phi_{POSS} = 20\%$ and PCLF, respectively. As POSS loading increases above $\phi_{POSS} = 10\%$, thermal stability is enhanced which is likely due to the ability of POSS to degrade at a lower temperature than PCLF and protect the surface layer of the polymer matrix by slowing the diffusion of oxygen [5,6].

Table 4.3 Thermal Properties of PCLF, PCLF-*co*-POSS and POSS.

Sample	T_d (°C)	T_{m1} (°C)	T_{m2} (°C)	T_c (°C)	ΔH_m (J/g)	X_c (%)
PCLF	415 (420)	39.6 (39.5)	45.8	17.1 (12.9)	62.2 (43.3)	46.1 (30.7)
5%	397 (415)	35.5 (35.5)	41.9	15.2 (1.8)	47.2 (40.6)	36.8 (30.3)
10%	413 (418)	35.1 (37.6)	43.1	8.0 (2.5)	46.5 (32.3)	38.3 (25.4)
20%	418 (423)	33.5 (28.4)	42.8	5.7 (-22.6)	32.2 (20.7)	29.8 (18.3)
POSS	391	-	-	-	-	-

* Data in parenthesis indicate values of crosslinked PCLF and PCLF-*co*-POSS.

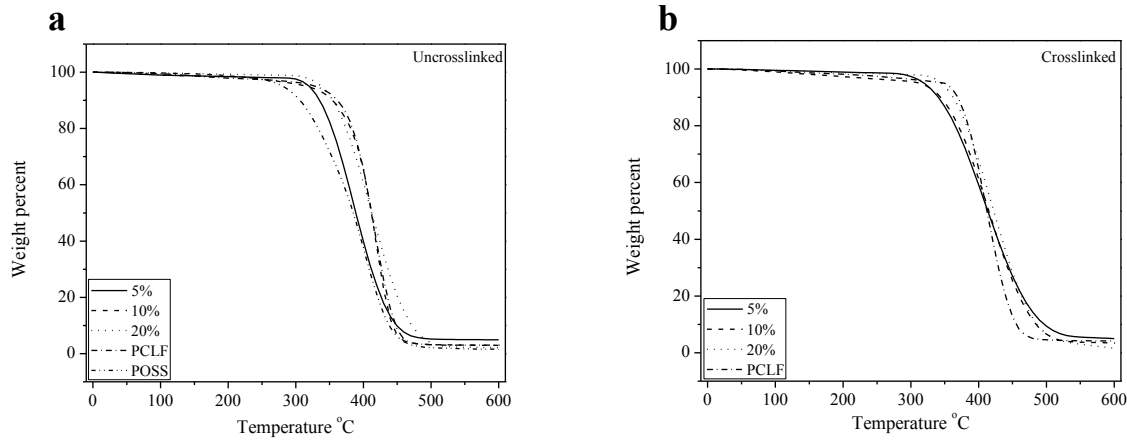


Figure 4.5 TGA curves of (a) PCLF, PCLF-*co*-POSS, and POSS and (b) photo- crosslinked PCLF and PCLF-*co*-POSS.

DSC curves (Figure 4.6) were used to gather the thermal properties such as melting temperature (T_m), crystallization temperature (T_c), and heat of fusion (ΔH_m), for PCLF, PCLF-*co*-POSS, POSS, and crosslinked PCLF and PCLF-*co*-POSS samples. Crystallinity (X_c) for uncrosslinked and crosslinked samples was calculated by using the equation $X_c = [\Delta H_m / (1 - \phi_{POSS} \Delta H_m^c)] \times 100\%$ and $X_c = [\Delta H_m / (1 - \phi_{POSS} \Delta H_m^c) \times 95.7\%] \times 100\%$, where ϕ_{POSS} was 0%, 5%, 10%, and 20%, respectively. The heat of fusion for completely crystalline PCL is 135J/g [7]. Uncrosslinked samples exhibited lower ΔH_m and X_c with higher compositions of POSS in the copolymer. The increase in T_m relative to higher ϕ_{POSS} for uncrosslinked samples can be attributed to the high crystalline nature of the POSS monomer with a T_m of 172.9 °C [8]. Crosslinked samples exhibited lower ΔH_m , X_c , and T_c than uncrosslinked samples as ϕ_{POSS} was increased, which was likely because chain motions were suppressed by the crosslinks.

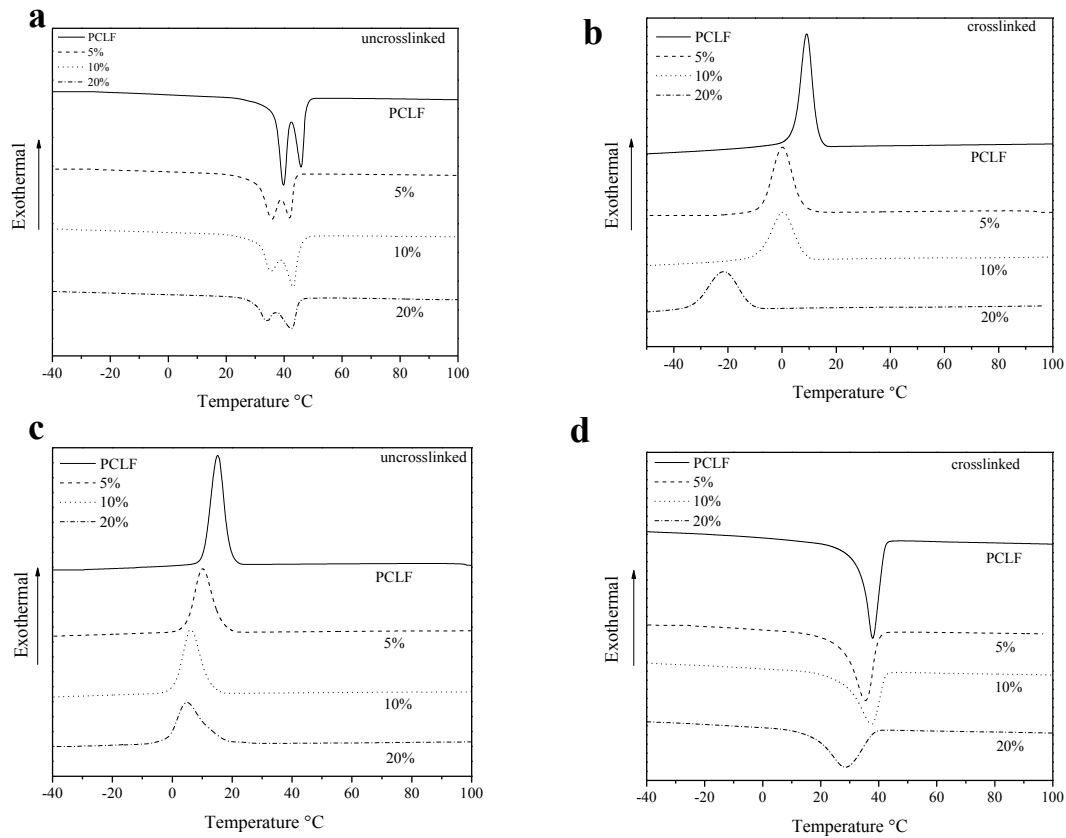


Figure 4.6 DSC (a) heating curve of PCLF and PCLF-*co*-POSS (b) photo-crosslinked PCLF and PCLF-*co*-POSS. (c) cooling curves of PCLF and PCLF-*co*-POSS (d) photo-crosslinked PCLF and PCLF-*co*-POSS.

4.8 Cell attachment and proliferation

Cell attachment and proliferation studies were performed by using mouse pre-osteoblastic MC3T3-E1 cells and rat primary aortic smooth muscle cells cultured on PCLF and PCLF-*co*-POSS disks. The purpose of this experiment was to determine the potential use of crosslinked PCLF and PCLF-*co*-POSS as biodegradable and injectable scaffolds to promote orthopedic and cardiovascular regeneration. The amount of MC3T3-E1 cells and SMCs at days 1, 2, and 4 post-seeding on PCLF and PCLF-*co*-POSS showed similarities with the positive control of tissue culture polystyrene (TCPS), thereby indicating that the PCLF and PCLF-*co*-POSS substrates were non-cytotoxic in the time considered for cell attachment and proliferation studies. All of the

substrates examined in this study provided necessary microenvironments for MC3T3-E1 cell and SMC attachment and proliferation, as indicated by the spread-out phenotype (Figures 4.7a and 4.8a).

4.8.1 MC3T3-E1 cells cultured on PCLF and PCLF-co-POSS disks

Mouse pre-osteoblastic MC3T3-E1 cell attachment at 4 h was significantly higher for PCLF-co-POSS ($\phi_{\text{POSS}} = 10\%$ and 20%) than crosslinked PCLF. Crosslinked PCLF-co-POSS ($\phi_{\text{POSS}} = 10\%$ and 20%) cell attachment values resembled similar results to that of the positive control (TCPS) (Figure 4.7b). The proliferation of MC3T3-E1 cells over a 4 day period (Figure 4.7c) indicated similar results to the trend seen for cell attachment, as proliferation was significantly enhanced on PCLF-co-POSS ($\phi_{\text{POSS}} = 10\%$ and 20%) when compared to crosslinked PCLF and PCLF-co-POSS with $\phi_{\text{POSS}} = 5\%$. Adding POSS at ϕ_{POSS} of $= 5\%$, 10% , and 20% enhanced both cell attachment and proliferation greater than crosslinked PCLF alone, therefore indicating the MC3T3-E1 cell preference for stiffer substrates, which was consistent with recent literature [9,10]. The proliferation index (PI) of MC3T3-E1 cells (Figure 4.7d) increased from 1.2 ± 0.8 on crosslinked PCLF to 1.6 ± 0.6 on the stiffer PCLF-co-POSS ($\phi_{\text{POSS}} = 20\%$), further indicating the preference of stiffer substrates for MC3T3-E1 cells.

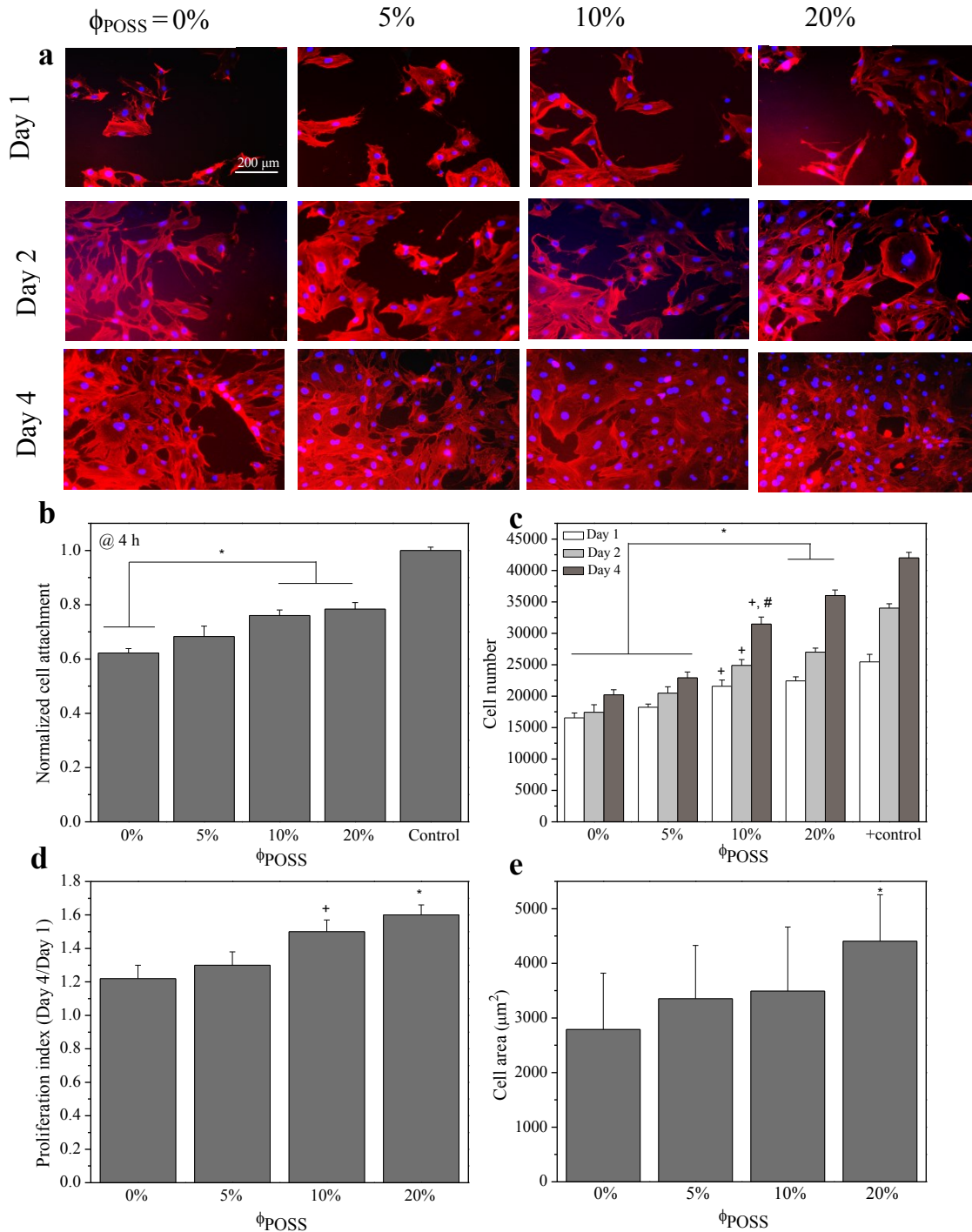


Figure 4.7 MC3T3-E1 cell attachment and proliferation. (a) Fluorescent images stained with rhodamine-phalloidin (red) and DAPI (blue) on crosslinked PCLF and PCLF-co-POSS disks at days 1, 2, and 4 post-seeding. (b) Normalized cell attachment at 4 h. (c) Cell numbers at days 1, 2, and 4. (d) Proliferation index of MC3T3-E1 cells. (e) MC3T3-E1 cell area at 1 day. *, $p < 0.05$ relative to PCLF for cell attachment and cell area, and PCLF and $\phi_{\text{POSS}} = 5\%$ for cell number and PI. +, $p < 0.05$ relative to PCLF for cell number and PI. #, $p < 0.05$ relative to $\phi_{\text{POSS}} = 5\%$ at day 4. Scale bar of 200 μm is applicable to all.

4.8.2 SMCs cultured on PCLF and PCLF-co-POSS disks

Rat primary aortic SMCs were also studied on their ability to attach and proliferate on crosslinked PCLF and PCLF-co-POSS disks. Cell attachment was evaluated at 4 h and showed similar results to the cell attachment of MC3T3-E1 cells, where cell attachment was significantly higher for PCLF-co-POSS ($\phi_{\text{POSS}} = 10\%$ and 20%) when compared to crosslinked PCLF and PCLF-co-POSS ($\phi_{\text{POSS}} = 5\%$) (Figure 4.8b). SMCs showed better attachment on all samples when compared to MC3T3-E1 cells. SMC proliferation was examined over a 4 day period at days 1, 2, and 4. SMC proliferation was significantly improved on PCLF-co-POSS ($\phi_{\text{POSS}} = 20\%$) disks when compared to crosslinked PCLF and PCLF-co-POSS ($\phi_{\text{POSS}} = 5\%$) (Figure 4.8c). All POSS-containing ($\phi_{\text{POSS}} = 5\%$, 10% , and 20%) samples showed better cell attachment and proliferation than crosslinked PCLF, similarly to the study conducted with MC3T3-E1 cells. The results shown for SMCs follow a similar trend as discussed for MC3T3-E1 cells and was likely due to SMCs affinity to attach and proliferate on stiffer substrates [11,12]. The PI of SMCs (Figure 4.8d) increased from 1.33 ± 0.7 on crosslinked PCLF to 1.7 ± 0.6 on PCLF-co-POSS ($\phi_{\text{POSS}} = 20\%$); however, the PI for PCLF-co-POSS ($\phi_{\text{POSS}} = 10\%$ and 20%) are nearly identical.

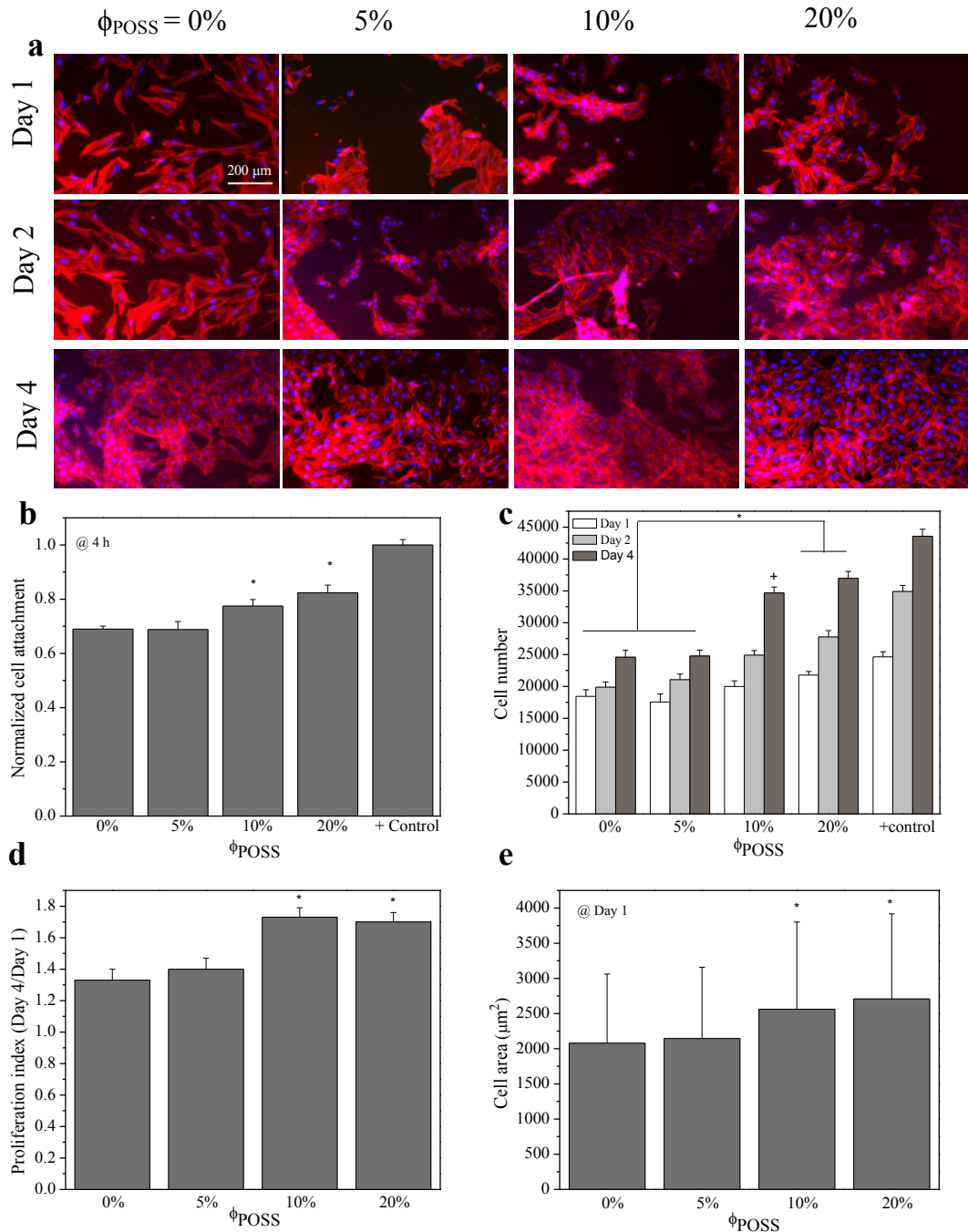


Figure 4.8 SMC cell attachment and proliferation. (a) Fluorescent images stained with rhodamine-phalloidin (red) and DAPI (blue) on crosslinked PCLF and PCLF-co-POSS disks at days 1, 2, and 4 post-seeding. (b) Normalized cell attachment at 4 h. (c) Cell numbers at days 1, 2, and 4. (d) Proliferation index of SMCs. (e) SMC cell area at 1 day. *, $p < 0.05$ relative to PCLF and $\phi_{\text{POSS}} = 5\%$ for all graphs. +, $p < 0.05$ relative to PCLF at day 4. Scale bar of 200 μm is applicable to all.

4.9 Focal adhesions

Focal adhesions (FAs) for both MC3T3-E1 cells and SMCs were analyzed using fluorescent images. FAs were characterized to determine cell adhesion, as FAs are the closest contact with regards to cells and the underlying substrate, and act as signal carriers to the extracellular matrix (ECM) [13,14]. Cytoskeleton F-actin was stained red with RP and vinculin-stained green was used to amplify the FA protrusions. FAs were quantified by cell density, i.e., FAs per cell, average FA area, and FA elongation, which is the inverse of circularity.

4.9.1 MC3T3-E1 focal adhesions

MC3T3-E1 focal adhesion density was significantly higher on all stiffer POSS-containing substrates when compared to crosslinked PCLF. The stiffest substrate PCLF-co-POSS ($\phi_{\text{POSS}} = 20\%$) showed to have statistically significant higher FA cell area and elongation when compared to all other samples, PCLF and PCLF-co-POSS ($\phi_{\text{POSS}} = 5\%$, and 10%). Fluorescent confocal microscopy images confirmed that FA protrusions are more prominent on the substrates containing larger POSS fractions, as indicated by the arrows (Figure 4.9).

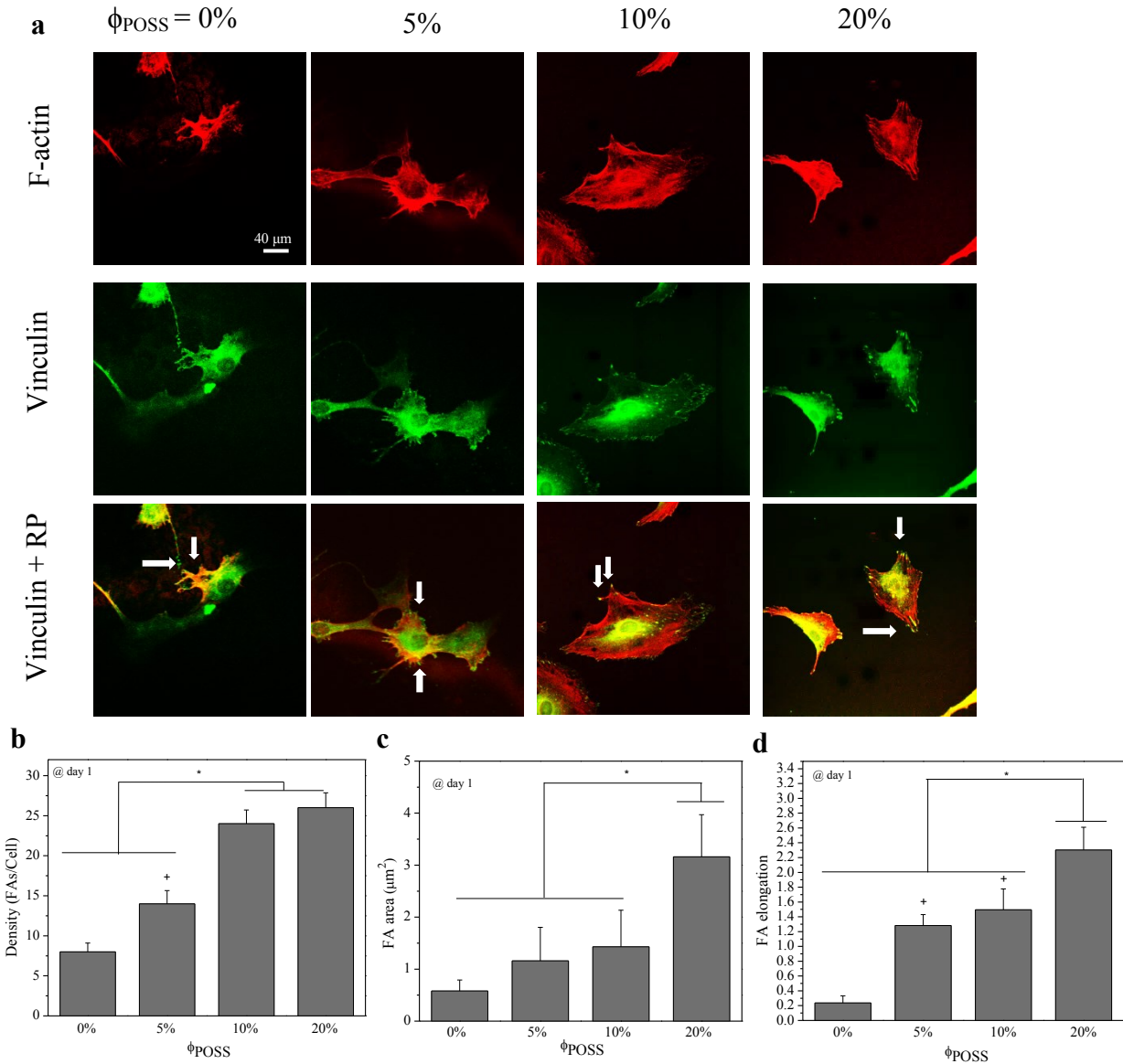


Figure 4.9 (a) Fluorescent images of MC3T3-E1 cells stained with RP (red) top row, vinculin (green) middle row, and RP + vinculin bottom row. (b) FA density. (c) FA area. (d) FA elongation. *, $p < 0.05$ relative to PCLF and $\phi_{\text{POSS}} = 5\%$ for density and relative to all other samples for area and elongation. +, $p < 0.05$ relative to PCLF for all data. Arrows indicate FA protrusions. Scale bar of 40 μm is applicable to all.

4.9.2 SMC focal adhesions

SMC FAs were characterized and quantified similarly to MC3T3-E1 cells. FA density was significantly higher on PCLF-co-POSS ($\phi_{\text{POSS}} = 10\%$ and 20%) substrates, indicating SMC

favorability for stiffer substrates (Figure 4.10). As surface stiffness and FA density increases, cell mechanotransduction mechanisms involving the crosstalk between actin and adhesion complexes, i.e., FAs, tend to activate integrins during cell attachment [15,16]. Cell area and elongation was significantly higher for PCLF-co-POSS ($\phi_{\text{POSS}} = 20\%$) when compared to all other samples. FA protrusions are indicated by the arrows.

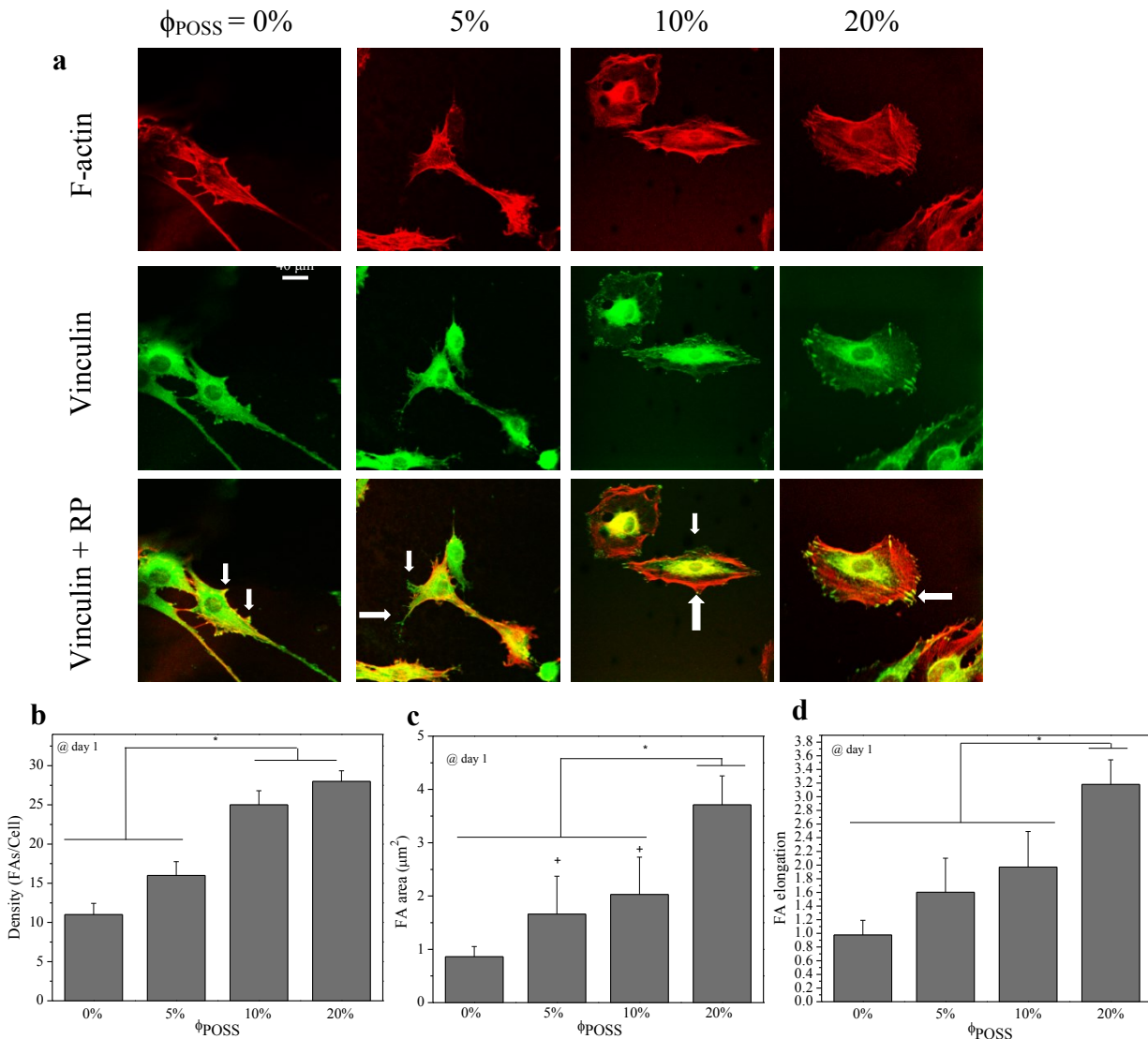


Figure 4.10 (a) Fluorescent images of SMCs stained with RP (red) top row, vinculin (green) middle row, and RP + vinculin bottom row. (b) FA density. (c) FA area. (d) FA elongation. *, $p < 0.05$ relative to PCLF and $\phi_{\text{POSS}} = 5\%$ for density and relative to all other samples for area and elongation. Arrows indicate FA protrusions. Scale bar of 40 μm is applicable to all.

4.10 Cell differentiation

4.10.1 ALP and calcium content

Early stages of MC3T3-E1 cell differentiation was characterized by examining alkaline phosphatase (ALP) activity and calcium content, which are two indicators of osteoblast differentiation. The ALP activity and calcium content was examined after being cultured for 7 and 14 days [17]. ALP activity and calcium content was maximized on PCLF-co-POSS ($\phi_{\text{POSS}} = 20\%$), showing a statistically significant difference when compared to crosslinked PCLF (Figure 4.11). The results indicate that POSS-containing substrates promote greater ALP activity and calcium content, which was likely due to MC3T3-E1 cells being able to sense POSS after the proliferative period [14,18]. It should be noted that ALP activity was maximized at week one, which is because of its role as an early bone marker [19]. Meanwhile, mineralization increased after one week, as indicated by an increase in calcium content.

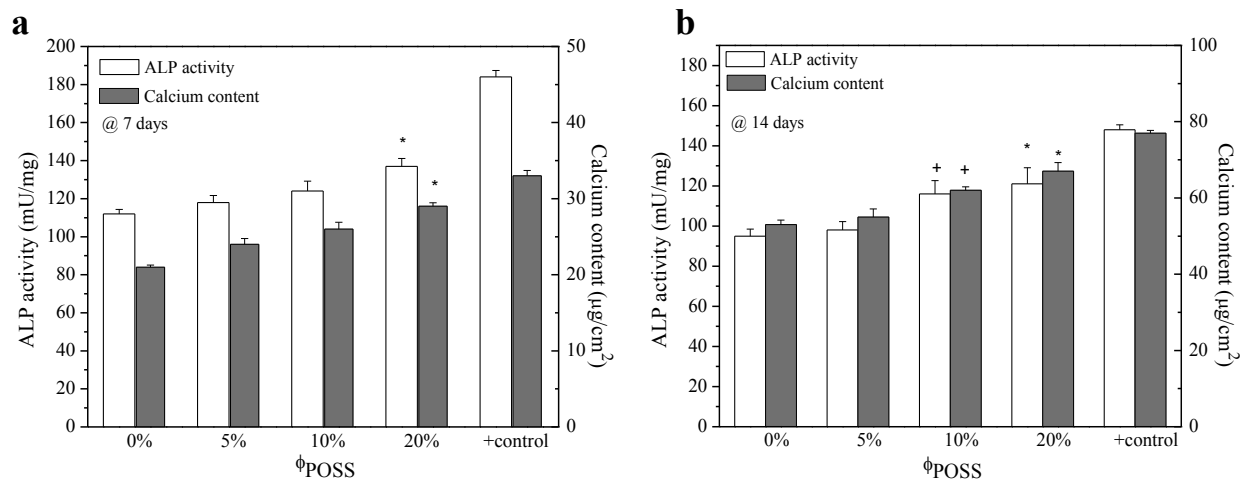


Figure 4.11 ALP activity and calcium content of MC3T3-E1 cells cultured on crosslinked PCLF and PCLF-co-POSS for (a) 7 days. (b) 14 days. *, $p < 0.05$ relative to PCLF at 7 days and PCLF and $\phi_{\text{POSS}} = 5\%$ at 14 days. +, $p < 0.05$ relative to PCLF.

4.10.2 MC3T3-E1 Gene Expression

Gene expression of MC3T3-E1 cells was analyzed after being cultured on crosslinked PCLF, and PCLF-co-POSS ($\phi_{\text{POSS}} = 5\%$, 10% , and 20%), for 14 days. Reverse transcriptase (RT) and real-time PCR were used to quantify ALP and osteocalcin (OCN) expression levels relative to GAPDH. The ALP gene in MC3T3-E1 cells was used as an early indicator of osteoblast differentiation since their peak expression level occurred at 7 days [19-21]. OCN expression was used as a late maker of osteoblastic differentiation, which reached its maximum expression levels after 14 days. The difference between early and late differentiation markers can explain the higher expression levels of OCN when compared to ALP. Even though, the differentiation markers have varied expression levels over time, the dependence upon ϕ_{POSS} was similar (Figure 4.12).

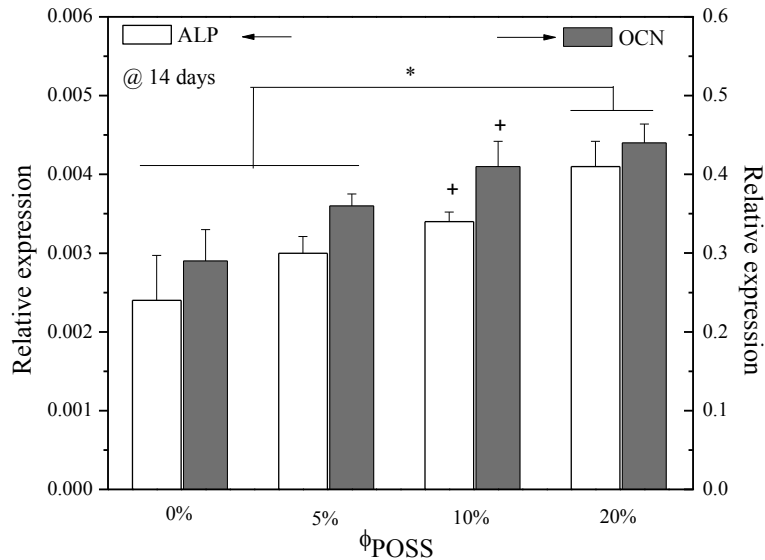


Figure 4.12 MC3T3-E1 gene expression levels relative to GAPDH at 14 days. ALP expression (white). OCN expression (gray). *, $p < 0.05$ relative to PCLF. +, $p < 0.05$ relative to PCLF and $\phi_{\text{POSS}} = 5\%$.

4.10.2 SMC Gene Expression

SMC gene expression was observed after being cultured on PCLF and PCLF-*co*-POSS ($\phi_{\text{POSS}} = 5\%$, 10% , and 20%), for 4 days. Smoothlin and calponin for contractile SMCs were the gene markers examined. [22,23]. Expression of both smoothlin and calponin relative to GAPDH showed a similar trend in expression with varied ϕ_{POSS} . Gene expression was significantly higher on PCLF-*co*-POSS ($\phi_{\text{POSS}} = 10\%$ and 20%) when compared to crosslinked PCLF and PCLF-*co*-POSS ($\phi_{\text{POSS}} = 5\%$) (Figure 4.13).

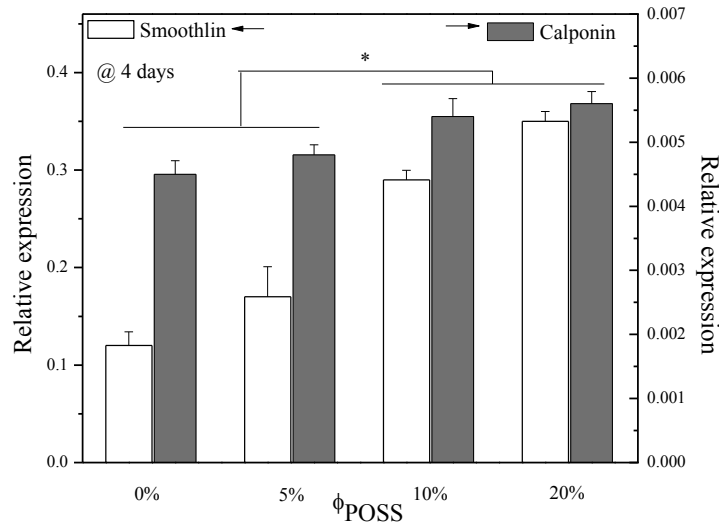


Figure 4.13 SMC gene expression relative to GAPDH at 4 days. Smoothlin expression (white). Calponin expression (gray). *, $p < 0.05$ relative to PCLF and $\phi_{\text{POSS}} = 5\%$.

4.10 Conclusions

Novel injectable, photo-crosslinkable, and degradable PCLF-*co*-POSS nano-hybrid polymer networks with varied POSS loading ($\phi_{\text{POSS}} = 0\%$, 5% , 10% , and 20%) were synthesized and photo-crosslinked via UV light. Results showed that the increase of ϕ_{POSS} lead to enhanced photo-crosslinking, as characterized by the gel fraction and swelling ratio. Further, higher ϕ_{POSS} resulted in increased stiffness, as indicated by DMA tensile testing. Mouse pre-osteoblastic

MC3T3-E1 cells and rat primary aortic SMCs favored the stiffer substrates with greater ϕ_{POSS} fractions, which was evident from increased cell attachment, proliferation, mineralization, and gene expression. Finally, when comparing the MC3T3-E1 and SMC response on PCLF-co-POSS substrates, SMCs had a greater affinity for the substrates, as evident by an increased cell number and proliferation index. This study clearly demonstrated the ability of POSS to improve physical properties of PCLF networks as well as, enhance the favorability for cell environments.

References

1. Jabbari, E., Wang, S., Lu, L., Gruetzmacher, J. A., Ameenuddin, S., Hefferan, T. E., Yaszemski, M. J. (2005). Synthesis, Material Properties and Biocompatibility of a Novel Self-Crosslinkable Poly(caprolactone fumarate) as an Injectable Tissue Engineering Scaffold. *Biomacromolecules*, 6(5), 2503–2511.
2. Horikx, M. (1955). Chain Scissions in a Polymer Network. *Journal of Polymer Science*, 19, 445-454.
3. Bouklas, N., Huang, R. (2012). Swelling Kinetics of Polymer Gels: Comparison of Linear and Nonlinear Theories. *Soft Matter*, 8(31), 8194-8203.
4. Wang, S.; Kempen, D. H.; Yaszemski, M. J.; Lu, L.(2009) The Roles of Matrix Polymer Crystallinity and Hydroxyapatite Nanoparticles in Modulating Material Properties of Photo-crosslinked Composites and Bone Marrow Stromal Cell Responses. *Biomaterials*. 30(20), 3359-70.
5. Liu, Y., Huang, Y., Liu, L. (2008). Influence of Methacryl Polyhedral Oligomeric Silsesquioxane on the Thermal and Mechanical Properties of Methylsilicone Resin. *Journal of Applied Polymer Science*, 2989-2995.
6. Lewicki, J., Pielichowski, K., Jancia, M., Hebda, E., Albo, R., Maxwell, R. (2014). Degradative and Morphological Characterization of POSS Modified Nanohybrid Polyurethane Elastomers. *Polymer Degradation and Stability*, (104), 50-56.
7. Wang, S., Yaszemski, M. J., Knight, A. M., Gruetzmacher, J. A., Windebank, A. J., Lu, L. (2009). Photo-crosslinked Poly(ϵ -caprolactone fumarate) Networks for Peripheral Nerve Regeneration: Physical Properties and Preliminary Biological Evaluations. *Acta Biomaterials*, 5(5), 1531–1542.

8. Cai, L., Chen, J., Rondinone, A. J. Wang, S. (2012), Injectable and Biodegradable Nanohybrid Polymers with Simultaneously Enhanced Stiffness And Toughness for Bone Repair. *Advanced. Functional. Materials*, 22: 3181–3190.
9. Wang, K., Cai, L., Zhang, L., Dong, J. And Wang, S. (2012), Biodegradable Photo-Crosslinked Polymer Substrates with Concentric Microgrooves for Regulating MC3T3-E1 Cell Behavior. *Advanced Healthcare Materials*, 1: 292–301.
10. Keogh, M., O'Brien, F., Daly, J. (2010). Substrate Stiffness and Contractile Behaviour Modulate the Functional Maturation of Osteoblasts on A Collagen–GAG Scaffold. *Acta Biomaterialia*, 6(11), 4305-4313.
11. Yeung T, Georges PC, Janmey PA. Effects of Substrate Stiffness on Cell Morphology, Cytoskeletal Structure and Adhesion. *Cell Motility and Cytoskeleton* 2005; 60:24-34
12. Choquet D, Felsenfeld DP, Sheetz MP. Extracellular Matrix Rigidity Causes Strengthening of Integrin-Cytoskeleton Linkages. *Cell* 1997;88:39-48
13. Stein, G., Lian, J., Owen, T. (1990). Relationship of Cell Growth to the Regulation of Tissue-Specific Gene Expression during Osteoblast Differentiation. *FASEB J.* 4(13), 3111-3123.
14. Wang, K., Cai, L., Wang, S. (2011). Methacryl-Polyhedral Oligomeric Silsesquioxane as a Crosslinker for Expediting Photo-Crosslinking of Poly(propylene fumarate): Material Properties And Bone Cell Behavior. *Polymer*, 52(13), 2827-2839.
15. Chen, C. (2008). Mechanotransduction - A Field Pulling Together? *Journal of Cell Science*, 121, 3285-3292.

16. Parsons, J. T., Horwitz, A. R., Schwartz, M. A. (2010). Cell Adhesion: Integrating Cytoskeletal Dynamics and Cellular Tension. *Nature Reviews. Molecular Cell Biology*, 11(9), 633–643.
17. Isama, K., Tsuchiya, T. (2003). Enhancing Effect of Poly(L-Lactide) on the Differentiation of Mouse Osteoblast-Like MC3T3-E1 Cells. *Biomaterials*, 24(19), 3303-3309.
18. Suzuki, A., Palmer, G., Bonjour, J., Caverzasio, J. (1998). Catecholamines Stimulate the Proliferation and Alkaline Phosphatase Activity of MC3T3-E1 Osteoblast-like Cells. *Bone*, 23(3), 197-203.
19. Hronik-Tupaj, M.; Rice, W. L.; Cronin-Golomb, M.; Kaplan, D. L.; Georgakoudi, I. Osteoblastic Differentiation and Stress Response of Human Mesenchymal Stem Cells Exposed to Alternating Current Electric Fields. *Biomed Eng Online* 2011, 10, 9.
20. Siebers, M. C.; Brugge, P. J.; Walboomers, X. F.; Jansen, J. A. Integrins as linker proteins between osteoblasts and bone replacing materials. A critical review *Biomaterials* 2005, 26, 137.
21. Owen, T., Aronow, M., Shalhoub, V., Barone, L., Wilming, L., Tassinari, M., Stein, G. (1990). Progressive Development of the Rat Osteoblast Phenotype In Vitro: Reciprocal Relationships in Expression of Genes Associated with Osteoblast Proliferation and Differentiation During Formation of the Bone Extracellular Matrix. *Journal of Cellular Physiology*, 143(3), 420-430.
22. Sobue K, Hayashi K, Nishida W. (1999) Expressional Regulation of Smooth Muscle Cell-Specific Genes in Association with Phenotypic Modulation. *Molecular Cell Biochemistry*; 190:105-118.

23. Wang C, Yin S, Cen L, Liu Q, Liu W, Cao Y, Cui L. (2010) Differentiation of Adipose-Derived Stem Cells into Contractile Smooth Muscle Cells Induced by Transforming Growth Factorbeta1 and Bone Morphogenetic Protein-4. Tissue Engineering Part A, 6(4):1201-1213.

**Chapter V. Regulation of MC3T3-E1 Cells on Smooth and Microgrooved PCLF-co-
POSS/HA Nanocomposite Substrates**

Abstract

Regulation of mouse pre-osteoblastic MC3T3-E1 cells was examined on photo-crosslinked substrates of poly(ϵ -caprolactone fumarate) (PCLF) and polyhedral oligomeric silsesquioxane (POSS), which were copolymerized via polycondensation with a POSS weight fraction of ($\phi_{\text{POSS}} = 20\%$). To enhance this study further and improve the surface chemistry of the polymer nanocomposite, PCLF-*co*-POSS was supplemented with 20% hydroxyapatite (HA). HA was homogeneously integrated into the PCLF-*co*-POSS network and material properties as well as, cell behavior were analyzed and compared with PCLF-*co*-POSS. The addition of HA within the polymer network resulted in enhanced mechanical properties. To examine the effect of surface topography, smooth PCLF-*co*-POSS, PCLF-*co*-POSS/HA and microgrooved PCLF-*co*-POSS/HA was studied on its ability to influence cell behavior. The integration of HA showed to improve mechanical properties and MC3T3-E1 cell behavior as attachment, proliferation, mineralization, and differentiation were enhanced. Further, microgrooved surface features significantly improved mineralization and gene expression over substrates with smooth surfaces.

5.1 Introduction

The purpose of this study was to regulate mouse pre-osteoblastic MC3T3-E1 cell behavior by incorporating 20% hydroxyapatite (HA) nanoparticles into PCLF-co-POSS ($\phi_{\text{POSS}} = 20\%$) to form photo-crosslinked nanocomposites. MC3T3-E1 cell behavior was examined on smooth $\phi_{\text{POSS}} = 20\%$, PCLF-co-POSS/HA, and microgrooved PCLF-co-POSS/HA substrates. Microgroove dimensions that were used measured $5 \mu\text{m} \times 12 \mu\text{m}$ (groove width \times groove depth). Since PCLF-co-POSS ($\phi_{\text{POSS}} = 20\%$) substrates proved to promote cell attachment and proliferation better than PCLF and PCLF-co-POSS ($\phi_{\text{POSS}} = 5\%$, and 10%), the introduction of HA into the $\phi_{\text{POSS}} = 20\%$ polymer network was thought to further enhance cell behavior (e.g., cell attachment, proliferation, mineralization, focal adhesions, and gene expression) because of the prominent role that HA plays in bone composition. In this study physical, mechanical, and thermal properties of PCLF-co-POSS ($\phi_{\text{POSS}} = 20\%$) and PCLF-co-POSS/HA substrates were compared along with their ability to influence MC3T3-E1 cell behavior.

5.2 Results and Discussion

5.2.1 Photo-crosslinking

Gel fractions and swelling ratios of PCLF-co-POSS/HA were compared to PCLF-co-POSS ($\phi_{\text{POSS}} = 20\%$) after photo-crosslinking. HA particles were able to suspend in the PCLF-co-POSS solution to ensure homogenous HA distribution in the crosslinked network. PCLF-co-POSS/HA, swelling ratios (S) and gel fractions (Γ) were calculated by the equations, $S = [(1 - \phi_{\text{HA}}) \times \Gamma_0 \times S_0] / [(1 - \phi_{\text{HA}}) \times \Gamma_0 + \phi_{\text{HA}}]$ and $\Gamma = \phi_{\text{HA}} + (1 - \phi_{\text{HA}}) \times \Gamma_0$, where S_0 and Γ_0 were the experimental swelling ratio and gel fraction for the pure PCLF-co-POSS network, respectively. The “theoretical” gel fraction of PCLF-co-POSS/HA differs from PCLF-co-POSS because HA is

insoluble in CH_2Cl_2 . The addition of HA increased the gel fraction while lowering the swelling ratio (Figure 5.1) [1]. This result is similar to recent literature regarding the addition of HA into PCLF networks [1,2]. The addition of HA in the polymer network resulted in a higher gel fraction since HA particles are insoluble in CH_2Cl_2 .

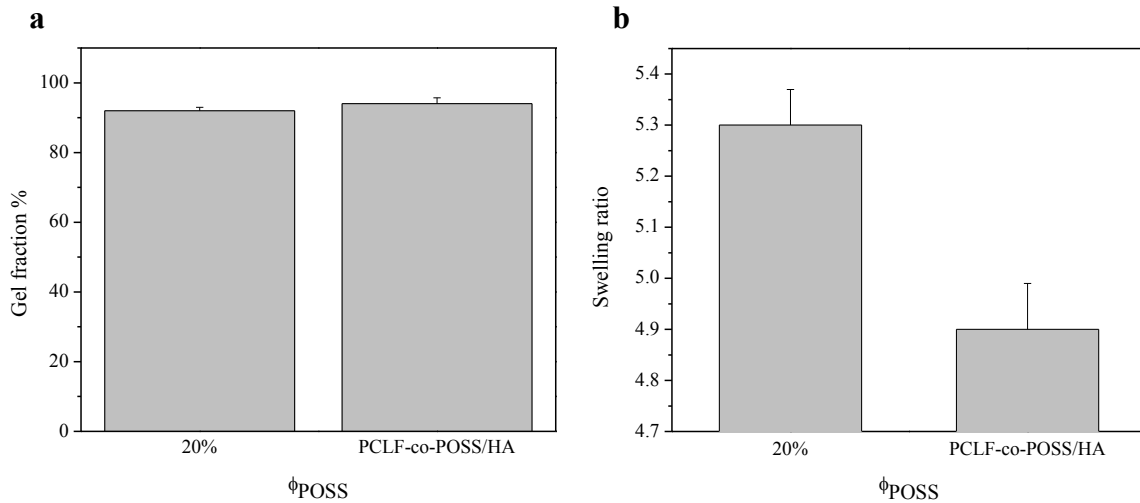


Figure 5.1 (a) Gel fractions and (b) swelling ratios of PCLF-co-POSS/HA.

5.2.2 Thermal and Mechanical Properties

Thermal and mechanical properties of PCLF-co-POSS were slightly altered after introducing HA into the polymer network (Figure 5.2a). The modulus of elasticity (E) was greater for the HA-containing nanocomposite; however, the incorporation of HA lead to brittle behavior of the polymer matrix, as evident by reduced elongation [1]. With the incorporation of HA, osteoconductivity can be enhanced along with material stiffness, to promote a favorable environment for bone tissue engineering applications [1-4]. Thermal stabilities of PCLF-co-POSS ($\phi_{\text{POSS}} = 20\%$) and PCLF-co-POSS/HA are demonstrated below (Figure 5.2b). Thermal degradation (T_d) of PCLF-co-POSS ($\phi_{\text{POSS}} = 20\%$) and PCLF-co-POSS/HA occurred in a single

step, where the onset of degradation was at 423 ° and 415 °C for PCLF-*co*-POSS ($\phi_{\text{POSS}} = 20\%$) and PCLF-*co*-POSS/HA, respectively. As indicated in a previous report, HA nanoparticles were stable at temperatures up to 600 °C [1]. The weight fraction of residue at 600 °C was ~20 for PCLF-*co*-POSS/HA, which shows good agreement to the 20% HA weight fraction within the polymer network. Thermal properties were determined by DSC (Figures 5.2c and 5.2d). Melting temperature (T_m), crystallization temperature (T_c), and crystallinity (X_c) remained similar (Table 5.1). X_c was calculated by the following equation, $X_c = [\Delta H_m / (\phi_{\text{PCL}} \Delta H_m^\circ)] \times 100\%$, where ΔH_m° is the known value of 135 J/g for completely crystalline PCL, and the composition of PCL in the nanocomposite is $\phi_{\text{PCL}} = (1 - \phi_{\text{HA}}) \times 97.5\%$ [5].

Table 5.1 Thermal properties of crosslinked $\phi_{\text{POSS}} = 20\%$ and PCLF-*co*-POSS/HA.

Sample	T_d (°C)	T_{m1} (°C)	T_c (°C)	ΔH_m (J/g)	X_c (%)
PCLF- <i>co</i> -POSS	423	28.4	-22.6	20.7	18.3
PCLF- <i>co</i> -POSS/HA	415	29.7	-26.9	15.4	19.7

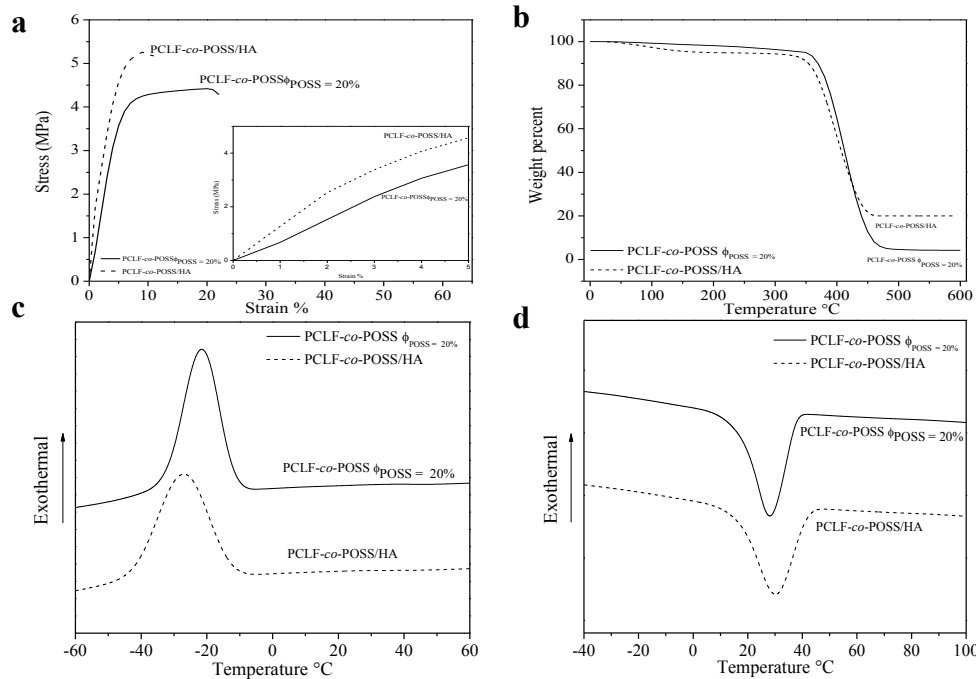


Figure 5.2 Thermal and mechanical properties of crosslinked $\phi_{\text{POSS}} = 20\%$ and PCLF-*co*-POSS/HA. (a) Stress vs strain curves (b) TGA curves (c) DSC cooling curves (d) DSC heating curve.

5.2.3 Surface topography characterization

Surface topography of PCLF-*co*-POSS ($\phi_{\text{POSS}} = 20\%$) and smooth/microgrooved PCLF-*co*-POSS/HA samples were imaged using scanning emission microscopy (SEM). Figure 5.3 shows the unique surface characteristics of each sample. The higher gel fraction of the PCLF-*co*-POSS/HA led to slightly smoother surfaces when compared to PCLF-*co*-POSS ($\phi_{\text{POSS}} = 20\%$) [6,7]. Microgrooved PCLF-*co*-POSS/HA is shown (Figure 5.3c) with a groove width of 5 μm .

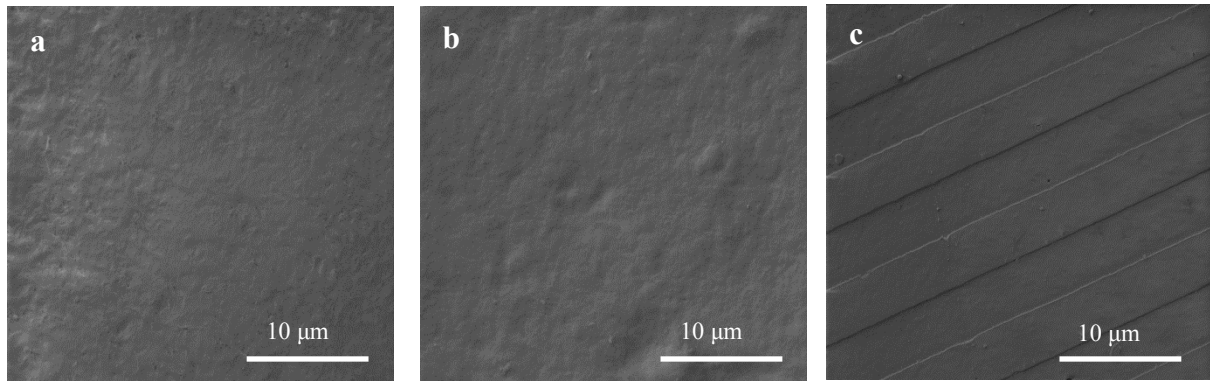


Figure 5.3 SEM images of (a) $\phi_{\text{POSS}} = 20\%$. (b) smooth PCLF-*co*-POSS. (c) microgrooved PCLF-*co*-POSS/HA.

5.3 Cell attachment and proliferation

MC3T3-E1 cells were seeded onto crosslinked PCLF-*co*-POSS ($\phi_{\text{POSS}} = 20\%$), PCLF-*co*-POSS/HA, and microgrooved PCLF-*co*-POSS/HA disks. Cell attachment was determined 4 h post-seeding and cell proliferation was analyzed after 1, 2, and 4 days. Both smooth and microgrooved PCLF-*co*-POSS/HA showed greater attachment and proliferation when compared to PCLF-*co*-POSS ($\phi_{\text{POSS}} = 20\%$) as shown in Figure 5.4. The proliferation index (PI) increased from 1.63 ± 0.6 for PCLF-*co*-POSS ($\phi_{\text{POSS}} = 20\%$) to 1.76 ± 0.8 and 1.76 ± 0.7 for smooth and microgrooved PCLF-*co*-POSS/HA, respectively. Microgrooved PCLF-*co*-POSS/HA influenced cell behavior as indicated by the vertical alignment. As indicated below (Figure 5.4), cells react

to different micro/nano topographies through the “contact guidance” effect [8-13]. Elongation of cells on microgrooved substrates was also observed. Cell alignment and elongation on microgrooved substrates occurs when cells sense forces thereby, influencing cells to adjust to the topography of the substrate and maintain optimal force equilibrium [14]. Although cell alignment was impacted by microgrooves, cell attachment and proliferation was not significantly influenced [15,16].

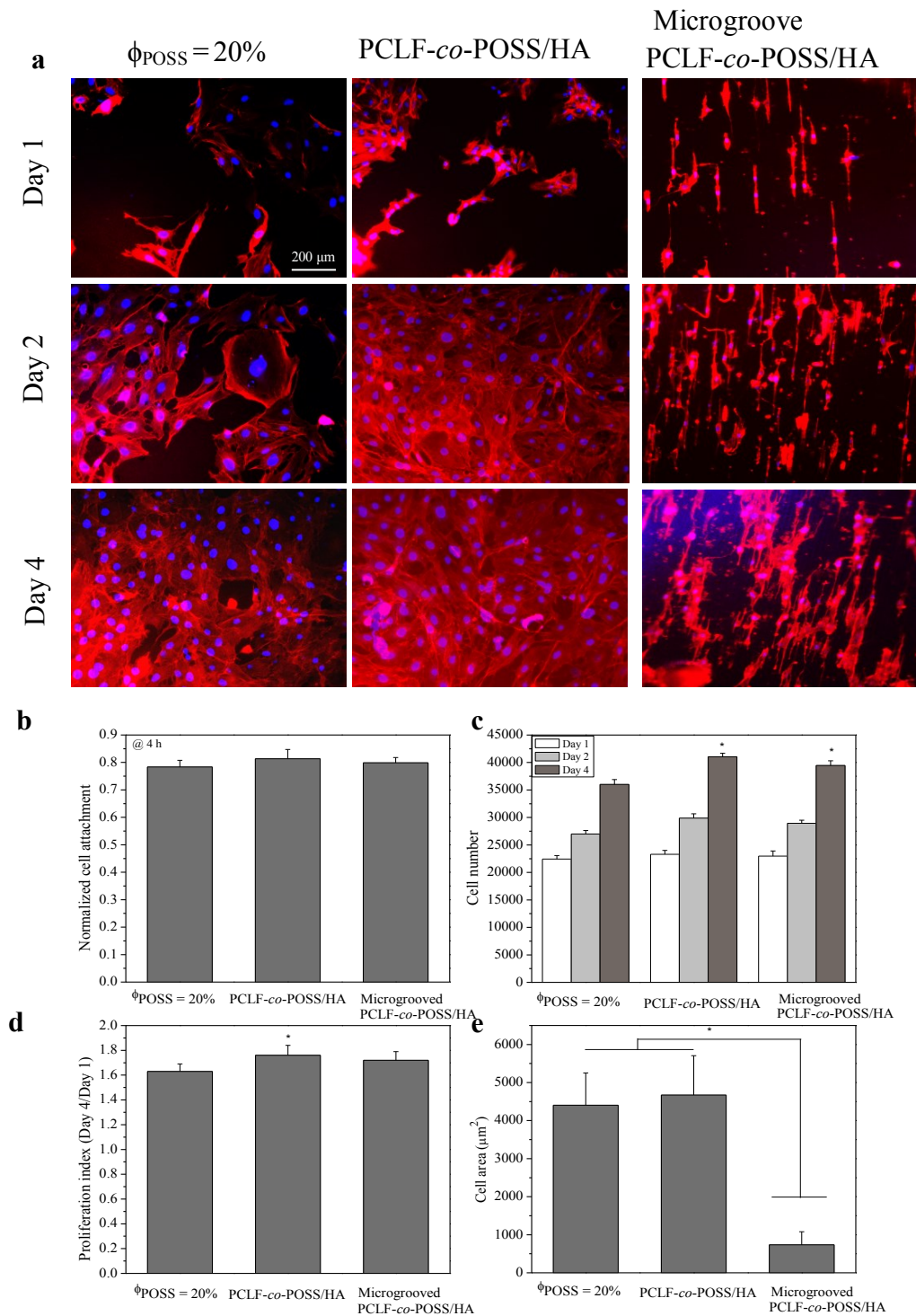


Figure 5.4 MC3T3-E1 cell attachment and proliferation. (a) Fluorescent images stained with rhodamine-phalloidin (red) and DAPI (blue) on $\phi_{\text{POSS}} = 20\%$ and PCLF-*co*-POSS/HA disks at days 1, 2, and 4 post-seeding. (b) Normalized cell attachment at 4 h. (c) Cell numbers at days 1, 2, and 4. (d) Proliferation index of MC3T3-E1 cells. (e) MC3T3-E1 cell area at 1 day. *, $p < 0.05$ relative to $\phi_{\text{POSS}} = 20\%$ for cell number at 4 days, PI, and relative to microgrooved PCLF-*co*-POSS/HA for cell area. Scale bar of 200 μm is applicable to all.

5.3.1 Focal adhesions

MC3T3-E1 focal adhesions (FAs) on smooth PCLF-*co*-POSS ($\phi_{\text{POSS}} = 20\%$), PCLF-*co*-POSS/HA, and microgrooved PCLF-*co*-POSS/HA were examined via confocal microscopy after being cultured for 1 day. FAs are complex macromolecule complexes which serve to physically anchor the actin cytoskeleton to integrins that interact with the surrounding extracellular matrix (ECM) [17]. FA density and elongation on both smooth and microgrooved PCLF-*co*-POSS/HA nanocomposites showed to have a statistically significant increase when compared to PCLF-*co*-POSS ($\phi_{\text{POSS}} = 20\%$), shown in Figure 5.5. Because PCLF-*co*-POSS/HA had higher mechanical properties and a more favorable surface chemistry, FA expression was increased [18]. FA elongation was significantly higher on microgrooved substrates, as they tend to attach to grooves or ridges in an oriented fashion [18-20].

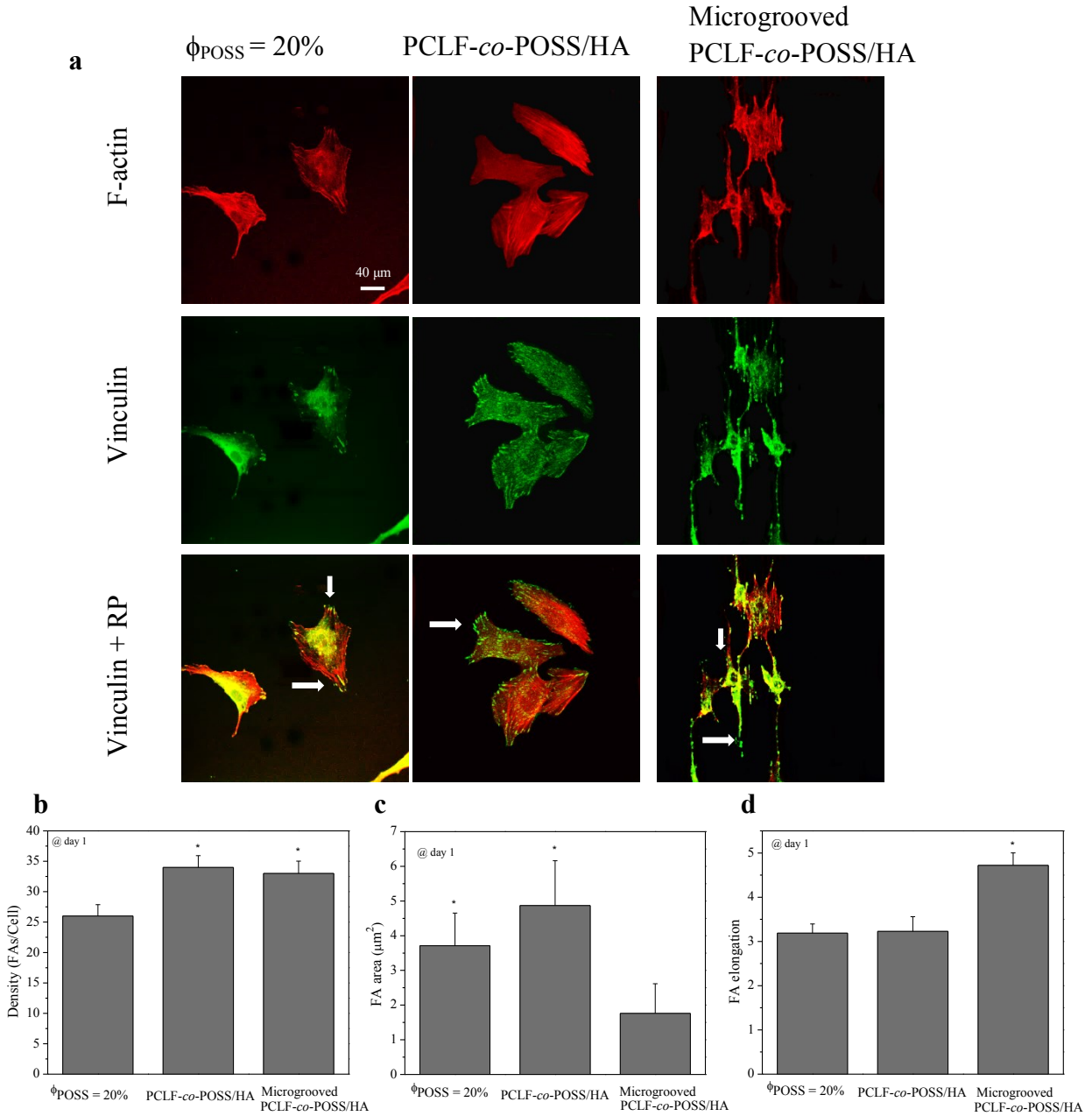


Figure 5.5 (a) Fluorescent images of MC3T3-E1 cells stained with RP (red) top row, vinculin (green) middle row, and RP + vinculin bottom row. (b) FA density. (c) FA area. (d) FA elongation. *, $p < 0.05$ relative to $\phi_{\text{POSS}} = 20\%$ for density, microgrooved PCLF-*co*-POSS for FA area, and relative to all other samples for elongation. Arrows indicate FA protrusions. Scale bar of 40 μm is applicable to all.

5.4 ALP activity and calcium content

Mineralization of MC3T3-E1 cells cultured for 7 and 14 days on PCLF-*co*-POSS ($\phi_{\text{POSS}} = 20\%$) and (smooth and microgrooved) PCLF-*co*-POSS/HA was determined by examining alkaline phosphatase (ALP) activity and calcium content, which are two indicators of osteoblastic differentiation [21,22]. The surface topography used here was smooth for PCLF-*co*-POSS ($\phi_{\text{POSS}} = 20\%$) and PCLF-*co*-POSS/HA, along with a microgrooved PCLF-*co*-POSS/HA substrate with a groove width of 5 μm and a groove depth of 12 μm . Both ALP activity and calcium content were significantly higher on the HA-containing substrates, which can be attributed to the favorable surface chemistry and mechanical properties induced from HA incorporation [2]. Further, microgrooved PCLF-*co*-POSS/HA substrates demonstrated higher ALP activity and calcium content over smooth PCLF-*co*-POSS ($\phi_{\text{POSS}} = 20\%$) and PCLF-*co*-POSS/HA (Figure 5.6). Enhanced mineralization on microgrooves suggested that cell alignment and confinement within the channels induces early differentiation and complements cell-cell interactions with the underlying substrate [2,23,24]. Alignment of osteoblasts has shown to alter cellular functions via altered regulation of cytoskeletal components, which explains the increase in mineralization and subsequent bone deposition [23-25].

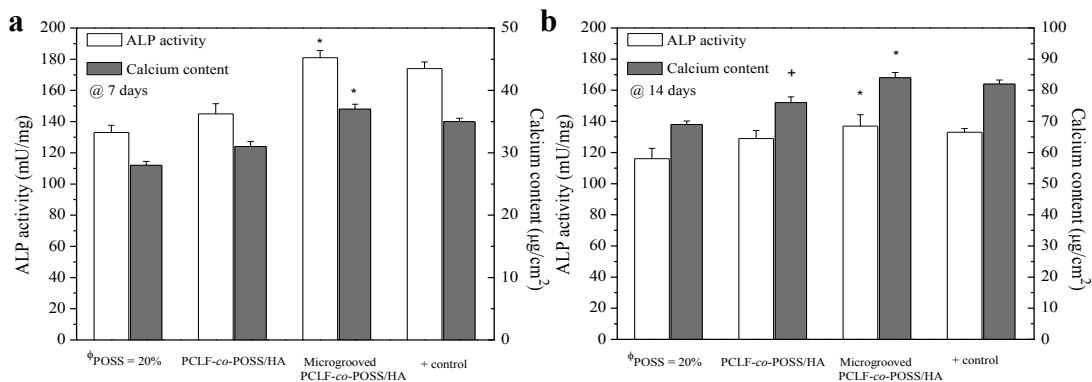


Figure 5.6 ALP activity and calcium content of MC3T3-E1 cells cultured on crosslinked $\phi_{\text{POSS}} = 20\%$, PCLF-*co*-POSS/HA and microgrooved PCLF-*co*-POSS/HA for (a) 7 days. (b) 14 days. *, $p < 0.05$ relative to all samples at 7 days and $\phi_{\text{POSS}} = 20\%$ at 14 days. +, $p < 0.05$ relative to $\phi_{\text{POSS}} = 20\%$.

5.5 Gene expression

Gene expression of MC3T3-E1 cells was determined after being cultured for 14 days on smooth PCLF-*co*-POSS ($\phi_{\text{POSS}} = 20\%$), PCLF-*co*-POSS/HA, and microgrooved PCLF-*co*-POSS/HA. Differentiation gene markers osteocalcin (OCN) and osteopontin (OPN) were quantified as indicators of osteoblastic maturation and mineralization [2,25]. mRNA expression of bone differentiation markers shown are relative to GAPDH (Figure 5.7). Since MC3T3-E1 cells were cultured for 14 days, both OCN and OPN were analyzed, as they are late differentiation gene markers which reach their maximum levels and continue to grow into the mineralization stage [26]. Gene expression here showed a similar trend to ALP activity and calcium content dependence upon HA-containing and microgrooved substrates. Microgrooved PCLF-*co*-POSS/HA samples showed to upregulate gene expression levels for OCN and OPN greater than the smooth PCLF-*co*-POSS ($\phi_{\text{POSS}} = 20\%$) and PCLF-*co*-POSS/HA. It is likely that microgrooves are capable of providing a favorable microenvironment for cells by allowing for better alignment and deformation of nuclei, thereby resulting in altered positioning of chromosomes and probability of gene expression [2,24-28]. Specifically, greater OCN expression can be achieved by constraining the nuclear shape of osteoblasts, induced from alignment [29]

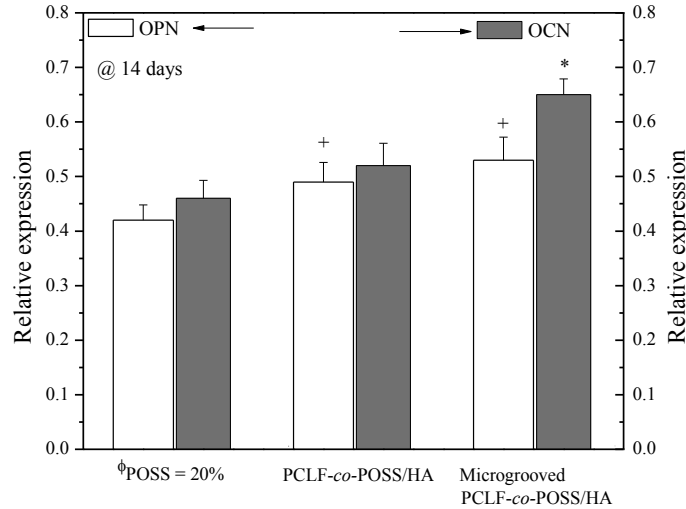


Figure 5.7 MC3T3-E1 gene expression levels relative to GAPDH at 14 days. OPN expression (white). OCN expression (gray). *, $p < 0.05$ relative to $\phi_{\text{POSS}} = 20\%$ for OPN and all samples for OCN.

5.6 Further discussion

By enhancing surface chemistry and topography, cellular fate can be tuned to achieve favorable bone regeneration. Overall, the stiffer substrates containing HA nanoparticles improved MC3T3-E1 cell attachment, proliferation, and gene expression over PCLF-co-POSS substrates. Crosslinked and microgrooved PCLF-co-POSS/HA substrates substantially improved mineralization of MC3T3-E1 cells relative to smooth substrates. Although microgrooves had minimal impact on cell proliferation relative to smooth surfaces, cell orientation was changed, causing cells to align in the corresponding direction of the microgrooves. Microgrooved PCLF-co-POSS/HA induced nuclei and focal adhesion distortion, as indicated by increased elongation. Elongation and alignment are important factors to consider, as aligned osteoblasts have the ability to promote the development of functional cell polarity thereby, favoring mineralization and bone formation [23]. Recent studies have quantified the aspect ratio of surface features by dividing groove depth by groove width, to study human dermal fibroblast alignment and proliferation [30]. Literature suggested that cell alignment can be better achieved with a higher

aspect ratio [30]. In this chapter, results suggested that MC3T3-E1 cells alignment responded well on deeper and narrower grooves ($5\ \mu\text{m} \times 12\ \mu\text{m}$, groove width \times groove depth). The results have suggested that substrates with tunable surface chemistry and topography can achieve desirable effects for bone remodeling and regeneration.

5.7 Conclusions

Here PCLF-*co*-POSS ($\phi_{\text{POSS}} = 20\%$) along with smooth and microgrooved PCLF-*co*-POSS/HA nanocomposites were fabricated and evaluated on their abilities to regulate mouse pre-osteoblastic MC3T3-E1 cell behavior. Characterization of the nanocomposites revealed that the homogeneously dispersed HA nanoparticles within the PCLF-*co*-POSS network increased gel fraction and stiffness. The increase in stiffness and improvement in surface chemistry induced by the incorporation of HA showed to improve MC3T3-E1 favorability for the polymer substrates, as cell attachment, proliferation, and differentiation was enhanced. It was also evident that microgrooved PCLF-*co*-POSS/HA substrates upregulated MC3T3-E1 mineralization and gene expression, which are good indicators of osteogenesis. This study displayed how surface chemistry and topography can influence cell behavior for orthopedic tissue engineering applications.

References

1. Lee, K., Wang, S., Yaszemski, M., Lu, L. (2008). Physical Properties and Cellular Responses to Crosslinkable Poly(propylene fumarate)/Hydroxyapatite Nanocomposites. *Biomaterials*, 29(19), 2839-2848.
2. Henry, M., Cai, L., Liu, X., Zhang, L., Dong, J., Chen, L., Wang, S. (2015). Roles of Hydroxyapatite Allocation and Microgroove Dimension in Promoting Preosteoblastic Cell Functions on Photocured Polymer Nanocomposites through Nuclear Distribution and Alignment. *Langmuir*, 31(9), 2851-2860.
3. Woodard, J., Hildore, A., Lan, S., Park, C., Morgan, A., Eurell, J., Johnson, A. (2007). The Mechanical Properties and Osteoconductivity of Hydroxyapatite Bone Scaffolds with Multi-Scale Porosity. *Biomaterials*, 28(1), 45-54.
4. Chu, T., Orton, D., Hollister, S., Feinberg, S., Halloran, J. (2002). Mechanical and In Vivo Performance of Hydroxyapatite Implants with Controlled Architectures. *Biomaterials*, 23(6), 1283-1293.
5. Cai, L., Wang, S. (2009). Poly(ϵ -caprolactone) Acrylates Synthesized Using a Facile Method For Fabricating Networks to Achieve Controllable Physicochemical Properties and Tunable Cell Responses. *Polymer*, 51, 164-177.
6. Wang, S., Yaszemski, M. J., Knight, A. M., Gruetzmacher, J. A., Windebank, A. J., Lu, L. (2009). Photo-Crosslinked Poly(ϵ -caprolactone fumarate) Networks for Peripheral Nerve Regeneration: Physical Properties and Preliminary Biological Evaluations. *Acta Biomaterials*, 5(5), 1531–1542.
7. Wang, S., Kempen, D., Yaszemski, M., Lu, L. (2009). The Roles of Matrix Polymer Crystallinity and Hydroxyapatite Nanoparticles in Modulating Material Properties of Photo-

crosslinked Composites and Bone Marrow Stromal Cell Responses. *Biomaterials*, 30(20), 3359-3370.

8. Harbers, G. M.; Grainger, D. W. Cell-Material Interactions: Fundamental Design Issues for Tissue Engineering and Clinical Considerations. in *Introduction to Biomaterials*; Guelcher, S. A., Hollinger, J. O., Eds.; CRC Press: Boca Raton, FL, 2005; pp 15-45.

9. Bettinger, C., Langer, R., Borenstein, J. (2009). Engineering Substrate Topography at the Micro- and Nanoscale to Control Cell Function. *Angewandte Chemie International Edition*, 48(30), 5406-5415.

10. Flemming, R., Murphy, C., Abrams, G., Goodman, S., Nealey, P. (1999). Effects of Synthetic Micro- and Nano-Structured Surfaces on Cell Behavior. *Biomaterials*, 20(6), 573-588.

11. Chen, S., Shi, X., Chinnathambi, S., Wu, H., Hanagata, N. (2013). Generation of Microgrooved Silica Nanotube Membranes with Sustained Drug Delivery and Cell Contact Guidance Ability by Using a Teflon Microfluidic Chip. *Science and Technology of Advanced Materials*, 14.

12. Vasiev, I., Greer, A., Khokhar, A., Stormonth-Darling, J., Tanner, K., Gadegaard, N. (2013). Self-folding Nano- and Micropatterned Hydrogel Tissue Engineering Scaffolds by Single Step Photolithographic Process. *Microelectronic Engineering*, 108, 76-81.

13. Dalby, M. (2006). Topographically Induced Direct Cell Mechanotransduction. *Medical Engineering & Physics*, 27(9), 730-742.

14. Ingber, DE. Cellular Tensegrity: Defining New Rules of Biological Design That Govern the Cytoskeleton. *J. Cell Sci.* 1993; 104:613-627.

15. Wang, J., Grood, E., Florer, J., Wenstrup, R. (2000). Alignment and Proliferation of MC3T3-E1 Osteoblasts in Microgrooved Silicone Substrata Subjected to Cyclic Stretching. *Journal of Biomechanics*, 33(6), 729-735.
16. Kenar, H., Kose, G., Hasirci, V. (2006). Tissue Engineering of Bone on Micropatterned Biodegradable Polyester Films. *Biomaterials*, 27(6), 885-895.
17. Thomas, C. H., Collier, J. H., Sfeir, C. S., Healy, K. E. (2002). Engineering Gene Expression and Protein Synthesis by Modulation of Nuclear Shape. *Proceedings of the National Academy of Sciences of the United States of America*, 99(4), 1972–1977.
18. Kuo, J. (2013). Mechanotransduction at Focal Adhesions: Integrating Cytoskeletal Mechanics in Migrating Cells. *Journal of Cellular and Molecular Medicine*, 17(6), 704-712.
19. Geiger, B.; Spatz, J. P.; Bershadsky, A. D. Environmental Sensing through Focal Adhesions. *Nat. Rev. Mol. Cell. Biol.* 2009, 10, 21–33.
20. Biggs, M. J., Dalby, M. (2010). Focal Adhesions in Osteoneogenesis. *Proceedings of the Institution of Mechanical Engineers. Part H, Journal of Engineering in Medicine*, 224(12), 1441–1453.
21. Birmingham, E., Niebur, G., Mchugh, P., Shaw, G., Barry, F., Mcnamara, L. (2012). Osteogenic Differentiation of Mesenchymal Stem Cells is Regulated by Osteocyte and Osteoblast Cells in a Simplified Bone Niche. *European Cells and Materials*, 23, 13-27.
22. Cai, L. Guinn, A. Wang, S. (2011) Exposed Hydroxyapatite Particles on the Surface of Photo-crosslinked Nanocomposites for Promoting MC3T3 Cell Proliferation and Differentiation. *Acta Biomaterialia.*, 7, 2185–2199.

23. Wang, K.; Cai, L.; Zhang, L.; Dong, J.; Wang, S. (2012) Biodegradable Photo-crosslinked Polymer Substrates with Concentric Microgrooves for Regulating MC3T3-E1 Cell Behavior. *Advanced. Healthcare Materials.* 1, 292–301.
24. Stein, G. S.; Lian, J. B.; Stein, J. L.; Van Wijnen, A. J.; Montecino, M. (1996) Transcriptional Control of Osteoblast Growth and Differentiation. *Physiological Review.* 76, 593–629.
25. B. Chehroudi. J. Ratkay. D.M. Brunette. (1992) The Role of Implant Surface Geometry on Mineralization In Vivo And In Vitro—A Transmission and Scanning Electron-Microscopy Study. *Cell Mater,* 2 , pp. 89–104.
26. Wu, X., Wang, S. (2012). Regulating MC3T3-E1 Cells on Deformable Poly(ϵ -caprolactone) Honeycomb Films Prepared Using a Surfactant-Free Breath Figure Method in a Water-Miscible Solvent. *ACS Applied Materials & Interfaces,* 4, 4966-4975.
27. Siebers, M., Brugge, P., Walboomers, X., Jansen, J. (2005). Integrins as Linker Proteins between Osteoblasts and Bone Replacing Materials. A Critical Review. *Biomaterials,* 26(2), 137-146.
28. Wu, X.; Wang, S. (2013) Biomimetic Calcium Carbonate Concentric Microgrooves with Tunable Width for Promoting MC3T3-E1 Cell Functions. *Advanced. Healthcare Materials.* 2 (2), 326–333.
29. Dahl, K. N. Ribeiro, A. J. S. (2008) Lammerding, J. Nuclear Shape; Mechanics; and Mechanotransduction. *Circulation. Research.* 102, 1307– 1318.
30. Crouch, A., Miller, D., Luebke, K., Hu, W. (2009). Correlation of anisotropic cell behaviors with topographic aspect ratio. *Biomaterials,* 30(8), 1560-1567.

Chapter VI. Summary

A series of biodegradable, injectable, and photo-crosslinkable nano-hybrid polymer composite networks were developed for bone and cardiovascular tissue engineering (TE) applications. With the increase in demand to repair diseased and injured tissue, polymers have emerged in the field of regenerative medicine to improve current treatment options, and therefore offer options to reduce invasive surgical procedures.

In the first study, poly (ϵ -caprolactone fumarate) (PCLF) was synthesized via polycondensation. PCLF was then copolymerized with 1,2-propanediol isobutyl POSS in varied weight fractions ($\phi_{\text{POSS}} = 5\%, 10\%, \text{ and } 20\%$) to form the copolymer PCLF-*co*-POSS. Physical properties of PCLF and PCLF-*co*-POSS were examined, and data revealed that the increase in POSS content lead to enhanced crosslinking density and material stiffness, as indicated by higher gel fractions and modulus of elasticity, respectively. Thermal properties were also examined, and results suggested that POSS had the ability to improve the thermal stability of the polymer network. After physical and thermal characterization, crosslinked PCLF and PCLF-*co*-POSS substrates were evaluated on their ability to regulate mouse pre-osteoblastic MC3T3-E1 cells and rat primary aortic smooth muscle cells (SMCs). The cell studies conducted aimed to evaluate MC3T3-E1 cell and SMC attachment, proliferation, and differentiation. Throughout the study, it was found that cell behavior was regulated upon the dependence of ϕ_{POSS} . The increased weight fractions of ϕ_{POSS} showed to increase cell numbers, mineralization, and gene expression, all of which are indicators of osteogenesis. Further, SMCs studies showed similar results, as the increase in ϕ_{POSS} also promoted cell attachment, proliferation, and gene expression. Both PCLF and PCLF-*co*-POSS samples showed to effect cell attachment and proliferation similarly to the tissue culture polystyrene (TCPS), thereby suggesting that cytotoxicity to cells was negligible.

In the proceeding study, hydroxyapatite (HA) nanoparticles were homogenously implemented into the PCLF-*co*-POSS ($\phi_{\text{POSS}} = 20\%$) network to enhance surface chemistry for bone TE applications. Three samples were developed including, PCLF-*co*-POSS (smooth and microgrooved) and PCLF-*co*-POSS/HA. Both physical and thermal characteristics of the polymer nanocomposites were analyzed. The addition of HA into the polymer network increased gel fractions and lowered swelling ratios, which was likely because HA nanoparticles are insoluble in CH_2Cl_2 . Mechanical properties were altered by the HA nanoparticles, as the polymer network exhibited a more brittle behavior and the modulus of elasticity was increased over PCLF-*co*-POSS ($\phi_{\text{POSS}} = 20\%$). Scanning emission microscopy (SEM) was used to confirm the surface topography of the PCLF-*co*-POSS (smooth and microgrooved) and PCLF-*co*-POSS/HA substrates. SEM revealed the dimensions of the microgrooved surface with a 5 μm groove width and 12 μm groove depth. MC3T3-E1 cell attachment, proliferation, and differentiation was examined to evaluate the effects that surface chemistry and topography plays on regulating cell behavior. Cell attachment and proliferation was slightly enhanced on PCLF-*co*-POSS/HA, which was because of the enhanced surface chemistry rather than surface topography. Surfaces containing microgrooves changed the orientation of cells and promoted cell alignment via “contact guidance”. Further, microgrooved surfaces showed to increase mineralization and gene expression over both smooth PCLF-*co*-POSS and PCLF-*co*-POSS/HA substrates.

In summary, I developed a series of novel biodegradable polymer composite networks with tailorable mechanical, thermal, chemical, and topographical properties for regulating cellular behavior. The studies conducted showed to promote favorable microenvironments for bone and smooth muscle cells, therefore indicating their uses for various TE applications.

Vita

Charles Sprague was born in Houston, TX. He attended Louisiana Tech University from 2009 to 2013, where he received a B.S. degree from the College of Engineering and Science with a major in Biomedical Engineering. In the fall of 2013, he enrolled at The University of Tennessee, in the Department of Mechanical, Aerospace, and Biomedical Engineering (MABE). That fall he joined Prof. Shanfeng Wang's group in the Department of Materials Science and Engineering. He received a Master of Science Degree in Biomedical Engineering from the University of Tennessee in August 2015.